THE
PHYSICAL REVIEW
A Journal of Experimental and Theoretical Physics Established by E. L. Nichols in 1893
VOL. 54, NO. 2 JULY 15, 1938 SECOND SERIES

Solar Diurnal Variation of Cosmic-Ray Intensity as a Function of Latitude

JULIAN L. THOMPSON
Ryerson Physical Laboratory, University of Chicago, Chicago, Illinois
(Received May 21, 1938)

The cosmic-ray data collected by A. H. Compton and R. N. Turner on the Pacific Ocean from March 17, 1936 to January 18, 1937 have been analyzed for a possible change with latitude of the solar diurnal intensity variation. A new geomagnetic latitude curve is shown based on these data and designed to remove periodic fluctuations due to unequal distribution of data with time. A method of combining data from a wide latitude range is developed and applied. Solar diurnal variation curves for latitudes ranging from 54.7° N to 40° S (geomagnetic) show no substantial variation in either amplitude or phase. The mean amplitude of the first harmonic of a Fourier analysis is found to be 0.24 percent with time of maximum being 14 hr. 06 min.

THE study of the solar diurnal variations of cosmic-ray intensity at various latitudes, of which a preliminary survey was published previously[1] has now been carried out in more detail. The data used in this study were those obtained by A. H. Compton and R. N. Turner in observations on the Pacific Ocean covering a period of about a year. A Carnegie model C cosmic-ray meter, mounted on the Canadian Australasian Steamship Company's motor ship Aorangi, was carried on 12 voyages between Vancouver, Canada and Sydney, Australia from March 17, 1936 to January 18, 1937. The meter has been described in detail elsewhere[2] and many of the results of the observations previously reported and discussed by Compton and Turner.[3]

The fact that the data at the various latitudes were all recorded by one instrument is a distinct advantage. Experience has demonstrated the difficulty of obtaining results from several meters, even of the same type, which shall be sufficiently consistent for the comparison of variations of small magnitude. Another advantage is that the data for any particular latitude were not obtained continuously, but at intervals distributed throughout the entire period of observation. There are for example on the average 6 days readings in each 2.5° of latitude. Had the meter been operated continuously for this length of time in one zone, and then moved on to the next, several sources of error might easily have influenced the results. Any seasonal change in the variation would have increased or decreased the observed difference due to latitude change, and it would have been difficult to correct equally for any great difference in barometric conditions in the various zones. In addition, slow changes in the constants of the meter itself, if such had occurred, would have been difficult to detect.

There is, however, an unfortunate feature of this method of gathering data for this type of

[1] J. L. Thompson, Phys. Rev. **52**, 140 (1937).
[2] A. H. Compton, E. O. Wollan and R. D. Bennett, Rev. Sci. Inst. **5**, 415 (1934).
[3] A. H. Compton and R. N. Turner, Phys. Rev. **52**, 799 (1937).

study. Since the average cosmic-ray intensity varies by more than 10 percent in going from the latitude of Vancouver or Sydney to the equator, and since this distance is traversed in somewhat less than two weeks, the change in intensity during a twenty-four hour period from this cause is several times as great as the anticipated diurnal variation. Two courses are open to avoid the serious errors introduced by this circumstance: (1) one may, in finding the diurnal effect for a particular latitude, use only data from a latitude zone so narrow that the variation due to change of latitude is inappreciable; or (2) one may endeavor to correct the data for this latitude effect and thus make possible the combining of data from a wide latitude zone. In the present case, the former method is ruled out by the fact that most of the data would be discarded and one would have a hopelessly small amount of data with which to work. This is accentuated by the fact that since the vessel was on a regular schedule, the south-bound trips encountered a given latitude at almost the same time of day every time, and similarly the north-bound trips, giving only portions of the day for which any data would be available at all. Consequently, the method was adopted of correcting the data for latitude effect and then of combining the results from a comparatively wide latitude zone.

Since latitudes are recorded to 0.1°, it is necessary to have average ionization values for each 0.1° if individual readings are to be adjusted.

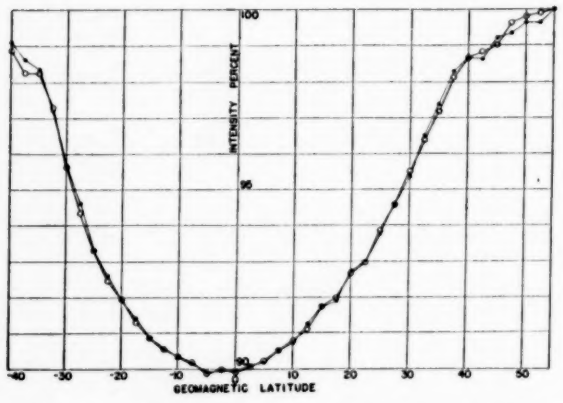

FIG. 1. Mean latitude effect on Pacific Ocean of eleven trips from March 27, 1936 to January 18, 1937. Data of Compton and Turner, showing difference between simple means averaged for each latitude range (black circles) and hourly means over the complete day for each latitude (open circles).

The first necessity in making such a latitude correction is a latitude-effect curve, from which the average ionization value for any latitude may be obtained. The latitudes used in this work are geomagnetic and not geographic, since the latitude effect is in the main a magnetic one. The customary procedure in constructing such a curve is to take the average value of all the data within zones of say 2.5° of latitude and assign that average value to the mean latitude of the zone. This gives a series of points which may be connected by straight-line segments or which may be used to guide in the drawing of a smoothed curve. In this particular case it seemed advisable to treat the data in a somewhat different manner. Since the trips were made on regular schedule, the times of arrival at and departure from principal ports of call were nearly the same on all trips. Thus the total data from all trips were in most 2.5° latitude zones markedly concentrated in certain portions of the day. For example, in the 2.5° zone whose mean latitude is 52.5°, there were 7 and 8 readings each for hours during the night, and only 3 for several of the daytime hours, and this variation was not exceptional. If an average ionization is to be arrived at which will be, as is certainly necessary, independent of any solar diurnal variation, the sampling must be made uniformly from all the hours of the day. To achieve this, the average hourly values were first found, and these in turn averaged over the twenty-four hours in order to fix the true average for the zone. A certain amount of statistical error is introduced by this procedure, since hours with few data are given equal weight with those for which many data are available. It seems clear, however, that where one is restricted to a certain number of data it is more important to eliminate systematic errors as far as possible. The extent to which this has been accomplished may be judged from the comparison of the latitude curve so obtained with that drawn in the more usual manner, as shown in Fig. 1. In general it will be seen that this procedure has been justified, inasmuch as the curve plotted in the usual way shows periodic fluctuations not present in the present curve. Not all of the irregularities are removed, however, and in particular that portion between latitudes 40°N and 54.7°N while im-

proved is still irregular. At 5°S and also at 37.5°S it is definitely more irregular than the original curve.

From the average ionizations obtained in this manner for every 2.5°, values were calculated for every 0.1° by direct linear interpolation. This was done without reference to any curve, although it would correspond to drawing straight-line segments between successive points to form the latitude curve. Despite the fact that the "true" latitude-effect curve must be a smooth curve, the points obtained actually represent the best averages for the various zones, and each point represents about the same number of data. Thus there is no logical way to decide through which points the smooth curve should pass, and linear interpolation offered the best use of the data.

With these values for each 0.1° at hand, each individual hourly value from the original data was adjusted by subtracting the average for the particular latitude at which it was taken. This resulted in transforming the more than 4000 hourly ionization values into hourly deviations from the mean. Insofar as the latitude variation of intensity was concerned, these deviations could be combined from as wide a range of latitudes as desired. The divisions chosen were a 20° zone embracing the geomagnetic equator, two 15° zones to the south and two to the north, and an additional 14.7° zone to the north, extending to but not including Vancouver at the northern extreme, and Auckland, New Zealand at the southern. Data from that portion of the course lying between Auckland and Sydney were not used, since there was but a very small variation in latitude in this portion, and a large variation in longitude.

In each zone except the northernmost, the correction to mean solar time was made by applying the appropriate correction for the mean longitude of the zone, since the variation of mean solar time over the zone was less than one hour. In the case of the zone between 40°N and 54.7°N, since the time variation was 72 minutes, the zone was divided into two parts, and appropriate corrections applied to each part before the data were combined.

It will be noted from the dates given that the period of observation did not cover a full year.

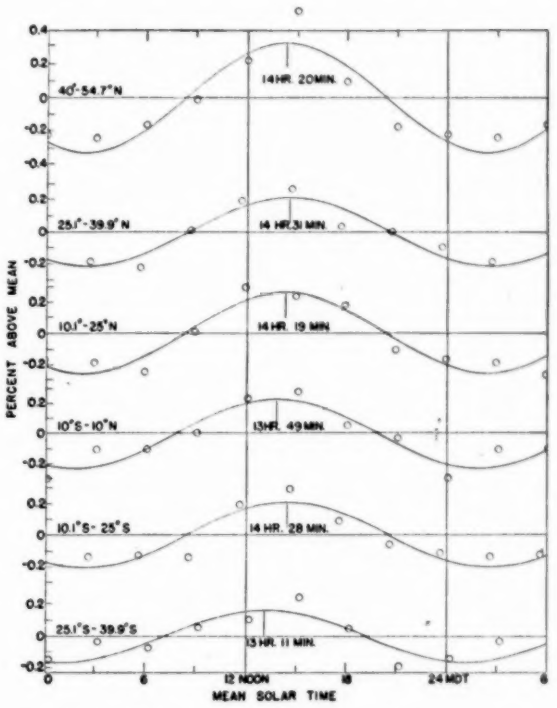

FIG. 2. Three-hourly means and first harmonic curves, showing solar time variations of cosmic rays at different latitudes on Pacific Ocean.

Since it is entirely possible that the diurnal variation may change with the season, the data were further grouped by seasons, and when the mean deviation for each hour had been found for each season, these seasonal averages were in turn averaged to find the yearly mean. In making the seasonal divisions, the solstices and equinoxes were taken as the mid-points of the respective seasons, rather than the dividing points.

From these average hourly deviations, the first harmonic of a Fourier analysis has been calculated, and also the three-hourly averages, both of which have been plotted. These graphs are given in Fig. 2, and a summary of the results in Table I. While it seems by no means necessary to assume an harmonic variation of intensity over the twenty-four hour period, the plotted three-hour means show a reasonably close approach to such a variation. On this assumption it is seen that the amplitude of the solar diurnal variation of intensity is substantially the same for the various latitude zones covered, and of the order of 0.24 percent. If the value of 0.33 percent found for the latitude zone 40°N − 54.7°N be excluded,

TABLE I. *Solar diurnal variation of cosmic-ray intensity at various latitudes.*

	GEOMAGNETIC LATITUDE	AMPLITUDE OF DAILY VARIATION, PERCENT	TIME OF MAXIMUM
1.	40°–54.7° N	0.33	14 hr. 20 min.
2.	25.1–39.9	0.22	14 31
3.	10.1–25.0	0.26	14 19
4.	10 S–10 N	0.23	13 49
5.	10.1–25.0 S	0.21	14 28
6.	25.1–39.9 S	0.17	13 11

the mean amplitude for all zones is 0.22 percent. Since this zone is the region in which the latitude variation shows the least regularity in these data, considerable doubt is justified as to the significance of this larger amplitude. There also seems to be no significant variation in the time of maximum, whose mean value for all latitudes is 14 hr. 06 min., with a maximum deviation of 55 minutes.

These results are in reasonable agreement with the amplitude of 0.20 percent with maximum at noon, reported by Hess and Graziadei[4] from the records of three years continuous observations at 2300 meters altitude. Other comparable results are the 0.19 percent amplitude, maximum at 9 hr. reported by R. L. Doan[5] at Chicago from the records of five meters operating simultaneously over a period of 10 days of exceptionally small barometric variation, and the 0.17 percent, maximum at 11 hr., reported by Forbush[6] from a critical analysis of data from 273 days record taken at Cheltenham, Maryland (geomagnetic latitude 50.4°).

The irregularity in the present data, noted above, occurs just on the "knee" of the latitude-effect curve, and a continuation of the study to much higher latitudes both north and south under the same conditions is much to be desired.

In conclusion, the author wishes to express his thanks to Professor A. H. Compton for suggesting the problem and making available the reduced data which have been used, and sincere appreciation for his helpful discussions during the course of the work.

[4] V. F. Hess and H. T. Graziadei, Terr. Mag. **41**, 9 (1936).

[5] R. L. Doan, Phys. Rev. **49**, 107 (1936).

[6] S. E. Forbush, Terr. Mag. **42**, 1 (1937).

On the Sidereal Time Variation of the Cosmic Radiation

HANNES ALFVÉN
Forskningsinstitutet för Fysik, Vetenskapsakademien, Stockholm, Sweden
(Received January 13, 1938)

If it is supposed that the positive and negative cosmic-ray particles are not equal in number, the resulting space charge will be neutralized by slowly moving ions which should follow the motion of the stars. If the cosmic-ray particles are not isotropic relative to the stellar system, as for example if they do not share the motion of galactic rotation, the relative motion of the slow ions and the cosmic-ray particles of opposite sign produces in effect an electric current. Calculation shows that the resulting magnetic field may become as great as 10^{-1} gauss if there is a considerable difference between the number of positive and negative particles. It is shown that the anisotropy corresponding to even a small sidereal time variation of the cosmic radiation would imply such great magnetic fields as to bend the paths of cosmic-ray particles in curves of radii small compared with interstellar distances. Therefore, the high degree of isotropy of the cosmic radiation is a necessary consequence of the fact that it consists mainly of charged particles and does not tell us anything about the place of origin of the radiation.

THE sidereal diurnal variation of the cosmic radiation is usually considered to be of fundamental importance for the problem concerning the origin of cosmic radiation. Especially, the absence of a marked intensity variation with the position of the Milky Way has been thought to exclude the generation of the radiation within our galaxy. This opinion would no doubt be correct if the cosmic radiation consisted of uncharged particles, which always travel rectilinearly through space. But as it has been shown that at least the main part of the radiation consists of charged particles, we must take into consideration that their path is rectilinear only in the absence of electric and magnetic fields, or in other words, only if the mutual interaction between the particles is negligible.

In interstellar space there is a multitude of charged particles with energies ranging from thermal to cosmic-ray energies. In order to distinguish between the slow particles and the cosmic rays we shall call a charged particle in space a "cosmic-ray particle" if the probability that it is deviated considerably when passing a thin sheet of matter (let us say 0.001 g cm^{-2}) is small. In another case we call it a "slow particle."

As the density of interstellar matter in our galaxy is about 10^{-25} g cm^{-3} the interaction between a cosmic-ray particle traveling for example 10^4 light years ($=10^{22}$ cm), and interstellar matter is negligible. On the other hand the slow particles, most of which are likely to be electrons and ions with thermal energies, collide so frequently with interstellar matter that they must share the motion of this matter, at least to a considerable extent. Thus, in our galaxy the slow particles take part, more or less, in the galactic rotation.

Now the east-west effect indicates that there are more positive than negative particles in cosmic radiation. As Swann[1] has pointed out, an excess of positive particles in cosmic radiation gives rise to an enormous charge in interstellar space if not neutralized by particles of the opposite sign. We must therefore assume that there is an excess of negative slow particles which has almost exactly the same value as the excess of positive cosmic-ray particles.

As now the slow particles within our galaxy take part in the galactic rotation we have (in a fixed system) a rotating negative space charge. If the cosmic radiation is *isotropic in a system moving with the galactic rotation*, it constitutes a positive rotating space charge exactly neutralizing the effect of the negative charge. But if the cosmic radiation is anisotropic in the rotating system, i.e., if on our earth we measure a sidereal time variation, the difference in motion between the positive and negative charge constitutes a current through space. The current density is no doubt very small, but as the cross section of the current is likely to be enormous, the magnetic field of the current is not at all negligible.

In order to show that even a small sidereal time variation of the cosmic radiation gives rise to enormous magnetic fields, let us assume that the

[1] W. F. G. Swann, Phys. Rev. **44**, 124 (1933).

Compton-Getting theory[2] is correct. For convenience we approximate the galactic system to a uniform circular disk with the radius $R=5\cdot10^{22}$ cm and the thickness $b=10^{22}$ cm, and which is rotating uniformly with the angular velocity $\omega=10^{-15}$ sec.$^{-1}$. According to Compton-Getting an observer moving with the system and situated at the distance r from the center would measure a relative excess of $4r\omega/c$ particles in the direction of the motion as compared with the opposite direction. If as a mean n negative and $n(1+\eta)$ positive particles (singly charged) hit a unit surface per second, the current density is

$$i=4r\omega n\eta e/c, \text{ e.m.u. cm}^{-2}$$

where $$e=1.6\cdot10^{-20} \text{ e.m.u.}$$

We assume that our observer finds no other current than this in space and no resultant space charge. This means that the excess of negative slow particles takes part in the galactic rotation and, to an observer in a fixed system, constitutes a current i with the same direction and magnitude (but for a small relativity correction). This is in accordance with the relativity theory: because the resultant space charge is zero (in the moving system) the current in the fixed and in the moving system must be equal to the first approximation ($v\ll c$).

It is now easy to calculate the magnetic field of the current. As the thickness of the disk is small compared with the radius, the magnetic field in the center is approximately

$$H=2\pi\int_0^R \frac{ibdr}{r}=\frac{8\pi n\eta ebR\omega}{c}.$$

Putting $n=0.2$ cm^{-2} sec.$^{-1}$ and $\eta=0.1$, we find

$$H\sim0.1 \text{ gauss!}$$

Hence, the consequence of a sidereal time variation as predicted by the Compton-Getting theory is that there must exist a magnetic field of the order of magnitude of one-tenth of a gauss in galactic space. This field is strong enough to bend the path of a 10^{10} ev particle to a circle with a radius smaller than that of our earth!

Against this argument may be objected that the excess of positive particles might be smaller than 10 percent ($\eta=0.1$) as assumed here. This objection is quite reasonable as our definition of cosmic radiation also includes smaller energies than those accessible to measurements. Moreover, the magnetic field might be compensated to a certain extent by other currents. But even if for example the positive excess were only 0.001 percent ($\eta=10^{-5}$) and moreover some unknown currents reduced the magnetic field by a factor of let us say 10^{-5}, the field would amount to 10^{-10} gauss, and this is enough to give a 10^{10} ev particle a radius of curvature of only 0.3 light year. As the magnetic field is perpendicular to the galactic plane it is impossible that a certain direction in this plane is favored by an excess of particles; in other words, a sidereal time variation of the Compton-Getting type is impossible.

Even a more local anisotropy of the charged particle component of the cosmic radiation seems to be very improbable. If the relative amplitude of the sidereal time variation is α, and we assume that this anisotropy is constant within a long cylinder with a radius of only 0.1 light year and the axis points in the direction of the anisotropy, the current within this cylinder generates a magnetic field

$$H\sim4\cdot10^{-4}\alpha \text{ gauss}$$

at the surface of the cylinder. A measurable sidereal time variation ($\alpha>10^{-4}$) gives a magnetic field $H>4\cdot10^{-8}$ gauss, so that a 10^{10} ev particle has a radius of curvature of <0.001 light year. This seems to be very improbable.

Consequently, a measurable sidereal time variation of the charged particle component of the cosmic radiation seems to be excluded. The experimentally found sidereal time variation must therefore be due either to a neutral component or, which perhaps is most probable, of secondary origin.

As the isotropy of the cosmic radiation is a mere corollary to the fact that most part of the radiation consists of charged particles, it is impossible to draw conclusions about the place of origin of the radiation from its isotropy. Consequently, the radiation may very well be generated within our galaxy, as predicted by the double star theory.[3]

[2] A. H. Compton and I. A. Getting, Phys. Rev. **47**, 817 (1935).

[3] H. Alfvén, Zeits. f. Physik **105**, 319, 633 (1937); **107**, 579 (1937); Ark. f. mat. astron. fys. **B25**. No. 29. April (1937).

The Silver L Series X-Ray Spectrum: Line Widths, Wave-Lengths, Relative Intensities, Satellites, and Widths of Energy Levels

LYMAN G. PARRATT
Cornell University, Ithaca, New York
(Received April 16, 1938)

With a new two-crystal vacuum spectrometer a systematic and precise study of 36 L series emission lines of silver has been made which includes measurements of wave-lengths, relative intensities, line widths and indices of asymmetry. These lines include 21 satellite lines. The contours of the three L absorption edges of silver were also recorded. From these data have been determined the widths of all the energy levels for single ionization of silver. From the widths of satellite lines are discussed the widths of certain states of double ionization.

INTRODUCTION

RECENT developments in x-ray spectroscopy are the quantitative correlations of (1) widths of x-ray emission lines and widths of absorption limits; (2) widths of "parent" lines and relative intensities of "satellite" lines; and (3) relative intensities, widths and wave-length positions of satellites. These are separate aspects of the problem of double (or multiple) ionization. The importance of multiple ionization was realized many years ago in connection with the Auger effect, with satellites and with certain fine structure in absorption edges, but only recently has the synthetic development of the physical concepts of the several phenomena reached the point where interrelating generalizations can be seen.[1]

The present paper reports the first systematic investigation of a complete L series spectrum with an instrument, a two-crystal vacuum spectrometer, having sufficiently high resolving power to measure the pertinent spectral properties. This study of 36 L series emission lines of silver ($Z=47$) includes measurements of wave-lengths, relative intensities, line widths and indices of asymmetry. These lines include 21 satellite lines. The contours of the three L absorption edges of silver were also recorded. From these data have been determined the widths of all the energy levels for single ionization (and in some cases for double ionization) of silver in the manner followed by Richtmyer, Barnes and Ramberg[2] in the case of gold. The contours of the absorption edges are found to abound with secondary structure and, although too complex to allow a simple direct measurement of energy level widths, promise exciting possibilities in quantitative studies of the Brillouin zones or crystal lattice energy levels in metallic silver or of energy levels in nongaseous substances in general.

EXPERIMENTAL

Spectrometer

The new two-crystal vacuum spectrometer differs but little in general design from its prototype.[3] The inside diameter of the tank has been increased from 50 to 60 cm; the distance between the crystals from 12 to 13.5 cm.

The ionization chamber, made of steel, is 3.5 cm in diameter and 9 cm in length; and has a window in the rear to allow the exit of unabsorbed x-rays. The collector rod has been extended to form a loop around the entrance window so as to collect more of the ions before recombination in the fore part of the chamber. Thin Cellophane (or Kodapak, less absorbing but also less tough), 0.5 mil thick, is used as the entrance window and is made electrically conducting by a negligibly thin aluminum foil placed on the window's inside. A conducting window is essential in facilitating saturation of the ion currents produced by radiations of widely differing intensities or of widely differing penetrations in the gas in the chamber.

To provide easy control of the gas pressure in the ion chamber and to allow the use of a very thin window that will support but a fraction of an atmosphere pressure, the gas inlet to the ion

[1] For recent papers illustrating this progress see F. K. Richtmyer, Rev. Mod. Phys. **9**, 391 (1937) and references.
[2] F. K. Richtmyer, S. W. Barnes and E. G. Ramberg, Phys. Rev. **46**, 843 (1934).
[3] L. G. Parratt, Phys. Rev. **41**, 553 (1932); Rev. Sci. Inst. **5**, 395 (1934) and **6**, 387 (1935).

chamber is connected by a flexible tube through the base plate (supporting the spectrometer) to the outside of the tank. Trouble with residual ionization (α-particles, etc.) is materially reduced by operating with a minimum gas pressure in the chamber.

The ionization currents were amplified with a WE-D96475 electrometer tube mounted adjacent to the ion chamber inside of the evacuated tank. The Barth[4] circuit was used with a maximum sensitivity of about 200,000 mm/volt/meter. Any one of five high resistors, in about equal and known steps from 10^9 to 10^{12} ohms, could be placed in the control-grid circuit by a switching device manipulated outside of the tank.

Linearity of the recording system was certified by comparisons of the absorption coefficient of silver for Ag$L\alpha_1$ radiation for each of two thicknesses of silver foils which reduced the ionization currents by factors of about 2 and 900, respectively. The two coefficients agreed within the experimental error of about 2 percent.

Crystals

Unfortunately the calcite crystals A_4B_4, exhaustively studied[5] some time ago, have deteriorated, spectrometrically speaking, during the intervening time. The reflecting characteristics of these crystals, cleaved and etched, have changed in $2\frac{1}{2}$ years as shown in Table I. The beginning of this change was suspected earlier.[5] These crystals were kept in a vacuum about ten months and were exposed to air in the laboratory about twenty months. Fortunately, repeated etching processes were successful in restoring the crystals to their earlier degree of perfection (or even slightly better, as shown in Table I) and so, as used in this study, the crystals may be called perfect crystals[5] of class I.

TABLE I. *Change with time in reflectivities of etched calcite crystals. Measured with* Mo$K\alpha$ *radiation, wave-length 0.71*A.

	1935	1937	1937 AFTER RE-ETCHING
(1, −1) full width	5.2″	8″	5.0″
(1, +1) full width	21.0″	27″	21.0″
Percent reflection in first order	66	40	67

[4] D. B. Penick, Rev. Sci. Inst. **6**, 115 (1935).

[5] L. G. Parratt, Rev. Sci. Inst. **6**, 387 (1935) and L. G. Parratt and F. Miller, Jr., Phys. Rev. **49**, 280 (1936).

X-ray tube

The specially designed x-ray tube is clamped in a vertical position onto the side of the tank. Through a sylphon bellows at each end of the tube, adjustments can be made to place either the filament or the target at any point in the space near the center of the tube. These adjustments greatly facilitate regulation of the shape and size of the focal spot, allow the best part of the target surface (important with powder targets) to be used as the focal spot, and permit easy alignment of the focal spot and slit. The surface of the target is inclined 30 degrees with respect to the path of the central ray to the first crystal.

To reduce the intolerable tungsten condensate on the target a shielded filament similar in design to the one described by Dershem[6] was found to work satisfactorily when the excessive heat produced by radiation from the filament was adequately dissipated. The grid-wire in this unit was found to be a very insensitive control and was dispensed with entirely.[7] The type of filament unit found most satisfactory[8] consisted of two cylindrical spiral filaments, about 20 turns of 5 to 7 mil tungsten, $\frac{1}{16}$″ in diameter and $\frac{1}{2}$″ long, connected in series, placed behind and offset on either side of a rectangular hole, $\frac{3}{16}$″$\times\frac{1}{2}$″, cut in the blind end of a steel tube $\frac{3}{4}$″ in diameter. With a uniform focal spot 7×5 mm, as used in the present study, this unit delivered more than 100 ma at 15 kv, although the steel shield was then red hot. To avoid this heating, which, for steady operation of the tube, requires an almost impractical outgasing process, oxide-coated filaments were tried but their emission was too spotty, the focal spot was not uniform, and there was a high probability of burning a small hole through the target. Carefully activated thoriated tungsten filaments served very well as long as a good vacuum was maintained. Adequate water-cooling of the shield is a better solution.

Targets

Several specimens of silver were used as targets to rule out spurious lines due to impurities. Gold

[6] E. Dershem, Rev. Sci. Inst. **7**, 86 (1936).

[7] One of the requirements of Dershem's filament design was the elimination of light direct from the filament and scattered from the target. In satisfying this requirement the grid-wire and deflecting shield serve an important function.

[8] Pierce, Olson and MacMillan, Rev. Sci. Inst. **8**, 145 (1937), describe another shielded filament unit, similar to the present one.

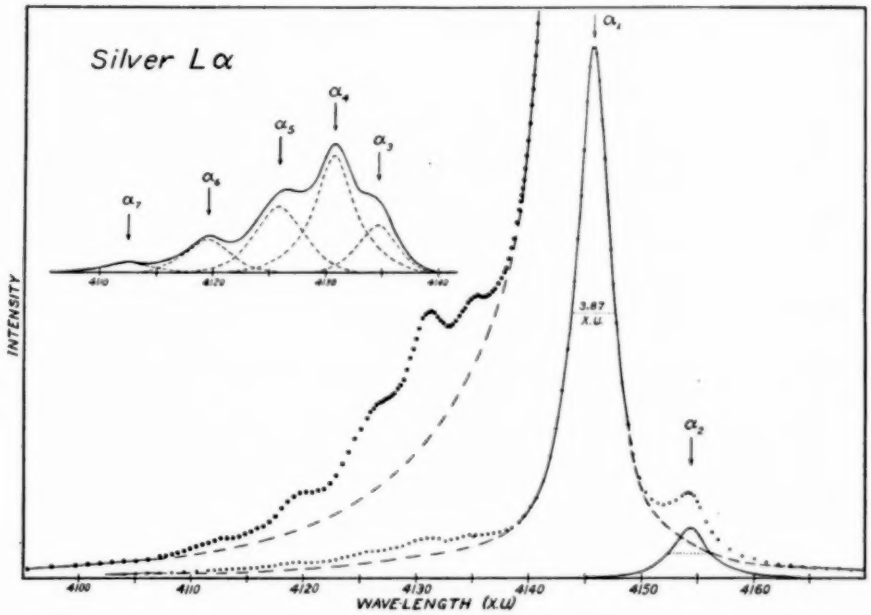

FIG. 1. Intensity plot (ionization recordings) of the Ag$L\alpha$ region. The upper satellite region, on the short wave-length side of α_1, is replotted with the intensity scale increased 6.3 times. Five component satellite lines have been sketched in.

was chosen as the target for producing the continuous radiation because of freedom from the M series lines in the spectrum range studied and because of the practical difficulties in making satisfactory targets of higher elements.

The tube voltage[9] was maintained at 15 kv for the emission spectrum and at 12 kv for the absorption curves. The lower voltage for the continuous radiation was used (1) to prevent gold L series lines from being excited and coming through in third-order reflection, and (2) as a practical compromise between the intensity of the continuous radiation in first order and the unwanted continuous radiation in second-order reflection.[10]

[9] See L. G. Parratt, Phys. Rev. **49**, 133 (1936) for description of the voltage supply.

[10] The ratio of the coefficients of reflection of each of the two crystals for reflection in first- and in second-order aids in minimizing the intensity of the second-order radiation. This ratio, 16 to 1 for the second crystal as interpolated from measurements by Parratt and Miller, reference 5, gives an effective ratio of about $1.5\times(16)^2$ or 400 for the coefficient of reflection of *both* crystals (400 in angular measure or about 50 in wave-length measure). The factor 1.5 is designed to take care (approximately) of the polarization of the beam upon reflection at the first crystal. The differential absorption of the first- and second-order beams is a hinderance in this minimization of second-order intensity.

Working x-ray intensity

The peak intensity of the $L\alpha_1$ line at 4.15A with the tube operating at 15 kv and 40 ma produced an ionization current of 6×10^{-13} ampere, equivalent to a full sensitivity scale deflection of 12,000 cm.

The intensity of the continuous radiation at 3.9A with the tube operating at 12 kv and 60 ma produced an ionization current of 1.2×10^{-14} ampere, a full sensitivity scale deflection of 250 cm, which could be read and repeated with a precision of about one percent.

MEASUREMENTS

Ionization curves

Figures 1 and 2 are reproductions of the α and the β lines of the observed Ag(47) L series spectrum. Fig. 2 is a composite of several overlapping sections recorded at different "sittings." The lower curve in Fig. 2 is plotted to an intensity scale magnified 15 times with respect to the scale in the upper curve. The accuracy with which the data were recorded is indicated by the consistency of the points on these curves.

In taking these data the base line or zero in-

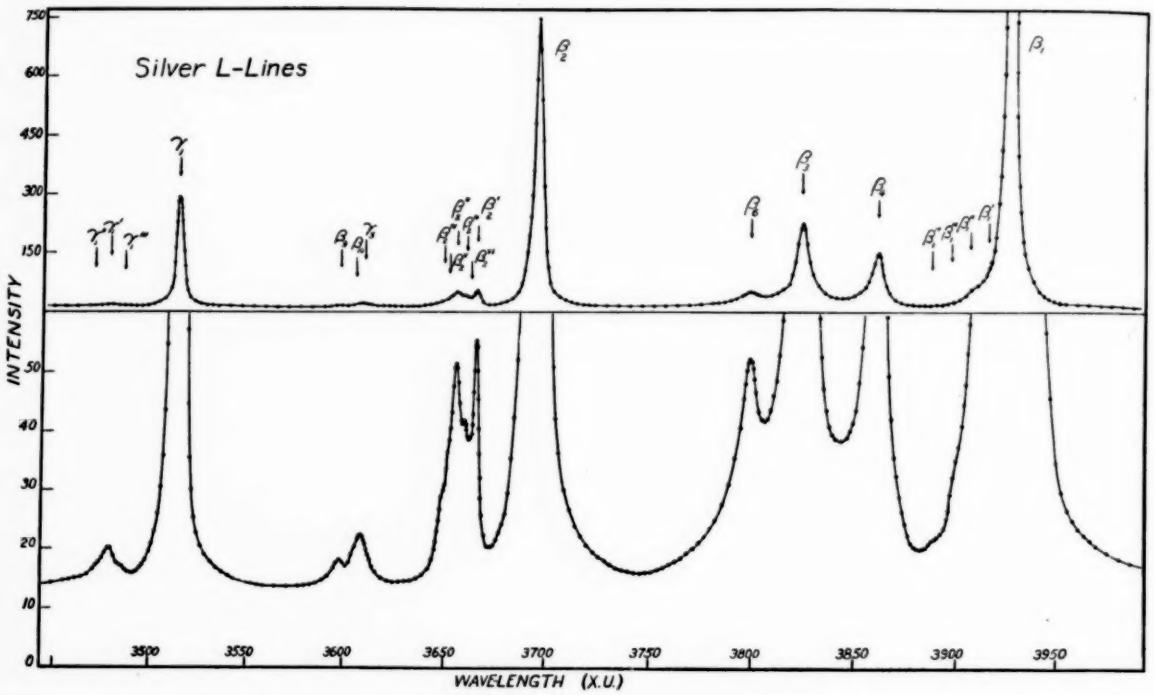

FIG. 2. Intensity plot (ionization recordings) of the Ag$L\beta$ region. The lower curve is plotted to an intensity scale 15 times the scale of the upper curve. The accuracy in measuring the various properties of most of these lines is limited not by the low intensity nor by the intensity readings but by the arbitrary resolution into component structure. The overlapping of these lines in inherent and cannot be reduced appreciably by increasing the resolving power of the (two-crystal) spectrometer with which their contours are recorded. The peak of the β_1 line is 4.8 times as high as the β_2 peak; the peak of the α_1 line, the strongest line of the series, is 8.25 times as high as the β_2 peak.

tensity was determined many times in the progress of each curve by placing temporarily a thick lead absorber in the beam. This procedure reduces the danger in the assumption of no "zero drift" or of uniform "zero drift." Also, this use of a complete absorber obviates the (all-too-frequent) interpolation to get the base-line between the "ends" or minima of such curves. Such an interpolation desirably ignores the background of continuous and of scattered radiation but also undesirably "fixes" arbitrarily the height and wave-length extent of each "line." In measuring line widths and relative intensities it is necessary, however, to discount the undesired background, especially for the weaker lines, such as η or β_6, β_9 or γ_5 (see the lower plot of Fig. 2). As yet we are forced to an arbitrary distinction between true line and background from the observed contours; a satisfying distinction can be made only when the complete intensity plot, including true line and background, is before us.

Figure 3 is the observed contour of the $\gamma_{2,3}$ lines. This contour illustrates a major difficulty in studies of this kind: The line widths are so great that close-lying lines seriously overlap one another and defy a unique resolution into components. An attempt at such a resolution is, of course, imperative in making a measurement of relative intensity, line width, shape or wave-length position. This overlapping is characteristic of the lines themselves and *cannot be reduced* appreciably by increasing the resolving power of the spectrometer.

The difficulty in resolving the α structure into component lines has been discussed in an earlier paper[11] with the conclusion that, in the analysis of contours recorded with practically infinite instrumental resolving power, we must resort to an arbitrary "reasonable" resolution, determined by the observer's best judgment.

Another poignant example of arbitrary but "reasonable" resolution is illustrated by the $L\beta_2$ satellite contour and components, Fig. 4.

The observed contour of the L_{III} absorption limit of silver, shown in Fig. 5, is the average of

[11] L. G. Parratt, Phys. Rev. **50**, 598 (1936).

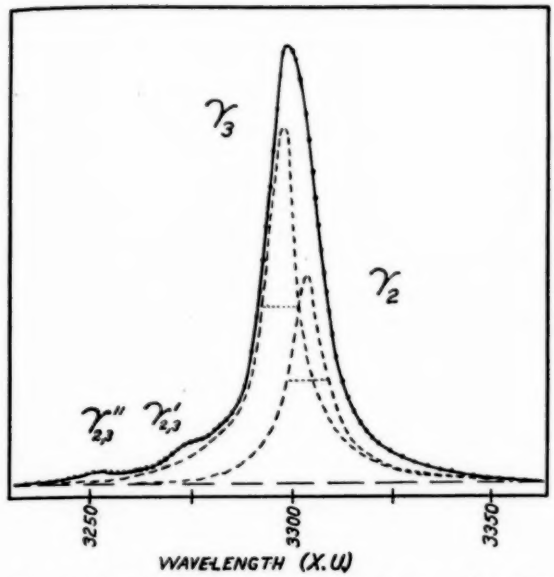

FIG. 3. The observed contour of the Ag$L\gamma_{2,3}$ lines illustrates the difficulty and the arbitrariness of the necessary resolution into components.

six curves taken with four different Ag foils. The average thickness of the absorbing foils was about 12,000A, which is the calculated optimum thickness, i.e., the thickness which gives the maximum relative change in the intensity at the L_{III} edge, when the absorption coefficients listed in the *Handbook of Chemistry and Physics*[12] are used.

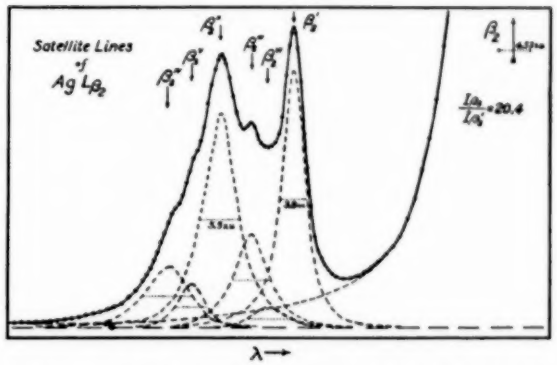

FIG. 4. The observed contour of the Ag$L\beta_2$ satellite structure is resolved into six components. Theory indicates that forty components of varying relative intensities and mostly unresolved should be present. The satellite line $L\beta_2'$ is less wide, 3.8 x.u. (3.5 x.u. corrected), than the "parent" line $L\beta_2$, 4.53 x.u. (4.1 x.u. corrected); this is the first satellite (or double ionization) line to be so reported. See text.

[12] *Handbook of Chemistry and Physics*, 19th edition, p. 1381.

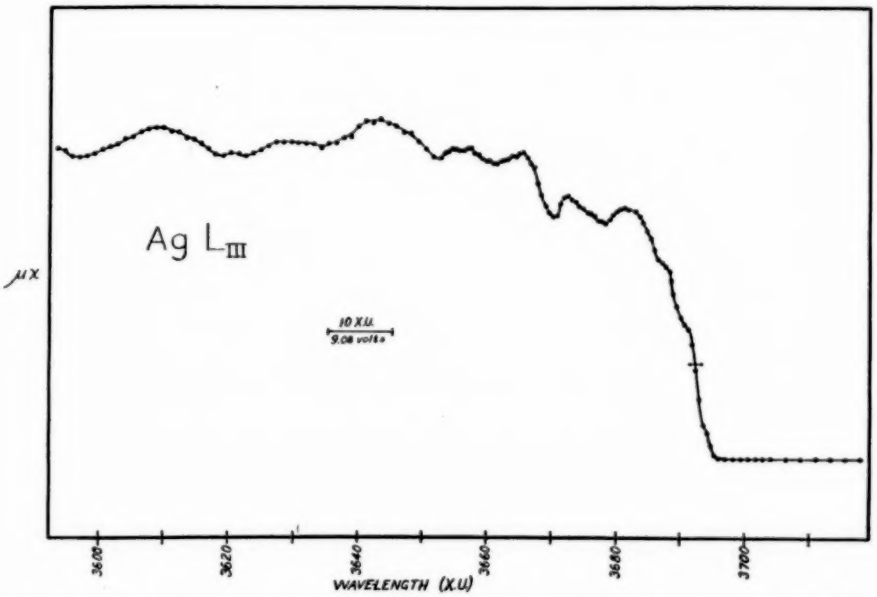

FIG. 5. The absorption (coefficient) of silver in the wave-length region of the AgL_{III} absorpton limit. In addition to the main absorption edge are found a series of absorption maxima. These maxima represent resonance absorption lines (or zones) corresponding to the ejection of the $(2p_{3/2})$ electron to outer unfilled energy levels. Atomic or optical levels are engaged in the resonance lines lying within about 9 electron volts (ionization potential of Cd(48), $Z=47+1$) from the main edge; crystal lattice energy levels (or zones) are involved in the more removed maxima. The width of the Ag$L\alpha_1$ line is indicated by the length of the arrow on the main edge: The width of the L_{III} energy state must be less than the length of this arrow.

Except in studying the details in small wave-length ranges, the large wave-length extent of these curves required that both crystals, the positions of the x-ray tube and of the ion chamber *all* be adjusted simultaneously as the recordings were in progress. In this way, the same effective region of each crystal was used in reflection, and proper alignment of the focal spot, crystals and ion chamber was maintained at all times.

Correction for resolving power

Since the widths of L series lines are relatively great (2 to 10 times as great as of K series lines of the same wave-length) the utmost in resolving power in the spectrometer (using special quartz crystals or higher orders of reflection[5]) is not necessary; in fact, is a detriment in recording *weak* lines. For this work the numerical resolving power ($\lambda/d\lambda$) was about 11,000 to 12,000: The $d\lambda$ interval in first-order reflection was about equal to $\frac{1}{10}$ of the width, 3.45 x.u., of the narrowest observed line, β_1; or about 1/50 of the widest line, l, 22.2 x.u.

The correction to be applied to observed non-overlapping lines in obtaining the true line contours, for purposes of measuring true line widths and relative intensities, is perhaps small with the present resolving power but is much greater than the observational error in recording the curves. This statement is not true in the cases of very faint or badly overlapped lines. The correction formula previously proposed[5] in terms of the (1, −1) and (1, +1) widths in x.u.

$$W_T = W_0 - 2.9 W_c^{1.7} \qquad (1)$$

at half-maximum intensity, has been applied to the measured line widths in a somewhat arbitrary manner; the full correction was applied in cases of distinctly separate or naturally resolved lines, e.g., α_1 or β_1, and an arbitrary fraction of the full correction was applied in cases of overlapping lines, e.g., α_2, β_2'' or γ_3. It is obvious that the same or full magnitude of correction, Eq. (1), cannot be applied to these two types of lines without introducing another appreciable error in the overlapping lines. To correct *properly*, one must very arduously operate on the observed contour instead of on the resolved components. An approximate method for doing this has been proposed by Spencer and this double inverse graphical procedure has been used as a guide[13] in the corrections made in the present analyses for line widths and for relative intensities.

Wave-Lengths

The writer's spectrometer is not capable of absolute wave-length measurements but is capable of measuring accurately small wave-length intervals. The wave-lengths of the Lα_1, β_1 and γ_1 lines of Ag(47) given by Haglund[14] were used as standards. Listed in Table II are wave-length intervals and wave-lengths of lines referred to Haglund's measurements as indicated. These values are believed to be more accurate than wave-lengths heretofore reported for the AgL series lines. Unfortunately, the l and η lines are too far removed from the α_1 line to be included with the new data in this table.

The γ_5, β_9 and β_{10} region requires comment. The observed contour of this region includes two well defined maxima, Fig. 2, and a slight irregularity, indicating a third line, between them. Two interpretations of this contour are possible: (1) we may heed the slight irregularity and say three lines are present; or (2) we may conclude that only two lines are observed, say the β_9 and β_{10} or the β_9 and γ_5. In favor of the first interpretation, as herein adopted, are four arguments. First, the wave-length interval between β_9 and β_{10} should be the same as the interval between α_1 and α_2; both intervals are equal to the separation of the M_{IV} and M_V energy levels. The separation of the observed maxima, perhaps the β_9 and β_{10} lines, is 11.9 x.u. whereas the $\alpha_1 \rightarrow \alpha_2$ separation is but 8.5 x.u. Second, the width of each of just two components is greater than one might reasonably expect for the β_9 line and for either the β_{10} or γ_5 line according to a criterion to be discussed later. Third, the Burger-Dorgelo sum rules for relative intensities predict an intensity ratio of 1 to 0.67 for β_9 to β_{10}, whereas the observed intensity ratio of the two lines is 1 to 2.9. The sum rules also predict an intensity for γ_5 equal to one-half of the intensity of β_6 or a γ_5 intensity 0.7 of the in-

[13] R. C. Spencer, Phys. Rev. **38**, 618 (1931), and L. G. Parratt, Phys. Rev. **49**, 138 (1936).

[14] P. Haglund, Zeits. f. Physik **84**, 248 (1933). See also A. H. Compton and S. K. Allison, *X-Rays in Theory and Experiment* (D. Van Nostrand Co., Inc., 1935), p. 786, and M. Siegbahn, *Spektroskopie der Röntgenstrahlen*, second edition (Julius Springer 1931), p. 228.

tensity of the higher peak of the contour in question. Fourth, if we derive from the combination principle and the energy level diagram the wave-length of $\gamma_5(L_{II}N_I)$ we equate $1/\gamma_5=(1/\beta_1)+(1/\beta_6)-(1/\alpha_2)$ and obtain $\gamma_5=3608.5$ x.u., when the wave-lengths in Table II are used. In a sense, the consideration of such arguments partially defeats the purpose of the experiments which are carried out to obtain data *from* which, rather than *to* which, such arguments may be made, but we must concern ourselves with the identification and the assignment of names to the observed lines or components.

The wave-lengths of the lines β_9 and β_{10} are radically different from Coster's (see Table II). In order to make doubly sure of the present wave-length scale, the position of Sn$L\alpha_1$, 3592.57 x.u. from Siegbahn's tables, was measured and checked as a secondary standard.[15]

[15] The wave-length of Sn$L\alpha_1$ cannot be checked perfectly because of the discrepancies in the variously reported wave-lengths. We may refer the position of the Sn$L\alpha_1$ line to the wave-length of the intense and therefore easily measured Ag$L\beta_2$ line. The present observed separation of these two lines is 102 x.u. If we use Hjalmer's λ for Ag$L\beta_2$, 3693.8 x.u., we get 3591.8 x.u. for the λ of Sn$L\alpha_1$; if we use the present value for Ag$L\beta_2$, 3695.50 x.u., we get 3593.5 x.u. for Sn$L\alpha_1$. The two values thus obtained for the Sn line straddle the latest value given in Siegbahn's tables, 3592.57 x.u.,

TABLE II. *Wave-lengths of peaks of lines of the L series spectrum of silver (Z=47). The wave-lengths of the three lines γ_1, β_1 and α_1 as measured by Haglund are used here as standards to which all the other lines are referred. For ready comparison the satellite measurements by the Richtmyers have been referred to the present values as standards instead of to Coster's values.*

LINE	TRANSITION	SEPARATION (SECONDS OF ARC)	SEPARATION (X.U.)	WAVE-LENGTH (X.U.)	PREVIOUS MEASUREMENTS (X.U.)	OBSERVER*
$\gamma_{2,3}''$	Satellite	10870	264.3	3251.15	—	
$\gamma_{2,3}'$	"	10000	244.0	3271.45	3270	D
γ_3	L_IN_{III}	8920	215.8	3299.65	—	
$\gamma_{2,3}$	—	8870	214.4	3301.05	3299.8	C
γ_2	L_IN_{II}	8680	210.0	3305.45	—	
γ_1'''	Satellite	1790	42.9	3472.55	—	
γ_1'	"	1455	34.85	3480.60	3480	D
γ_1''	"	1130	27.1	3488.37	—	
γ_1	$L_{II}N_{IV}$	0	0	[3515.45]	3514.9	H_j, C
β_9	L_IM_V	3410	80.9	3596.35	3620	C
β_{10}	L_IM_{IV}	3765	89.3	3604.8	3630	C
γ_5	$L_{II}N_I$	3930	93.2	3608.6	3607.3	C
β_2^{iv}	Satellite	5626.5	133.2	3648.65	3648.2	R
β_2^{v}	"	5763	137.4	3652.9	—	
β_2''	"	5928.5	140.3	3655.75	3655.6	R
β_2'''	"	6110	144.6	3660.0	3660.4	R
β_2^{vi}	"	6201.5	146.6	3662.1	—	
β_2'	"	6355	150.9	3666.35	3665.4	R
$\beta_2^{(a)}$	"	—	—	—	3691.0	R
β_2	$L_{III}N_V$	7635	180.05	3695.50	3695.60	H
β_6	$L_{III}N_I$	12170	284.45	3799.90	3798.6	C
β_3	L_IM_{III}	4515	101.5	3825.00	3824.5	H_j, C
β_4	L_IM_{II}	2870	64.4	3862.10	3861.1	H_j, C
β_1^{iv}	Satellite	1560	33.5	3893.0	3893.4	R
β_1'''	"	1250	27.0	3899.5	3899.5	R
β_1''	"	880	19.0	3907.5	3907.0	R
β_1'	"	510	11.0	3915.5	3914.9	R
β_1	$L_{II}M_{IV}$	0	0	[3926.50]	3926.6	H_j, C
α_7	Satellite	1587	34.15	4111.60	4112.65	R
α_6	"	1203	25.85	4119.90	4119.45	R
α_5	"	915	19.6	4126.15	4125.75	R
α_4	"	690	14.75	4131.00	4130.75	R
α_3	"	510	10.9	4134.85	4135.05	R
α_1	$L_{III}M_V$	0	0	[4145.75]	4145.6	H_j, C
α_2	$L_{III}M_{IV}$	397	8.48	4154.25	4153.8	H_j, C
η	$L_{II}M_I$	—	—	—	4410.1	C
l	$L_{III}M_I$	—	—	—	4697.6	C

* D = Druyvesteyn, 1928. Siegbahn, reference 14.
C = Coster, 1922. Siegbahn, reference 14.
H_j = Hjalmar, 1921. Siegbahn, reference 14.
R = Richtmyer and Richtmyer, 1929. Reference 17.
H = Haglund, 1933. Reference 14.

Satellite lines

The $L\beta_2$ satellite lines also deserve further comment. Six β_2 satellites have been drawn under the observed contour of Fig. 4. Five of these correspond either to observed peaks or to observed irregularities of slope in the contour. The sixth, β_2^{vi}, is not observationally necessary until we adopt the criteria of (at least fair) symmetry and reasonableness of shape of the component lines. If we do not adopt such criteria we are not allowed to measure, or even to speak of, any of the individual components of such a group. Indeed, the assumption of six $L\beta_2$ satellite components is ultra-conservative in view of recent trends in theory: Richtmyer and Ramberg[16] predict forty separate components in this satellite group for gold, the transition ($2p3d \rightarrow 4d3d$).

The satellite line $L\beta_2^{(a)}$, at 3691.0 x.u. according to a measurement with the photographic method by Richtmyer and Richtmyer,[17] is not included in the present investigation. This is not a denial of the real existence of this line, but indicates, rather, an unwillingness on the writer's part to break up the extreme intimacy of $\beta_2^{(a)}$ and β_2.[18] This may be a case in which the technique of exposure (or overexposure) of a photographic plate may bring out for wave-length determination a faint line which is too faint, relative to an intense or a rapidly changing background (the side of a strong line), to show itself distinctly in a *linear* intensity plot. This possible advantage of the photographic method, notwithstanding its inferior resolving power, when in careful hands, has been anticipated before,[19] and, in a comparison of methods, is of considerable significance.

The γ_1 satellite contour is observed to be complex also, and the γ_1'' component is included mainly on the belief that the γ_1' component should have fair symmetry and a reasonable shape.

Two satellites accompanying the $\gamma_{2,3}$ lines are recognized in this study but there are indications that more than two components really exist.

Relative Intensities

To obtain transition probabilities from the observed relative intensities many troublesome corrections must be made,[20] such as corrections for absorption in the target, in the windows, in the air path, and in the ionization chamber; for variations in the coefficient of reflection of the crystal or crystals; and for ionization probabilities (which include the tube voltage). One correction which seems to have escaped adequate discussion in the literature so far and which is apt to be larger than some of those listed above is the correction for the resolving power of the spectrometer.

The relative intensity of two lines is defined as the ratio of the energy or power contained in one line with respect to that contained in the other line. This definition is subject to *two* experimental applications. In the first application the relative intensity is the ratio of the *maximum ordinates* of the two lines whose contours are recorded with a spectrograph or a spectrometer of *low resolving power*, an instrument whose effective $d\lambda$ interval or "spectral window" is many times greater (or wider) than the wave-length extent (or width) of each of the two lines being measured. In the second application relative intensity is the ratio of *areas* contained under the contours (plots of intensity *vs.* frequency) of the two lines when recorded with an instrument of infinite or, in practice, *very high resolving power*. In using an

reported by Wennerlöf. Hjalmer's value for Sn$L\alpha$ is 3592.2. These discrepancies, however, are too small to account for the 20 x.u. difference between the present wave-lengths and Coster's values for γ_5, β_9 and β_{10}.

[16] F. K. Richtmyer and E. G. Ramberg, Phys. Rev. **51**, 925 (1937).

[17] F. K. Richtmyer and R. D. Richtmyer, Phys. Rev. **34**, 574 (1929).

[18] It might be argued that additional component lines *should* exist on the short wave-length side of β_2 because of transitions between the L_{III} level and the levels just beyond the N_V level. Such lattice levels and their energy separations are shown in the absorption curve of Fig. 5. It is difficult to estimate the intensities one might expect for emission lines from these levels (excited states) but the fact that β_2 shows no especially peculiar shape between its peak and the β_2' satellite indicates that the intensities are low. (Part of the *width* of β_2 may be due to transitions from these levels in case the levels form an effective continuum.) However, an interpretation of this character for $\beta_2^{(a)}$ is, perhaps, not unreasonable.

[19] Compare, for example, the photographic and ionization recordings of identical spectral regions (1) of M. V. Dolejšek, Comptes rendus **174**, 441 (1922), and of L. G. Parratt, Phys. Rev. **49**, 502 (1936), (2) of M. H. Hulubei, Comptes rendus **201**, 544 (1935) and of C. H. Shaw and L. G. Parratt, Phys. Rev. **50**, 1006 (1936), (3) of F. K. and R. D. Richtmyer, Phys. Rev. **34**, 574 (1929) and of Fig. 1 of the present report, and (4) of A. W. Pearsall, Phys. Rev. **46**, 694 (1934) and of Fig. 4 of the present report.

[20] A. H. Compton and S. K. Allison, *X-Rays in Theory and Experiment* (D. Van Nostrand Co., 1935), p. 652.

instrument having a spectral window between these extremes, one must tackle the difficult task of correcting the observed contours.

It is not generally feasible to apply a low resolving power instrument to accurate relative intensity measurements because so few x-ray lines appear as single or non-overlapping lines. In the spectral region of Figs. 1 or 2, for example, it is difficult to choose a spectral window of the proper extent to include all of one and only one line with an intensity uncertainty of less than, say, a few percent. With the assumptions that, for a given window position, the width of the window is properly chosen to include *all* of one line and *none* of other lines, or with an attempt to correct adequately when the assumption is not valid, the magnitude of the attending error in the relative intensity measurement is dependent upon the complexity of the spectral region being studied. Uncertainties from this cause may be as great as *several hundred percent* in the intensity ratios of faint lines close to a strong line, as the $L\alpha_1\alpha_2$ doublet, or as satellite and "parent" lines.

Investigators have appreciated the need for instruments of higher resolving power in studying overlapping multiplets, but, in using such instruments, have often confused the two experimental interpretations of relative intensity, i.e., ratio of maximum ordinates and ratio of areas. This was, at first, not thought of as a serious confusion since it was not known then that x-ray lines have such widely differing shapes, particularly widths. Of course, if the two x-ray lines in question had identical widths (preferably zero widths) and shapes the two relative intensity interpretations would be the same. But they seldom do: The observed widths of the present L series lines for Ag (47) differ from each other by as much as a factor of 7 (e.g., the β_1 to l lines). Ideally, then, an instrument of practically infinite resolving power is to be preferred. The two crystal spectrometer comes closest to meeting this requirement, but does not quite reach it. To say that the width of the spectral window is but 1/5 or 1/10 or 1/20 of the width of the x-ray line is to tell but part of the story; the indefinite extent of the window as it tails out on either side and its entire integrated effect in the observed contours is the complete story.[21] Even with the two-crystal instrument, unless operated with special crystals, such as with quartz, or with crystals in higher orders of reflection, a correction for lack of infinite resolving power must be made.

There are, therefore, two uncertainties in relative intensity determinations due to resolution, (1) inherent in the analyzing spectrometer in not meeting the requirements for either of the two experimental interpretations of relative intensity of lines of different widths and shapes, and (2) a consequence of an arbitrary resolution of overlapping structure into the proper component lines even though recorded with an instrument having infinite resolving power. These effects of resolution are in part responsible for the discrepancies in the relative intensity values that have appeared in the literature, and in particular for the differences between the present measurements and the hertofore best measurements for the silver L series lines, e.g., those of Jönsson, of Pearsall, and of Hirsh.[22]

In Table III are listed the experimental relative intensities of the AgL series lines. In the third column are the ratios of observed peaks (maximum ordinates) corrected only for the continuous and scattered background. In the fourth column are ratios of the peaks of the previous column corrected for overlapping. In the fifth column are ratios of the areas corrected for background, for overlapping, for lack of finite resolving power, for coefficient of reflection of the crystals,[23] and for absorption in the two

[21] The problem of the effect of the crystal diffraction patterns is carefully discussed in connection with the short wave-length limit of the continuous spectrum by DuMond and Bollman, Phys. Rev. **51**, 400 (1937) and mentioned by Kirkpatrick and Ross, Phys. Rev. **51**, 529L (1937). See also Compton and Allison, reference 20, pp. 710–722, and reference 5.

[22] A. Jönsson, Zeits. f. Physik **46**, 383 (1928), A. W. Pearsall, Phys. Rev. **46**, 694 (1934), F. R. Hirsh, Phys. Rev. **48**, 722 (1935), and Hirsh and Richtmyer, Phys. Rev. **44**, 955 (1933).

[23] The coefficient of reflection of a crystal is defined as the area contained under the diffraction pattern of the crystal on which is incident unit intensity of radiation of the wave-length contained in the pattern. In obtaining relative intensity, the correction for the variation of the coefficient of reflection is, for each crystal, the reciprocal of the ratio of the two pattern areas for the two wave-lengths in question. This correction tacitly includes the *width* of the pattern (area$\sim$(width$\times$height)) and therefore includes a correction for the resolving power. But note that this aspect of the resolving power is merely that the *intensity* which a crystal reflects is approximately inversely proportional to

windows (Cellophane, combined thickness of 0.0017 inch). The x-rays are completely absorbed in the ion chamber. The corrections for the ionization probabilities and for absorption in the target have not been made because of the difficulties in their execution at this time.

The two corrections for resolution, somewhat arbitrary as shown above, are believed to in-

the width of the spectral window; it says nothing about the perturbations present in an observed contour due to the *changing slope* of the true or unperturbed contour. These perturbations, referred to in the text as inherent in the spectrometer, are really characteristic of the *interactions* of the spectrometer with the spectral region under observation: The observed curve is the integral of the product of the diffraction pattern and the true contour being studied. In a sense, then, two separate corrections must be made for the lack of infinite resolving power (in addition to the arbitrary resolution of lines if they overlap). In this connection it may be mentioned that to relative intensity measurements made with a single crystal spectrometer or spectrograph should be applied, in addition to the correction for coefficient of reflection of the crystal, a correction for the change in area of the spectral window when this area is determined by slit-geometry. This correction, a resolving power correction (where the resolving power is proportional to the tangent of the Bragg angle), is the ratio of the energy extents of the spectral windows for each of the two wave-lengths. For lines of large wave-length separation this correction is significant.

TABLE III. *Relative intensities of the lines of the L series spectrum of silver ($Z=47$). The most intense line, α_1, is taken as 100. The relative areas in column 5 include corrections for background, for overlapping of neighboring lines, for lack of infinite resolving power of the spectrometer, for coefficients of reflection of the two crystals, and for absorption in the x-ray path with the exception of the absorption in the target itself.*

		Present Measurements			Previous Measurements		
Line	Transition	Observed Peaks from Contour	Observed Peaks (corrected for overlapping)	Areas Corrected (not corrected for absorption in target)	Not Corrected	Corrected for Target Absorption, etc.	Observers*
β_4	$L_I M_{II}$	2.34	2.1	3.9	4.6	5.8	J
β_3	M_{III}	3.7	3.6	7.2	7.4	9.4	J
β_{10}	M_{IV}	—	0.030	0.043			
β_9	M_V	0.08	0.056	0.074			
γ_2	N_{II}	—	0.36	0.66			
γ_3	N_{III}	—	0.62	1.04			
$\gamma_{2,3}'$	Satellite	—	0.013	0.029			
$\gamma_{2,3}''$	"	—	0.013	0.029			
η	$L_{II} M_I$	0.27	0.27	2.0	2.0	2.2	J
β_1	M_{IV}	58.1	58.1	49.1	53	59	J
β_1'	Satellite	—	0.6	0.84			
β_1''	"	—	0.6	0.84			
β_1'''	"	—	0.2	0.28			
β_1^{iv}	"	—	0.07	0.10			
γ_5	N_I	0.16	0.13	0.28			
γ_1	N_{IV}	5.2	5.2	4.36	9.5	12	J
γ_1'	Satellite	0.12	0.10	0.10			
γ_1''	"	—	0.026	0.026			
γ_1'''	"	—	0.019	0.036			
l	$L_{III} M_I$	0.40	0.40	4.4	4.1	4.1	J
α_2	M_{IV}	15.6	9.2	8.61	12	12	J
α_1	M_V	100	100	100	100	100	
α_3	Satellite	7.57	1.37	1.64			
α_4	"	7.14	3.9	5.0	16% of α_1		
α_5	"	—	2.13	3.0			H
α_6	"	—	1.06	1.58	33% of α_1		
α_7	"	—	0.3	0.45			H and R
β_6	N_I	0.65	0.22	0.56			
β_2	N_V	12.1	12.1	11.9	20.2	21	J
$\beta_2^{(a)}$	Satellite	—	—	—			
β_2'	"	0.694	0.586	0.50			
β_2''	"	0.64	0.49	0.63			
β_2'''	"	0.48	0.22	0.27			P
β_2^{iv}	"	—	0.14	0.22	52.2% of β_2		
β_2^{v}	"	—	0.10	0.11			
β_2^{vi}	"	—	0.04	0.05			

* J = Jönsson, 1928. Recorded at 10 kv.
H = Hirsh, 1935. Recorded at 20 kv.
H and R = Hirsh and Richtmyer, 1933. Recorded at 20 kv.
P = Pearsall, 1934. Recorded at about 17 kv.

troduce the largest uncertainty, from 2 or 3 percent in most favorable cases and perhaps as much as 700 percent in the cases of the weak satellites, such as β_2'''.

The coefficients of reflection of the crystals had been carefully determined previously.[5] As defined in terms of the second reflection in a two-crystal spectrometer, the coefficient of reflection refers to a partially polarized x-ray beam. According to the theory of crystalline reflection, an unpolarized beam is, upon reflection at 45° ($\lambda=4.28$A with calcite), completely polarized; its intensity is therefore reduced to one-half for this reason alone. With a Bragg angle different from 45° the second reflection increases the polarization by further reducing the relative intensity of the π-component, but the fractional reduction of intensity of the whole beam at the second crystal is much less than at the first crystal. The intensities (calculated, not observed) of the π- and σ- components as reflected from the first and second crystals are given as integrals of $F(l)$ and $\Phi(k)$ functions in an earlier paper.[24] From these integrals and from the definition and units of R, the coefficient of reflection, one may ascertain the approximate correction to the intensity reflected from each crystal for the variation of R with wave-length. The resultant correction for both crystals together, as a reciprocal multiplying factor for each line, is

$$R=R_A\cdot R_B=\delta^2\sec^2\theta_0\csc^2\theta_0 \times\left\{\int_{-\infty}^{\infty}\Phi_\sigma(k)dk+\int_{-\infty}^{\infty}\Phi_\pi(k)dk\right\}D^2E^2, \quad (2)$$

where D is the dispersion factor (reciprocal radians to reciprocal spectral energy units) and E is the ratio of the experimental values of R_B to the calculated values ($E\approx 0.92$). The quantity δ is the unit decrement of the refractive index and θ_0 is the corrected Bragg angle. The $\Phi(k)$ functions include absorption of the x-rays in the crystals.

Until the target absorption and ionization probability corrections have been made the present relative intensity values must be considered as characteristic of the angle between the electron beam and the target face, 60°, the angle of the x-ray beam and target face, 30°, and of the tube voltage, 15 kv. These target and voltage corrections are small for lines whose wave-length separation is small and the present values may, for such lines, be taken as the approximate transition probabilities.

Argon gas at various pressures was used in the ion chamber for most of these studies. Argon is not entirely satisfactory because the K absorption edge occurs at about 3.857A, in the middle of the present wave-length range. To avoid uncertainties in the ion chamber corrections because of this absorption differential and to insure linearity of the intensity recording system for wave-lengths on either side of this absorption edge, a careful calibration was made with air at 2 atmospheres pressure and again with methyl bromide. For accurate studies of certain regions of the entire spectrum, e.g., the β_2 satellites or the $\gamma_{2,3}$ lines, and for accurate wave-length positions or for line widths and shapes, argon was used at a pressure reduced to a minimum as mentioned above; but, for the β_4 line (see Fig. 2) and for the relative intensities of the entire series, the peak intensities of the several "key" lines were taken quickly and consecutively without changing operation of the x-ray tube or the pressure of air (or of methyl bromide) in the ion chamber.

Only qualitative agreement is found between the present relative intensities and those of previous observations, Table III. Air in a point Geiger counter was used by Jönsson to detect the intensity. The photographic method was used in the other cases where comparison can be made, namely, in the measurements of the integrated satellite intensity (integrated over the total structure) by Hirsh, by Hirsh and Richtmyer, and by Mrs. Pearsall.[22]

Widths

Emission lines

The observed full widths at half-maximum intensity of the Ag L series lines are tabulated in Table IV, column four. The widths corrected for the finite resolving power are listed in column five. For strong and nonoverlapping lines the

[24] L. G. Parratt, Phys. Rev. **41**, 561 (1932), Table III. See Compton and Allison, reference 20, p. 725, for simplification of $\Phi(k)$.

uncertainties in the observed widths are about 2 percent; in the corrected widths about 8 (guess) percent. For weak lines appearing in an overlapping multiplet structure the uncertainties may be as large as 100 percent. In the last column are given the corrected widths in electron volts.

The wide variations in the observed line widths, from 3.0 x.u. to 21.5 x.u., is very striking. Similar variations, although somewhat smaller, have been observed before in L series lines, for example, for U(92),[25] for Au(79)[2] and for Pb(82).[26] Jönsson[22] also detected variations in the widths of L series lines; he observed the AgLl line to be 3 times as wide as Ag$L\beta_1$.

No general statements about the shapes of these lines can be made except that, with rare exceptions, the lines are not symmetrical. The asymmetries are given as indices[27] in the third column of Table IV. Note that the steep side, except for the α_1 line, is the long wave-length side of the line instead of the short wave-length side as in the case of asymmetrical $K\alpha_{1,2}$ lines.[28]

[25] J. H. Williams, Phys. Rev. **37**, 1431 (1931).
[26] R. E. Shrader, Phys. Rev. **49**, 644*A* (1936).

Widths of energy levels

The widths of x-ray lines are related in some manner to the widths of the energy levels of the radiating atoms. Of the several factors contributing to the mean lifetimes of the excited

[27] The index of asymmetry is defined as the ratio of that part of the line width on the long wave-length side of the maximum ordinate to that part of the width on the short wave-length side.
[28] L. G. Parratt, Phys. Rev. **50**, 1 (1936), and J. A. Bearden and C. H. Shaw, Phys. Rev. **48**, 18 (1935).

TABLE IV. *Widths of silver L series lines.*

LINE	TRANSITION	INDEX TO ASYMMETRY	OBSERVED WIDTHS (CORRECTED FOR OVERLAPPING) (SECONDS OF ARC)	WIDTHS (CORRECTED FOR RESOLVING POWER AND FOR OVERLAPPING) (X.U.)	ENERGY WIDTHS (CORRECTED) (ELECTRON VOLTS)
β_4	$L_I M_{II}$	0.9	330	7.1	5.9
β_3	M_{III}	1.0	360	7.8	6.6
β_{10}	M_{IV}	—	275	6.3	6.0
β_9	M_V	—	265	5.9	5.6
γ_2	N_{II}	—	400	9.7	11.0
γ_3	N_{III}	—	375	9.0	10.2
$\gamma_{2,3}'$	Satellite	—	?	?	?
$\gamma_{2,3}''$	"	—	?	?	?
η	$L_{II} M_I$	0.9	850	16.9	10.8
β_1	M_{IV}	1.0	155	3.0	2.4
β_1'	Satellite	—	225	5.0	4.0
β_1''	"	—	225	5.0	4.0
β_1'''	"	—	225	5.0	4.0
β_1^{iv}	"	—	225	5.0	4.0
γ_5	N_I	—	410	9.2	8.8
γ_1	N_{IV}	0.8	180	3.9	3.95
γ_1'	Satellite	—	200	4.5	4.5
γ_1''	"	—	200	4.7	4.7
γ_1'''	"	—	300	7.0	7.0
l	$L_{III} M_I$	0.9	1200	21.5	10.7
α_2	M_{IV}	—	162	3.1	2.2
α_1	M_V	1.05	178	3.26	2.34
α_3	Satellite	—	185	3.8	2.8
α_4	"	—	205	4.1	3.0
α_5	"	—	220	4.6	3.3
α_6	"	—	230	4.9	3.5
α_7	"	—	230	4.9	3.5
β_6	N_I	—	455	9.9	8.6
β_2	N_V	0.9	195	4.11	3.72
β_2'	Satellite	—	160	3.5	3.2
β_2''	"	—	235	5.2	4.8
β_2'''	"	—	235	5.2	4.8
β_2^{iv}	"	—	275	6.4	5.9
β_2^{v}	"	—	200	4.7	4.3
β_2^{vi}	"	—	225	5.2	4.8

states involved in the emission of the line, the dominating factors have an energy distribution given by the dispersion equation,

$$I(\nu)d\nu=\frac{\Gamma}{2\pi}\frac{d\nu}{(\nu_0-\nu)^2+(\Gamma/2)^2}, \qquad (3)$$

where Γ is the full width at half-maximum intensity of these factors.[2] An x-ray line emitted by a transition between two energy states, each of whose energy distribution is of the form given by Eq. (3), has a spectral distribution of the same form when Γ is interpreted[2] as the sum of the widths of the two involved states, A and B.

$$\Gamma_{\text{line}}=\Gamma_{A\text{ state}}+\Gamma_{B\text{ state}}. \qquad (4)$$

The simple sum relation of Eq. (4) is a well-known characteristic of the product of two dispersion curves. Γ_A or Γ_B is to be interpreted as a statistical width rather than as the actual width of the energy level or state of any *one* atom. Reciprocity between mean lifetimes of energy states and widths of energy states follows from the uncertainty principle.

With this interpretation of line widths it is apparent that the widths of energy states are of considerable significance: A schematic diagram of widths of energy states, once obtained, may be used to predict widths of emission lines[29] in much the same manner as energy level diagrams are used to predict wave-lengths of lines; and observed widths may be used to check the theory.[29]

There are 15 diagram lines and 13 energy levels; but unfortunately we cannot solve for the 13 unknowns by the method of a simultaneous solution using Eq. (4) because the equations are not independent.

A solution was proposed by Richtmyer, Barnes and Ramberg,[2] which involves an independent determination of one of the energy levels from a measurement of the width of an absorption limit. With the purpose of such a solution in mind the contours of the three AgL absorption limits were recorded. In Fig. 5 is reproduced the contour of the L_{III} absorption region. The amount of "secondary" and "fine" structure[30, 31] is seen to be very large, sufficient indeed to defeat the purpose intended in recording the contour.

Parenthetically, it is interesting to note that this absorption limit contour, Fig. 5, includes, superimposed on the L_{III} absorption state, a series of resonance absorption lines. These absorption lines involve the atomic or optical energy levels for lines lying close to the main absorption edge, and involve the crystal lattice energy levels for the lines farther removed from the main edge. It seems possible that in the near future we shall obtain considerable *precise* information about the outer energy levels or zones in the nongaseous states by the analysis of such accurately recorded curves.[32]

By Eq. (4), the width of the L_{III} state is less than the width of the $L\alpha_1$ emission line by an amount equal to the width of M_V. The corrected

[29] This assumes that we may neglect those width factors whose energy distributions are not of the form of Eq. (3). Such factors, mentioned in an earlier paper (Phys. Rev. **50**, 1 (1936)) on $K\alpha_{1,2}$ lines of elements of lower atomic numbers, are probably present in most if not all x-ray lines and the relative importance of their contributions is probably greater when the shapes of the observed lines are not symmetrical or are not given by Eq. (3). Strictly speaking, this assumption is not justified in the present study and the energy level widths obtained therefrom can have only a qualitative meaning but are certainly of the correct order of magnitude.

[30] Structure within the energy region defined by the minimum ionization potential of the atom (rather, of atom $(Z+1)$) is "fine" structure (Kossel); outside of this energy region is "secondary" structure (Lindsay-Kronig). The minimum ionization potential of Cd(48) is 9 electron volts. Kossel structure is supposed to be characteristic of vapor absorbers; Kronig structure of crystalline absorbers. The type of structure in Fig. 5 close to the L_{III} edge for crystalline silver is both fine and secondary structure and the distinction is of little or no significance.

[31] It is not possible to match this structure with that calculated from Kronig's equation

$$E(n)=((n^2h^2)/8md^2), \quad n^2=\alpha^2+\beta^2+\gamma^2 \qquad (5)$$

(where α, β, γ are Miller indices, d the grating space, m the electronic mass and h Planck's constant) but agreement is not to be expected when one considers (1) that Eq. (5) does not hold for small values of n because in this energy region the electron is not "free"; (2) that we do not know just where on the contour we should take $n=0$; and (3) that we are dealing with the region of the crystal lattice containing an ion (inner, L_{III}, electron missing), the perturbations due to which are not included in the simple theory.

[32] For further treatment of these matters the reader is referred to R. Smoluchowski, Phys. Rev. **50**, 201 (1936); Mott and Jones, *Properties of Metals and Alloys* (Oxford University Press, 1936), pp. 128–131, and references; and, for a systematic study (photographic method) of the L absorption limits of elements neighboring to Ag(47), to Arne Sandstrom, "An Investigation into X-Ray Absorption Spectra," Inaugural Dissertation, Upsala, 1935. See also R. Landshoff, Rev. Sci. Inst. **9**, 143 (1938).

width of the $L\alpha_1$ line is indicated by the length of the arrow near the center of the main edge in Fig. 5. The difficulties in resolving the observed contour into the L_{III} state and the component resonance lines are at this time insurmountable. Similar difficulties are encountered in ascertaining the width of the L_I or the L_{II} state, or, as we shall see presently, of the K state from the contour of the corresponding absorption limit.

Having found no direct solution for state widths, we proceed somewhat arbitrarily to estimate the width of the L_{III} energy state as 2.0 electron volts. From this as a base the widths of all the other energy levels have been calculated. These widths are given in Table V.

A few differences are found in the trends in the widths of the energy states of silver in Table V and of the widths of the energy states of gold, Table V of Richtmyer, Barnes and Ramberg.[2] L_{II} is wider than L_{III} for silver, the reverse is found for gold. The present M_{II} and M_{III} levels are seemingly very narrow in comparison with those of gold. These and other variations between Ag(47) and Au(79) are to be ascribed apparently to variations in the Auger width. Auger widths, sensitive to variations in the electronic architecture of the atoms, have not yet been sufficiently well evaluated for further discussion.

The width of the $K\alpha_1$ line of Ag has been measured by Allison[33] as 0.28 x.u. This width, when corrected for the finite resolving power of the crystals, is about 10 electron volts. We calculate an expected width of 8 electron volts for the silver K state when we assume the width of the L_{III} state to be 2 electron volts. Ross[34] has reported 34 electron volts, uncorrected, or 25 ev, "corrected" for resolving power, for the width of the K absorption limit of silver. In conforming to the present definition of the width of an absorption limit, Ross' corrected measurement is reduced to perhaps 17 ev. The difference between 8 (calculated) and 17 (observed) is apparently to be ascribed to unresolved fine or sub-Kronig structure in the K absorption contour. The fact that irregularities in the AgL_1 contour, involving the same "optical" levels by the selection rules, are found in the present study close to the main absorption edge means that such resonance absorption structure must be present, although as yet undetected, in the K contour also.

Resonance absorption lines are, of course, much less ambiguous when the absorber is a gas, and, indeed, have been recently measured and identified for A(18).[35] Incidentally, the width of each of these resonance lines for argon,

[33] S. K. Allison, Phys. Rev. **44**, 63 (1933).
[34] P. A. Ross, Phys. Rev. **44**, 977 (1933).
[35] Richtmyer and Parratt, Phys. Rev. **53**, 678*A* (1938).

TABLE V. *Widths of x-ray energy states of* Ag(47).

STATE	QUANTUM NUMBERS n	l	WIDTHS OBSERVED (ELECTRON VOLTS)	WIDTHS COMPUTED (ELECTRON VOLTS)	REMARKS
K	1	0	25	8.0	$K\alpha_1-L_{III}$ K limit by Ross; $K\alpha_1$ line by Allison
L_I	2	0	10(?)	5.3	$L_{III}+\beta_9-\alpha_1$, $L_{III}+\beta_{10}-\alpha_2$
L_{II}	2	1	6(?)	2.2	$L_{III}+\eta-l$, $L_{III}+\beta_1-\alpha_2$, $L_{III}+\gamma_5-\beta_6$
L_{III}	2	1	(2.0)	2.0	Basis of interpretation ($\alpha_1=L_{III}+M_V$)
M_I	3	0	—	8.6, 8.7	$\eta-L_{II}$, $l-L_{III}$
M_{II}	3	1	—	0.6	β_4-L_I
M_{III}	3	1	—	1.3	β_3-L_I
M_{IV}	3	2	—	0.2, 0.7, 0.2	β_1-L_{II}, $\beta_{10}-L_I$, α_2-L_{III}
M_V	3	2	—	0.34	α_1-L_{III}
N_I	4	0	—	6.6, 6.6	β_6-L_{III}, γ_5-L_{II}
N_{II}	4	1	—	5.7	γ_2-L_I
N_{III}	4	1	—	4.9	γ_3-L_I
N_{IV}	4	2	—	1.8	γ_1-L_{II}
N_V	4	2	—	1.7	β_2-L_{III}

one of which is very sharp and easily measured, gives directly the width of the K state of argon, the width of the optical level ($4P$) being negligible.

Widths of double ionization energy levels

Following a lead given in a recent paper by Richtmyer and Ramberg,[16] the width of the state, either initial or final, in the emission of a satellite (a double ionization) line may be taken as the sum of the widths of the two states (each of double ionization) involved. We may tentatively use the state widths derived from widths of single ionization lines, as listed in Table V. This is done with the argument that ". . . the absence of a single other electron is not likely to influence materially the probability per unit time that either one of the vacancies will be filled."[16]

As an example, the $L\alpha$ satellites arise from transitions $L_{III}M_{IV,V}$ to $M_{IV,V}M_{IV,V}$, so we may expect the widths of the $L\alpha$ satellite lines for silver to be $2+0.3+0.3+0.3=2.9$ electron volts. Actually, the observed widths of the $L\alpha$ satellite lines are from 2.8 to 3.5 electron volts as listed in Table IV. That the lines α_5, α_6 and α_7 are wider than 2.9 ev may be an indication that the observed contour should be resolved into more component lines than the five in the present analysis. Indeed, the calculations of Richtmyer and Ramberg[16] treat fifteen $L\alpha$ satellite components, transition ($2p3d \rightarrow 3d^2$), of which 8 are fairly intense. Only five components are drawn in the present experimental study because only five pronounced irregularities are present in the observed contour, but if one chose to so interpret the conclusions of the theory, one might sketch under the observed contour all fifteen lines.

The case of the widths of the satellites of $L\beta_2$ is especially interesting. These satellites supposedly arise from the transitions $L_{III}M_{IV,V} \rightarrow N_VM_{IV,V}$: the expected width for the satellites is $2+0.3+1.7+0.3=4.3$ electron volts, using the values in Table V. The observed widths of the $L\beta_2$ satellites are, with the exception of the β_2' line, from 4.8 to 5.9 ev. Here again we might sketch in more components than are indicated in Fig. 4, perhaps as many as the theoretical forty,[16] thereby reducing the widths of all the components to, say, 4.3 ev.

The $L\beta_2'$ satellite line is an unruly one. Surprisingly, this line is *narrower* than its "parent" line $L\beta_2$; the doubly ionized states involved in this satellite emission are longer lived than the singly ionized states which emit $L\beta_2$. No reasonable resolution of the observed contour, Fig. 4, can avert this conclusion. Another resolution, which eliminates β_2^{VI}, and makes β_2''' less wide but asymmetrical (with an index much less than unity) may possibly force the width of β_2' to equal β_2, but the shape of β_2' is then unreasonable. It is perhaps unnecessary to point out that the addition of more components of equal or of less widths serves to *decrease* component widths rather than to increase them.

That the β_2' line is less wide than the parent line β_2 may indicate that the absence of the second electron does materially influence the probability per unit time that the N_V vacancy will be filled. The absence of the second electron may disturb the energy relations of the various electron shells a sufficient amount to materially decrease the sensitive Auger width of N_V. No calculations on this point have been made. No matter what the explanation may be for the narrow β_2' line, one may not use with impunity the sum of the observed widths of singly ionized states to obtain the width of a satellite state; rather, in any given case, one must wait for supporting theoretical calculations. Consequently, in the present status of the investigation, no component satellite line has been assumed in a complex structure on the criterion of satellite widths.

It is quite possible that, while the argument presented above may not be valid in some cases, it may hold in other cases. That the satellites of β_1 are somewhat wider than the "expected" width of 3 ev may indicate either that their background, the side of β_1, has been sketched in too low or that more than four components are really present. Two of the satellites of γ_1 are of the "expected" width but the third, γ_1''', has some 2.5 ev excess width, possibly "evidence" of additional unresolved components.

One would expect the relation to hold best

with the $K\alpha$ satellite states, because the Auger widths in the $L_{II,\,III}$ states are of much less relative importance. Experimentally, the component widths of the $K\alpha_{3,\,4}$ group of satellites vary from 1.5 to 3 times the widths of the "parent" lines for element S(16) to Pd(46),[36] but we do not yet have information about the widths of the single ionization states.

[36] L. G. Parratt, Phys. Rev. **50**, 1 (1936); Shaw and Parratt, Phys. Rev. **50**, 1006 (1936).

JULY 15, 1938 PHYSICAL REVIEW VOLUME 54

The Continuous Absorption Spectrum of Iodine Monochloride in the Ultraviolet

JOHN L. BINDER
Pure Oil Company, Chicago, Illinois

(Received May 27, 1938)

It is shown that the absorption of light in ICl gas follows Beer's law, at least up to the concentrations used here, namely 4×10^{-4} mole/l. The absorption coefficients of ICl were measured at a number of wave-lengths and at several temperatures in the ultraviolet continuous band and the partial absorption coefficients derived from them. The effective amplitude of vibration of the electron producing this band was determined from the absorption coefficient curves. An attempt to measure the dissociation of ICl spectral-photometrically showed that the visible continuous band and the ultraviolet continuous band broadened out at high temperature to completely overlap the continuous ultraviolet band of Cl_2.

INTRODUCTION

As part of a program on the study of the continuous absorption of the halogens, the measurement of the absorption coefficients of ICl was undertaken. The continuous band reported[1] with maximum at 2400A was chosen rather than that in the visible because the iodine absorption on the short wave side is so weak that it can be neglected and the Cl_2 absorption on the long wave side is known. Such is not the case with the visible ICl continuum.

EXPERIMENTAL

The ICl was prepared[2] by mixing atomic proportions of pure solid I_2 and pure liquid Cl_2 in a closed vessel which had been evacuated. Samples for use were withdrawn into evacuated bulbs through "Breakoffskies." The compound was analyzed by titrating weighted amounts with standard $Na_2S_2O_3$ and also by precipitating the silver halides followed by a determination of the Ag in the precipitate. The results of the analyses agreed well and were within 1 percent of the theoretical mole percent values. In subsequent calculations the atomic ratio is taken to be 1 : 1 for this sample.

Since ICl decomposes readily and is very reactive, the quartz absorption cells were filled and the concentration of the gas in them found in the following manner. A weighed bulb of ICl was broken in an evacuated 6 l flask to which the cell was connected. When equilibrium was reached the cell was sealed off and the balance of the ICl frozen into a side tube on the flask which was then sealed off. The amount of ICl in the tube was found by titrating with $Na_2S_2O_3$ and a check obtained by weighing the broken glass of the bulb.

The absorption coefficients were measured by means of photographic photometry. The same type of apparatus and disposition was used as employed by Gibson and Bayliss[3] in the measurement of the absorption coefficients of Cl_2. However, the details of spectral photographic photometry were carried out as discussed by Ornstein, Moll and Burger.[4]

The same procedure of photographing the ICl spectrum and the calibration spectra was em-

[1] Cordes and Sponer, Zeits. f. Physik **63**, 338 (1930).
[2] By Elizabeth P. Baxter.
[3] Gibson and Bayliss, Phys. Rev. **44**, 188 (1933).
[4] Ornstein, Moll and Burger, *Objektive Spektralphotometrie* (Vieweg u. Sohn, Braunschweig 1932).

ployed as Gibson and Bayliss used for Cl_2. The screens used for the calibration spectra, described by Harrison,[5] were calibrated by means of a phototronic cell and microammeter and also by means of a thermopile and galvanometer.

The densities of the ICl spectrum and the calibration spectra were measured by means of a densitometer which was constructed in the laboratory machine shop. The light measuring part consisted of a General Electric PJ 22 photocell, an amplifier with a General Electric FP 54 Pliotron tube in a circuit described by DuBridge and Brown[6] and a high resistance galvanometer. The amplifier was linear over the range used, very stable and extremely sensitive.

From these density measurements and transmissions of the screens, either blackening or density curves were drawn for each wave-length and the ICl transmission at each wave-length was found by interpolating.

The ICl spectrum was photographed with two cells, one 20 cm long and one 10 cm long, filled with different concentrations of gas. The values of the absorption coefficients reported here are the averages of the results obtained from at least two plates for each cell except those at the highest temperature. These values were obtained with one cell.

Since ICl dissociates into I_2 and Cl_2, the usual expression for Beer's law

$$I/I_0 = e^{-\alpha c d}, \qquad (1)$$

where I is the intensity of the light transmitted by the gas, I_0 is the intensity of the incident light, c is the concentration of gas in moles per liter, d is the length of light path in the gas and α is the absorption coefficient, must be modified to take into account the absorption due to I_2 and Cl_2. Since the I_2 absorption in this region at these temperatures is so weak that it can be neglected, the equation for Beer's law becomes

$$I/I_0 = e^{-d(\alpha_1 c_1 + \alpha_2 c_2)}, \qquad (2)$$

where α_1 and c_1 refer to Cl_2 and α_2 and c_2 refer to ICl.

The absorption coefficients of Cl_2 at the temperatures studied were obtained by graphical interpolation from those reported by Gibson and Bayliss. The concentrations of Cl_2 at these temperatures were found from the data of McMorris and Yost[7] on the dissociation constants of ICl. The dissociation of Cl_2 into atoms is negligible at the temperatures studied here.[8]

TABLE I. *Absorption coefficients of* ICl *at various temperatures.*

λ(A)	293°K	387°K	489°K	685°K
3100	2.6	3.1	10.4	28.2
3075	9.5	12.7	16.9	
2994	17.1	19.1	27.1	50.0
2912	32.2	37.5	58.5	
2851	49.2	63.6	74.5	77.8
2804	73.6	84.9	90.5	
2762	97.0	106.9	108.6	112.1
2699	135.8	134.6	138.2	139.5
2644	166.6	164.4	155.5	169.3
2582	205.5	198.2	188.1	184.9
2562	219.1	209.5	193.6	190.6
2537	236.1	224.1	205.4	
2527	242.8	230.8	208.0	
2510	249.8	233.9	210.8	
2501				207.5
2487	255.8	239.9	215.0	
2479	261.5	242.1	217.1	
2465	264.3	245.9	217.8	
2462				212.5
2453	264.3	246.6	221.8	
2440				211.6
2438	264.3	247.6	222.0	
2413	265.0	248.8	222.3	
2406	265.0	248.1	221.7	211.0
2395	259.9	242.8	216.5	
2382				203.6
2370	254.1	234.7	215.9	
2359	240.3	227.3	208.6	
2348				193.5
2337	227.0	214.3	202.6	
2327				185.5
2308	204.1	201.5	190.4	
2289	192.8	183.5	178.1	
2267				166.2
2264	175.6	168.3	162.3	
2245	160.1	155.6	155.4	
2195	119.5	128.8	141.9	148.9
2165	95.9	103.0	113.1	123.2

Considering the errors of the various values used in calculating the absorption coefficients and the errors in the intensity measurements of the ICl, it is thought that these values, except those below 2250A, are accurate to at least 5 percent. The error at the short wave end of the curve is greater, probably about 10 percent, due to greater error in measuring the ICl intensities.

[5] Harrison, J. Opt. Soc. Am. **18**, 492 (1929).
[6] DuBridge and Brown, Rev. Sci. Inst. **4**, 532 (1933).
[7] McMorris and Yost, J. Am. Chem. Soc. **54**, 2247 (1932).
[8] Giauque and Overstreet, J. Am. Chem. Soc. **54**, 1931 (1932).

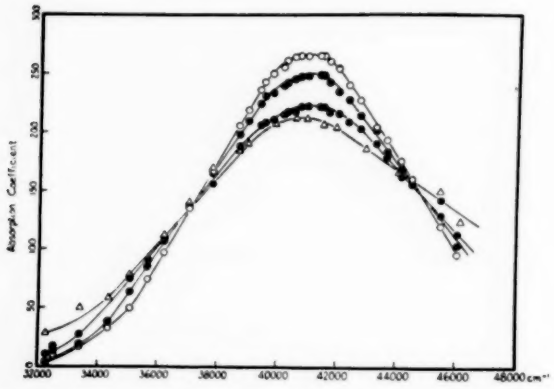

FIG. 1. Absorption coefficients. Open circles are for 293°K; circles with black centers, 387°K; solid circles, 489°K; and triangles, 685°K.

PARTIAL ABSORPTION COEFFICIENTS

As Gibson and Bayliss showed the absorption coefficient may be expressed by

$$\alpha=\frac{(\alpha_0+\alpha_1 e^{-E_1/kT}+\alpha_2 e^{-E_2/kT}\cdots)}{\sum_{v''} e^{-E_{v''}/kT}}, \qquad (3)$$

where α_0, $\alpha_1\cdots$ are partial absorption coefficients and the E's are energies of the various vibrational states. The denominator of this expression was evaluated by using, for the vibrational energy of the ground state of ICl,[9]

$$E/hc=384.6(v''+\tfrac{1}{2})-1.58(v''+\tfrac{1}{2})^2 \qquad (4)$$

and the following values obtained:

Temp.	293°	387°	489°	683°K
$\sum_{v''} e^{-E_{v''}/kT}$	1.183	1.324	1.487	1.820

Assuming the first few vibrational levels of the ground state of ICl to be equally spaced and taking the separation to be $\omega''=378.28$ cm^{-1}, we may write Eq. (3)

$$\alpha S_T=\alpha_0+\alpha_1 x+\alpha_2 x^2+\cdots,$$

where
$$x=e^{-378.28hc/kT}, \qquad (5)$$
$$S_T=\sum_{v''} e^{-E_{v''}/kT}.$$

At each wave-length the smoothed absorption coefficients obtained from Fig. 1 multiplied by the appropriate value of S_T were plotted against X. Extrapolating the curve so obtained to $X=0$, the value of the intercept on the ordinate, gives the value α_0 and the slope of the curve at that point the value α_1. The data are not accurate enough to obtain α_2 by this graphical method.

The values of the partial absorption coefficients α_0 and α_1 obtained in this way are given in Table II and Fig. 2.

EFFECTIVE AMPLITUDE OF VIBRATION

According to Mulliken[10] the effective amplitude of a vibrating electron is given by

$$P/e=0.0619\times10^{-8}\int \alpha_\nu d\nu/\nu,$$

where P is the effective electric moment of the electronic transition, e the electric charge and α_ν the absorption coefficient. If we approximate this integral as he suggests by using the curves of Fig. 1, the following values of P/e are obtained:

Temp.	20°C	114°C	216°C
P/e(CM)	0.0953×10^{-8}	0.0957×10^{-8}	0.0959×10^{-8}

DISSOCIATION CONSTANT OF ICl

An attempt was made to measure the dissociation constant of ICl by measuring the Cl_2 absorption in a cell filled with a large amount of ICl. This proved unsuccessful because it was found that at elevated temperatures the ICl absorption bands overlapped the continuous ultraviolet Cl_2 absorption band on both the long and short wave side of its maximum.

DISCUSSION

In view of the agreement in the results obtained using different concentrations of ICl and different lengths of light path in the gas there is no doubt that the absorption follows Beer's law up to a concentration of 4×10^{-3} mole/l.

The absorption curves show the flattening of the maximum and the broadening of the band with increasing temperature that is customary with such continuous bands. Temperatures high

[9] Jevons, *Report on Band Spectra of Diatomic Molecules*, Phys. Soc. (1932).

[10] Mulliken, Phys. Rev. **46**, 549 (1934).

enough to show two maxima in the absorption curve due to a greater contribution to the absorption of the second vibrational level were not reached. In view of the large dissociation of ICl it is doubtful that this could be done.

This work was done several years ago in the College of Chemistry at the University of California. I wish to acknowledge my indebtedness to Professor G. E. Gibson, who suggested the problem, for his interest and valuable advice.

TABLE II. *Partial absorption coefficients of* ICl.

ν (CM^{-1})	α_0	α_1	ν (CM^{-1})	α_0	α_1
32000	0	0	39500	278.2	6.0
32500	4.75	10.0	40000	297.7	0
33000	11.5	12.5	40500	303.8	0
33500	18.7	15.0	41000	306.5	0
34000	27.2	25.0	41500	304.8	2.5
34500	35.0		42000	295.0	5.0
35000	44.2	80.0	42500	270.0	11.0
35500	55.0	105.0	43000	245.0	25.0
36000	77.2	121.5	43500	219.8	56.5
36500	107.2	110.0	44000	195.0	65.0
37000	134.6	85.0	44500	168.7	80.0
37500	163.7	39.0	45000	144.2	96.5
38000	193.2	24.0	45500	115.0	107.5
38500	219.8	12.0	46000	87.0	117.5
39000	249.0	10.0			

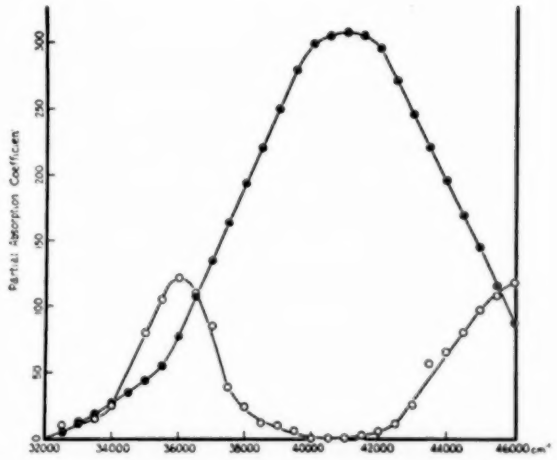

FIG. 2. Partial absorption coefficients. Circles with black centers are for α_0, and open circles for α_1.

The Infra-Red Absorption Spectrum of CD_4

ALVIN H. NIELSEN * AND HARALD H. NIELSEN
Mendenhall Laboratory of Physics, Ohio State University, Columbus, Ohio

(Received May 13, 1938)

The spectrum of CD_4 has been measured from 3.0μ to 10.5μ and three regions of absorption were observed. These bands with centers at 2992.8 cm^{-1}, 3103.7 cm^{-1}, 2259.0 cm^{-1}, and 995.86 cm^{-1} have been identified as $\nu_1+\nu_4$, $\nu_3+\nu_4$, ν_3, and ν_4 by analogy with CH_4. The line spacings obtained from these bands in CD_4 are $\Delta\nu_{\nu_1+\nu_4}=7.17$ cm^{-1}; $\Delta\nu_{\nu_3+\nu_4}=5.01$ cm^{-1}, $\Delta\nu_3=4.52$ cm^{-1}; $\Delta\nu_4=3.42$ cm^{-1} as compared with 5.3 cm^{-1}, 13.5 cm^{-1}, 9.77 cm^{-1} and 5.41 cm^{-1} for the same bands in CH_4. Values for the ζ's of Johnston and Dennison have been obtained and are as follows: $\zeta_3=0.1465$ and $\zeta_4=0.3535$. Utilizing the line spacings given above and the expression $\Delta\nu_3+\Delta\nu_4=3h/8\pi^2A$ derived by Johnston and Dennison the value 1.044×10^{-39} g cm^2 is obtained for the moment of inertia A.

I. INTRODUCTION

RECENT measurements on the infra-red absorption bands due to the spherically symmetrical hydrides of carbon,[1] silicon,[2] and germanium[3] have seemed sufficiently interesting to justify an examination also of the spectra of these molecules where the hydrogen atoms have been replaced by the isotope of mass 2. The deuterium variety of these compounds is in general not easily obtained, but the carbon tetra-deuteride may be prepared simply by allowing aluminum carbide to react with a very pure sample of deuterium oxide. It was found to be necessary to bake out the aluminum carbide for several days, while running a vacuum pump, to drive off all occluded water vapor. This serves to eliminate all the ordinary methane molecules caused by interaction of the carbide with water vapor in the atmosphere.

We wish in this paper to report on measurements which we have made on the spectrum of CD_4 prepared in the manner described above using D_2O of 99.5 percent purity. The purity of the final sample of gas used in these measurements was good enough so that the absorption bands due to even the most likely hybrid methanes remained unobserved.

For our measurements we made use of the same prism-grating spectrometer used by previous investigators working in this laboratory on similar experiments. Two different gratings were required; one ruled with 800 lines per inch for the region near 10.0μ, and another ruled with 3600 lines per inch for the 3.3μ and the 4.4μ regions. The slit widths used in this experiment included spectral intervals of 0.6 cm^{-1}, 0.8 cm^{-1}, 0.6 cm^{-1}, in the regions 3.3μ, 4.4μ, and 10.0μ, respectively. Two absorption cells made of glass tubing fitted with windows of polished rocksalt were used; one two centimeters long and the other ten centimeters long. The former was used for measurements on the fundamental vibrations and the latter on the combination bands. Regions of intense absorption were found at 3.3μ, 4.4μ and 10.0μ and these have been studied in detail.

II. EXPERIMENTAL RESULTS

The 4.4μ region

This region of absorption which corresponds to the 3.3μ band in the spectrum of CH_4 has been identified as ν_3 in Dennison's notation. The measurements for this band are plotted as percent absorption against a scale of frequencies in cm^{-1} and wave-lengths in μ and are shown in Fig. 1. The R branch of this band overlaps with the carbon dioxide fundamental making it impossible, because of atmospheric CO_2, to measure as many lines on this side of the band as in the P branch. Deflections of the galvanometer were made on each setting with the cell in the beam

* Assistant Professor at University of Tennessee, Knoxville.

[1] J. P. Cooley, Astrophys. J. **62**, 73 (1925); A. H. Nielsen and H. H. Nielsen, Phys. Rev. **48**, 864 (1935).

[2] W. B. Steward and H. H. Nielsen, J. Chem. Phys. **2**, 712 (1934); Phys. Rev. **47**, 828 (1935).

[3] W. B. Steward and H. H. Nielsen, Phys. Rev. **48**, 861 (1935).

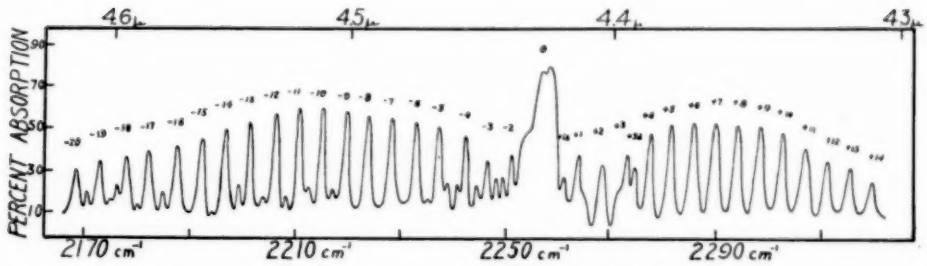

FIG. 1. Curve showing the ν_3 absorption band of CD_4 at 4.4μ.

and then out of the beam so percent absorption could be computed. It is believed that despite the CO_2 the line positions given are quite accurate. Readings were taken at spectral intervals of 0.9 cm^{-1}. Table I gives a list of the observed lines and their frequency positions.

The $\Delta\nu_3$ averaged over the whole band has been computed to be 4.52 cm^{-1} as compared with 9.77 cm^{-1} in CH_4. The center of the band, as determined from these measurements is at 2259.0 cm^{-1}. This value is in good agreement with the Raman spectrum value of 2258.0 cm^{-1} given by MacWood and Urey.[4]

The 10.0μ region

The fundamental vibration ν_4 of CH_4 gives rise to an absorption band near 7.7μ. For CD_4 the vibration ν_4 absorbs in the region of 10.0μ. The appearance of this absorption band as revealed by our measurements is shown in Fig. 2 where again percent absorption is plotted against a scale of frequencies in cm^{-1} and wave-lengths in μ. The deflections of the galvanometer for cell in, and cell out of, the beam were read at intervals of 0.6 cm^{-1}. The center of this band is set at 995.86 cm^{-1} which agrees with the value 987 cm^{-} predicted by Dennison and Johnston.[5] As in the corresponding band in CH_4 the central line or Q branch is extremely broad and converges toward smaller frequencies. Appreciable convergence of the rotational lines in the band is observed. The extreme lines in the P branch have a spacing of about 5.4 cm^{-1} while the extreme ones in the R branch have a spacing of about 2.5 cm^{-1}. From the average of the spacings over the whole band the $\Delta\nu_4$ is about 3.42 cm^{-1} as compared with 5.41 cm^{-1} in CH_4. An immediately obvious difference between this band and the ν_4 in CH_4 is that the lines on the high frequency side do not split up into multiplets. This may be due to the fact that the lines are appreciably closer together and thus more difficult to resolve. On the low frequency side the lines split into multiplets very early. Curve (b) Fig. 2 shows a strong peak observed in the first sample of gas made. This is clearly a Q branch of some hybrid molecule probably CHD_3 since on purification it shrinks and almost disappears as shown in (a) Fig. 2.

Table II lists the lines and their frequency positions numbered much in the same manner as

[4] G. E. MacWood and H. C. Urey, J. Chem. Phys. **4**, 402 (1936).

[5] D. M. Dennison and M. Johnston, Phys. Rev. **47**, 93 (1935).

TABLE I. *Frequencies of the lines in* ν_3.

LINE NO.	ν	LINE NO.	ν	LINE NO.	ν	LINE NO.	ν
+14	2319.2 cm^{-1}	+3a	2274.7 cm^{-1}	− 3	2246.9 cm^{-1}	−13a	2199.3 cm^{-1}
+13	2314.7	+3	2273.5	− 4	2242.3	−14	2196.5
+12	2310.5	+2	2268.7	− 5	2237.6	−15	2192.1
+11	2306.2	+1	2264.2	− 6	2232.9	−16	2187.5
+10	2301.9	+1a	2261.5	− 7	2228.4	−16a	2185.0
+ 9	2298.6	0	2259.0	− 8	2223.9	−17	2182.6
+ 8	2294.5	−1	—	− 9	2219.5	−18	2178.0
+ 7	2290.4	−2	2251.2	−10	2215.0	−19	2173.1
+ 6	2286.0	−2a	2249.5	−11	2210.6	−20	2168.5
+ 5	2282.0	−2b	2248.2	−12	2206.2		
+ 4	2277.9			−13	2201.2		

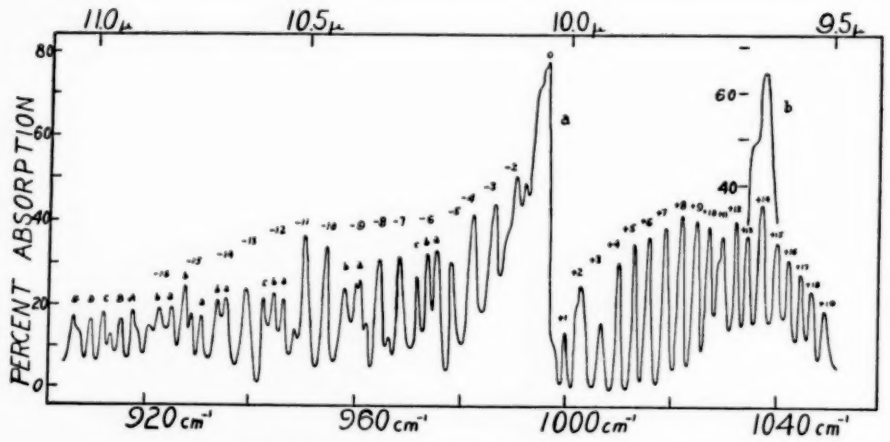

FIG. 2. Curve showing the ν_4 absorption band of CD_4 at 10.0μ.

in the work reported by us on ordinary methane.

The 3.3μ region

The absorption in this spectral region is the result of two overlapping bands identified by analogy from CH_4 as $\nu_1+\nu_4$ and $\nu_3+\nu_4$ with centers at 2992.8 cm^{-1} and 3103.7 cm^{-1}, respectively. The investigation of this region was made difficult by some atmospheric water vapor absorption since this work was done in the summer. Again percent absorption was plotted by taking readings with the cell in the beam and out of the beam. Deflections were taken at intervals on the circle corresponding to 0.9 cm^{-1}. The curve in Fig. 3 shows both bands fairly well resolved and plotted in percent absorption against a scale of frequency in cm^{-1} and wavelength in μ. Although the R branch of $\nu_1+\nu_4$ overlaps with the P branch of $\nu_3+\nu_4$ it is possible to obtain a fair value of the $\Delta\nu$ for each band. The $\Delta\nu_{\nu_1+\nu_4}$ is 7.17 cm^{-1} as compared with $\Delta\nu=5.3$ cm^{-1} for CH_4. The $\Delta\nu_{\nu_3+\nu_4}$ is 5.01 cm^{-1} as compared with 13.5 cm^{-1} for CH_4. The most important lines in these two bands are tabulated with their frequency positions in Table III.

III. Discussion of Results

The theory of the methane molecule taking into account first-order interactions between rotation and vibration has been discussed by Johnston and Dennison.[6] In this discussion they have pointed out that the spacing between rotational lines in a band is in general not related to the actual moment of inertia in any very simple manner. The following equation,

$$\Delta\nu_3+\Delta\nu_4=(2-\zeta_3-\zeta_4)h/4\pi^2A=3h/8\pi^2A$$

derived by them relates the actual moment of

[6] M. Johnston and D. M. Dennison, Phys. Rev. **48**, 868 (1935).

TABLE II. *Frequencies of the lines in ν_4.*

Line no.	ν	Line no.	ν	Line no.	ν	Line no.	ν
+19	1049.08 cm^{-1}	+6	1015.83 cm^{-1}	− 6 a	975.31 cm^{-1}	−14 a	935.20 cm^{-1}
+18	1046.57	+5	1012.59	− 6 b	973.42	−14 b	933.45
+17	1044.38	+4	1009.96	− 6 c	971.79	−15 a	930.97
+16	1042.19	+3	1006.76	− 7	968.83	−15 b	927.77
+15	1040.02	+2	1003.29	− 8	964.56	−16 a	925.08
+14	1036.93	+1	1000.14	− 9 a	960.33	−16 b	922.88
+13	1034.78	0	995.86	− 9 b	958.23	A	917.81
+12	1032.03	−1	—	−10	954.31	B	915.65
+11	1029.60	−2	990.22	−11	950.16	C	912.08
+10	1026.86	−3	986.59	−12 a	946.31	D	909.71
+ 9	1024.47	−4	982.44	−12 b	944.53	E	907.12
+ 8	1021.77	−5	978.04	−12 c	942.75		
+ 7	1018.79			−13	939.21		

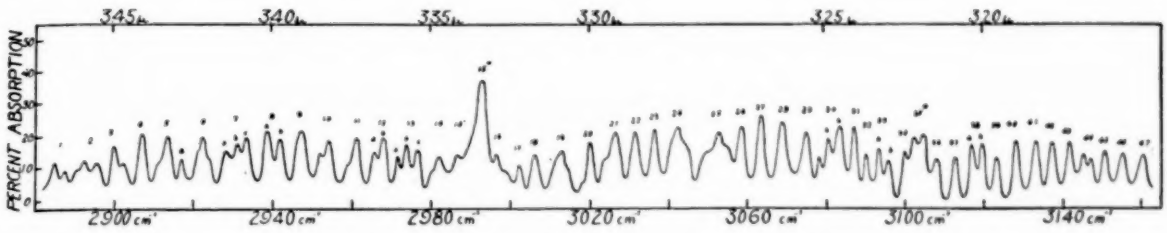

FIG. 3. Curve showing the combination bands $\nu_1+\nu_4$ and $\nu_3+\nu_4$ at 3.3μ.

TABLE III. *Frequencies of lines in $\nu_1+\nu_4$ and $\nu_3+\nu_4$. The lines with asterisks are the Q branches.*

LINE NO.	ν	LINE NO.	ν	LINE NO.	ν	LINE NO.	ν
1	2885.3 cm^{-1}	11	2961.1 cm^{-1}	21	3027.0 cm^{-1}	35*	3103.7 cm^{-1}
2	2894.2	12 *a*	2965.7	22	3031.9	36	3107.5
3	2900.3	12 *b*	2968.1	23	3036.8	37	3112.7
4	2907.5	13 *a*	2971.6	24	3042.9	38 *a*—17.2	3118.5
5	2913.7	13 *b*	2973.9	25	3050.2	38 *b*—19.8	
5*a*	2917.1	13 *c*	2976.9	26	3058.9	39	3123.6
6	2922.7	14	2982.7	27	3063.9	40	3128.2
7 *a*	2928.9	14′	2986.9	28	3069.5	41	3133.4
7 *b*	2931.2	15*	2992.8	29	3075.2	42	3138.0
7 *c*	2933.5	16	2996.4	30 *a*—80.8	3081.9	43	3141.9
8 *a*	2939.2	17	3002.3	30 *b*—84.0		44	3146.5
8 *b*	2942.1	18	3006.5	31	3087.1	45	3150.8
9	2947.8	19	3013.1	32	3090.3	46	3155.7
10	2954.1	20	3020.4	33 *a*—93.5	3094.7	47	3161.0
				33 *b*—96.0			
				34	3099.9		

inertia A to the measurable line spacings in ν_3 and ν_4, and also to the ζ_3 and ζ_4 which represent the magnitudes of an internal angular momentum due to the vibration of the molecule arising from the fact that ν_3 and ν_4 are triply degenerate. Choosing $\Delta\nu_3=4.52$ cm^{-1} and $\Delta\nu_4=3.42$ cm^{-1}, we obtain a value of 1.044×10^{-39} g cm^2 for A, which is about twice the value 5.47×10^{-40} g cm^2 for ordinary methane. It is also possible to calculate the ζ's. Since $\Delta\nu_3=(1-\zeta_3)h/4\pi^2A$ and $\zeta_3+\zeta_4=\frac{1}{2}$ we obtain the values $\zeta_3=0.1465$ and $\zeta_4=0.3535$. The theory further predicts that $\Delta\nu_4$ should be equal to $\Delta\nu_{\nu_1+\nu_4}$, and that $\Delta\nu_{\nu_3+\nu_4}=5h/16\pi^2A$. Experimentally it is found that $\Delta\nu_4=3.42$ cm^{-1} whereas the band $\nu_1+\nu_4$ shows a $\Delta\nu=7.17$ cm^{-1} which is not at all good agreement. An alternate explanation is that this band may be due to CHD_3 which should have a band in this region with a spacing of about 7 cm^{-1}.

Using the relation given by Johnston and Dennison for $\Delta\nu_{\nu_3+\nu_4}$ we obtain a value of 6.52 cm^{-1} as compared with the average value over the whole band of 5.01 cm^{-1}. This is not good agreement but is about as close agreement as was obtained in the case of ordinary methane.

The splitting up of rotation into multiple structure is not accounted for by their theory, but must no doubt be ascribed to interactions of higher order than the first between rotation and vibration.

Spectra of the Monochlorides of Nickel, Cobalt and Iron

KENNETH R. MORE*
Sloane Physics Laboratory, Yale University, New Haven, Connecticut
(Received May 21, 1938)

Emission spectra in the region 3800 to 6000A which are attributed to the molecules NiCl, CoCl, and FeCl have been excited by means of high frequency discharges in silica tubes containing $NiCl_2$ $CoCl_2$, and $FeCl_2$, respectively. Vibrational analyses of four systems of NiCl and three systems of CoCl are given. No regularities were found among the FeCl bands.

INTRODUCTION

EMISSION spectra attributed to the chlorides of iron, cobalt, and nickel were reported by Mesnage[1] in 1935. Mesnage suggests that most of the bands are due to the diatomic chlorides. Many of the bands reported form sequence-like structures. In the case of one group of bands attributed to NiCl Mesnage suggests a provisional assignment of vibrational quantum numbers. This quantum assignment is untenable because it leads to a value of about 1400 cm^{-1} for the ground state vibrational frequency of the NiCl molecule. This value is much too high for a molecule as heavy as NiCl.

In the present investigation the spectra in question were excited in a high frequency discharge and were photographed with a grating which gives much higher dispersion than did the spectrograph used by Mesnage. The data obtained lead to quite a different interpretation of the NiCl spectrum.

EXPERIMENTAL

The spectra under investigation were excited by the passage of a high frequency discharge through a fused silica tube which contained a small amount of $NiCl_2$, $CoCl_2$, or $FeCl_2$. The power was supplied by a radiofrequency oscillator having a two kilowatt power tube. The materials used were of the highest purity obtainable commercially. The silica tube was 1.5 cm in diameter and 25 cm in length. It was provided with external electrodes which were placed 12 cm apart. The discharge tube was evacuated with a Hyvac pump. In order to maintain a suitable pressure of the chloride vapor in the discharge the tube was heated externally by means of a Mecker burner. The tube was pumped while the discharge was in operation in order to prevent the pressure from becoming too high for the passage of the high frequency discharge. This was necessary because chlorine was formed by the dissociation of the triatomic chlorides.

The spectra were photographed in the second order of a 21-foot grating which was in a stigmatic mounting. The dispersion was about 2.5A per mm. Exposure times varied from fifteen minutes to two hours. Iron arc comparison spectra were recorded on all plates. Nickel and cobalt arc spectra were also recorded on the NiCl and CoCl plates, respectively. The latter served for the identification of the nickel and cobalt lines which were excited in the discharge.

DATA

The spectrum of nickel chloride extends from 3900 to 4800A, with the strongest bands in the region 4050 to 4450A. Most of the heads reported by Mesnage are found, together with many others. The bands all degrade to the red. Several groups of strong bands form rather closely spaced sequences. Partially resolved rotational structure extends for a considerable distance from the strong heads.

The cobalt chloride spectrum extends from 3800 to 5700A. As in the case of nickel chloride nearly all the bands reported by Mesnage are found, along with several others. The cobalt chloride bands also degrade to the red. Some of the bands form very closely spaced sequences, while many of the heads are not part of any obvious sequence array. Partially resolved rotational structure is observed in all the bands.

* Sterling Fellow.

[1] P. Mesnage, Comptes rendus **200**, 2072 (1935); **201**, 389 (1935).

Bands of iron chloride are observed in the region 4000 to 6000A. These bands do not resemble the NiCl and CoCl bands in appearance, inasmuch as few distinct heads and no rotational structure are found. Some of the heads degrade to the red, some to the violet, and some do not degrade definitely in either direction. None of the bands form obvious sequence arrays.

Analysis

Nickel chloride

Four prominent groups of heads are arranged in vibrational arrays and a fifth group in a sequence of double heads. The other bands present seem to be single heads, unrelated to the other heads observed. The wave numbers of the four systems analyzed, and the wave numbers of the other bands observed, are given in Tables I and II, respectively. It is found that for all the systems analyzed the $\Delta v=0$ sequence is strong and the $\Delta v=\pm 1, \pm 2$ sequences are weak. The intensity distribution thus follows a rather narrow Condon parabola. In the case of the systems analyzed the strong $\Delta v=0$ sequences consist of single strong heads which are probably Q heads. Weak heads which may be R heads are observed in some cases. For the $\Delta v=\pm 1, \pm 2$ sequences only Q heads are observed. The fifth system, for which only one sequence has been identified, consists of double heads of about equal intensity.

Table I. *Wave numbers of analyzed bands of* NiCl.

v' \ v''	0	1	2	3	4
		System 1			
0	22738.3				
1		22718.2	22302.6	21888.2	
2		23112.8	22697.3	22283.4	21871.3
3		23504.0		22676.3	
		System 2			
0	23222.7				
1		23200.7	22785.3		
2		23593.9	23177.7	22762.8	
3			23567.9	23152.7	22738.3
4					23125.9
5					23511.6
		System 3			
0	24129.6	23712.8			
1		24112.0	23697.6		
2			24094.7		
		System 4			
0	24614.7	24199.6			
1	25012.5	24596.7	24181.8		
2	25406.5	24991.3	24577.5		
3		25382.2	24968.8		

Table II. *Wave numbers of unanalyzed bands of* NiCl.

24417.7	24494.5	21246.1	21747.4
410.7	476.4	237.7	
387.6			
382.8	460.0	230.1	23333.3
359.1			
354.9	21911.0	21639.3	23757.6
331.9			
327.8	890.7	627.1	
305.4	871.3		24214.6
301.5		22289.8	
		283.4	

The Q heads of the four systems analyzed are represented by the following equations:

$$\nu=22747.6+400.2u'-1.35u'^2 \\ -419.2u''+0.88u''^2, \quad (1)$$

$$\nu=23232.7+397.3u'-1.18u'^2 \\ -417.2u''+0.35u''^2, \quad (2)$$

$$\nu=24138.5+401.3u'-1.05u'^2 \\ -419.2u''+1.20u''^2, \quad (3)$$

$$\nu=24623.2+400.7u'-1.58u'^2 \\ -416.6u''+0.55u''^2, \quad (4)$$

where $u=v+\frac{1}{2}$.

The electronic interval 484 cm^{-1} occurs between system 1 and system 2, and also between system 3 and system 4. This equality of intervals suggests that these systems arise from transitions involving a common doublet term. It is probable that this common doublet state is the ground state. If this is the case the two doublet systems arise from transitions to the ground state from two upper states which are either single or have practically the same electronic doubling.

The vibrational constants also suggest that systems 1 and 3 have a common lower state, as have systems 2 and 4. With this interpretation 1 and 2 must have a common upper state, and also 3 and 4, if the upper states are single. The differences between the vibrational constants which should thus be equal are within the limits to be expected because the constants are derived from head data. In the case of systems for which the frequencies of the upper and lower state are nearly equal, the use of head data instead of origin data reduces the accuracy with which the constants may be determined. It has already been pointed out that the upper states may be

electronic doublets with nearly equal splittings. In this case 1 and 2, and also 3 and 4, do not have common initial levels. The upper state vibrational frequencies are thus not necessarily equal.

A vibrational isotope effect due to the chlorine isotopes is found in only a few cases, probably because of the weakness of the bands for which the effect should be appreciable and because of the blending of weak heads with rotational structure. No isotope effect due to the nickel isotopes is observed.

The bands discussed are all attributed to the diatomic NiCl molecule. The appearance and arrangement of the bands support this interpretation. The observation of strong line spectra of Ni I and Cl I and only a very weak spectrum of molecular chlorine indicates that the high frequency discharge produces a considerable amount of complete dissociation of the $NiCl_2$ into atomic fragments. Under such conditions of excitation it is probable that the bands observed are due to the diatomic molecule NiCl rather than to the triatomic molecule $NiCl_2$. It is of course possible that some of the bands are due to impurities in the compounds used, but none of them have been identified as being due to any known spectrum. The partially resolved rotational structure has the same appearance in all the bands, indicating that all are due to the same molecule.

Since the low lying terms of Ni I are $3d^84s^2$, ^3F and $3d^94s$, ^3D, and the ground state term of Cl I is $3p^5$, ^2P, any Λ value from zero to four is possible for the ground state of the NiCl molecule. The multiplicity may be either doublet or quartet, with doublet the more probable. If the excited states of the NiCl molecule are built by the combination of a Cl I atom in the ground state with a Ni I atom in an excited state, as is probable, doublet terms of Λ values from zero to five are possible, together with terms of higher multiplicity.

A doublet interval of the order of 484 cm^{-1} in the ground state is reasonable for a $^2\Pi$ state, considering the multiplet splittings of the ground states of Ni I and Cl I. It is moreover a rather high value for a $^2\Delta$ or $^2\Phi$ state. Hence it is probable that the ground state of NiCl is $^2\Pi$. The two upper states involved in the four systems analyzed may have either negligible electronic doublet intervals or nearly identical intervals which

TABLE III. *Wave numbers of analyzed bands of* CoCl.

v' \ v''	0	1	2	3	4	5	6
				System 1			
0	22014.0						
1	22432.5	22012.0					
2		22426.9	22008.9				
3		22840.0		22005.5			
4			22832.6	22416.4	22001.2	21587.4	21174.8
5				22825.1	22408.4	21994.2	21581.4
6					22814.8	22401.0	21988.1
				System 2			
0	22402.7	21984.0	21565.6				
1		22398.8	21980.6	21562.9			
2		22812.6	22394.1	21976.5	21559.3		
3				22388.0	21971.2		
4				22798.1		21966.6	
				System 3			
0	22966.2	22546.2					
1	23383.4	22964.1					
2	23795.5	23378.0	22961.5				
3		23786.9	23371.8	22956.7			
4			23777.3	23362.1	22951.1		
5					23354.6		
6					23755.5	23347.5	

TABLE IV. *Wave numbers of unanalyzed bands of* CoCl.

22074.9	22182.4	23497.2	26079.5

are not zero. If the first is the case the terms are probably $^2\Sigma$, though a $^2\Delta$ term might have a negligible doublet interval. The appearance of the bands, with strong Q and very weak R heads, indicates transitions of the type $^2\Sigma \rightarrow {}^2\Pi$ or $^2\Delta \rightarrow {}^2\Pi$. The fact that slightly different values of ω are found for the apparently common upper state in both cases suggests that the upper terms may be $^2\Delta$, with different values of ω for the two members of a given doublet term. This evidence is not conclusive, however, because the observed differences in the ω' values may be due entirely to the errors which may arise when band head data are used. The fifth system mentioned has double heads of about equal intensity. This has the appearance of a $^2\Pi \rightarrow {}^2\Pi$ transition. If this is so only one member of the doublet is observed. The other bands reported are weaker than those discussed and do not fit any vibrational array. These unrelated bands suggest the existence of several excited electronic states of the NiCl molecule.

Cobalt chloride

The three groups of bands which form closely spaced sequences are fitted to vibrational arrays which are given in Table III. Each band in these arrays consists of a single head. The cobalt

chloride bands for which no analysis is made are given in Table IV. These bands seem to be single with no sequence structure like that which is so prominent in the case of the other bands. The heads of the three systems analyzed are given by the following equations:

$$\nu = 22014.6 + 420.0u' - 1.14u'^2 - 421.2u'' + 0.74u''^2, \quad (1)$$

$$\nu = 22404.3 + 416.6u' - 0.82u'^2 - 419.4u'' + 0.28u''^2, \quad (2)$$

$$\nu = 22967.3 + 420.0u' - 1.66u'^2 - 421.8u'' + 1.34u''^2, \quad (3)$$

where $u = v + \frac{1}{2}$.

The ground state electronic term of the CoCl molecule is probably a triplet with a Λ value of 0, 1, 2, 3, or 4, because the ground state of Co I is $3d^7 4s^2$, ^4F. Terms of singlet, triplet, and higher multiplicities are possible for the excited states of CoCl. No obvious electronic multiplets are observed in the spectrum. The three systems analyzed may be members of an electronic triplet, with intervals of 390 and 563 cm^{-1}. Usually the two intervals in a molecular triplet are more nearly equal than are these.

Iron chloride

On account of the absence of distinct heads in the spectrum of FeCl attempts at analysis have failed. It is probable that the lack of heads indicates that the rotational constants of the upper and lower states are nearly equal, while the lack of sequence structure suggests that the vibrational constants are also nearly equal. The fact that this equality is indicated for both the rotational and vibrational constants is consistent with the Mecke rule. In cases where the vibrational constants are nearly equal the bands for Δv not zero are usually weak. It is thus likely that the FeCl bands for which Δv is not zero are weak as well as diffuse, and are readily masked by other bands.

Discussion

It is of interest to compare the vibrational frequencies of the monochlorides of the elements of the first transition group of the periodic table. The frequencies are now known for TiCl,[2] CoCl, NiCl, and CuCl,[3] being 456, 421, 418, and 417 cm^{-1} respectively for the ground states. In addition the bands of TiCl degrade to the violet while the bands of CoCl, NiCl, and CuCl degrade to the red. The differences between the lower and upper state frequencies are approximately -47, $+3$, $+18$, and $+20$ cm^{-1} for TiCl, CoCl, NiCl, and CuCl, respectively. The difference is called positive if ω'' is greater than ω'. This trend indicates that ω' and ω'' may well be nearly equal for the FeCl molecule, since Fe is the element immediately preceding Co in the periodic table.

The decrease in the ground state frequency from the 456 cm^{-1} value for TiCl to the 418 cm^{-1} value for NiCl is greater than that expected from the mass change alone. It is thus evident that the force constant of the molecule must decrease somewhat with the addition of electrons to the incomplete $3d$ shell.

In conclusion the author wishes to express his appreciation to Professor W. W. Watson for stimulating discussions of this work.

[2] K. R. More and A. H. Parker, Phys. Rev. **52**, 1150 (1937).
[3] R. Ritschl, Zeits. f. Physik **42**, 172 (1927).

Mean Absorption and Equivalent Absorption Coefficient of a Band Spectrum

WALTER M. ELSASSER
California Institute of Technology, Pasadena, California

(Received May 23, 1938)

The note deals with the absorption of a band in which the lines have the dispersion form; the effect of the overlapping of neighboring lines upon the absorption is taken into account. The analytical problem can be solved for a periodic pattern of lines with equal intensity S, width 2α and distance d from each other. Simple expressions are derived for the limiting cases of small α/d (formula (8)) and large α/d. In the latter case the transmission by a layer of thickness x is given by

$$I = I_0 e^{-(Sx/d)\tanh(2\pi\alpha/d)}.$$

It appears that this formula gives a fairly good mean approximation even for small values of α/d, while the true transmission in this case is not exponential. It is shown that in problems of radiative transfer and radiative equilibria this approximate formula for the transmission can be used; *i.e.* the factor of x in the above exponent may be substituted in the equations of transfer as equivalent of a mean absorption coefficient.

THE theory of the absorption of spectral lines has been the object of extensive investigations.[1] The theory of infra-red band lines especially was developed by Dennison[2] and a comparison of the experimental and theoretical absorption of such bands has been carried out by Matheson.[3] It has also been directly proved in various cases[3, 4] that these lines have the dispersion form required by the theory of collision broadening. In these investigations it was assumed that the effect of the overlapping of neighboring lines is negligible, or the absorbing layers were chosen so thin that this condition was practically fulfilled. We want here to develop an elementary theory of the effects produced by the overlapping of lines in the absorption by layers of considerable thickness. This includes as a limiting case the transition from line absorption into continuous absorption when the line distance becomes smaller than the line width. Although the model considered here is somewhat too simplified to be directly applicable to the absorption of real band spectra, we are able to draw some interesting conclusions from it. The main difficulty of band spectra absorption lies in the fact that the *mean* absorption is not, in general, of the exponential type, $I = I_0 e^{-kx}$. (As frequently expressed in the older literature, the absorption does not follow Beer's law.) This introduces many mathematical complications, especially in problems of radiative energy transfer and radiative equilibria. Band spectra play a great role in terrestrial and stellar radiation transfer; for instance the radiative heat transfer in the earth's atmosphere takes place within two water bands and a CO_2 band. In this connection it seemed of particular interest to investigate the possibility of replacing the rapidly oscillating absorption coefficient of a band by a mean coefficient which only depends upon the much slower variation of the total line intensity from line to line. For numerous radiative transfer problems this yields a good approximation, as we shall see.

We shall confine our calculations to the case of lines which have the familiar dispersion form, as for instance that produced by collision broadening. The absorption coefficient for the individual line as function of the frequency has then the form

$$k(\nu) = \frac{S\alpha/\pi}{(\nu-\nu_0)^2+\alpha^2}, \tag{1}$$

where 2α is the width and S the total line intensity $\int k d\nu$. The amount of radiation, say Q, absorbed in a layer of optical thickness x is given by

$$Q = I_0 \int_{-\infty}^{+\infty} (1 - e^{-k(\nu)x}) d\nu,$$

where I_0 is the incident intensity. Now if x is very small, Q will of course be proportional to the total line intensity S. As soon as x becomes

[1] Ladenburg and Reiche, Ann. d. Physik **42**, 181 (1913); a comprehensive treatment in Max Born's treatise *Optik*.
[2] D. M. Dennison, Phys. Rev. **31**, 503 (1928).
[3] L. A. Matheson, Phys. Rev. **40**, 813 (1932).
[4] H. Becker, Zeits. f. Physik **59**, 601 (1929).

somewhat larger, the absorption will be complete in the core of the line while the amount of radiation absorbed in the wings still increases with increasing x. It can be shown that in this case a good approximation is obtained by neglecting α^2 in the denominator of (1). The integration can then readily be carried out and yields the result

$$Q=2(S\alpha x)^{\frac{1}{2}}I_0, \tag{2}$$

the absorption being proportional to the square root of the line intensity and the optical thickness. The formula must obviously be valid in a band spectrum provided the line width is small compared to the distance of successive lines and provided the fraction of radiation absorbed is small compared to unity so that the overlapping of the lines is negligible. Formula (2) has been verified experimentally in numerous instances.

We proceed now to the general case for which the width is not small compared to the line distance. In order to have a problem that is accessible to analytical treatment we shall consider an infinite sequence of lines, all having the same intensity S and a constant distance d from each other. Then the absorption coefficient is

$$k(\nu)=\sum_{n=-\infty}^{n=+\infty}\frac{S\alpha/\pi}{(\nu-nd)^2+\alpha^2}. \tag{3}$$

To evaluate the sum we note that (3) is an analytic function of ν which has single poles at the points $\nu=nd\pm i\alpha$. It is well known that under certain restrictions an analytic function $f(z)$ which has only single poles can be expanded in a sum of rational fractions corresponding to these poles[5] (Mittag-Leffler's theorem). If a_1, $a_2\cdots$ are the poles and b_1, $b_2\cdots$ the corresponding residues we have

$$f(z)=f(0)+\sum b_n\left(\frac{1}{z-a_n}+\frac{1}{a_n}\right).$$

By virtue of this theorem (3) may be written

$$k=(iS/2d)[\cot(\tau+i\beta)-\cot(\tau-i\beta)]$$

where

$$\tau=\pi\nu/d,\quad \beta=\pi\alpha/d. \tag{4}$$

[5] Whittaker-Watson, ch.7.4.

We may write instead of this

$$k=\frac{S}{2d}\cdot\frac{\sinh 2\beta}{\sin(\tau+i\beta)\sin(\tau-i\beta)}$$

$$=\frac{S}{d}\cdot\frac{\sinh 2\beta}{\cosh 2\beta-\cos 2\tau}. \tag{5}$$

If we introduce the mean fractional transmission $T=I/I_0$, we have

$$T=\frac{1}{\pi}\int_0^{\pi}e^{-k(\tau)x}d\tau. \tag{6}$$

Before evaluating (6) for the general case we shall consider the limits of small and of large β.

1. Small β

Here we have from (5)

$$kx=S\beta x/d\sin^2\tau=C/\sin^2\tau. \tag{7}$$

Substituting into (6) and introducing $1/\sin^2\tau=y$ as integration variable we get

$$T=\frac{1}{\pi}\int_1^{\infty}e^{-Cy}\frac{dy}{y(y-1)^{\frac{1}{2}}}.$$

It follows that

$$-\frac{dT}{dC}=\frac{1}{\pi}\int_1^{\infty}e^{-Cy}\frac{dy}{(y-1)^{\frac{1}{2}}}=\frac{e^{-C}}{\pi}\int_0^{\infty}\frac{e^{-Cz}}{Z^{\frac{1}{2}}}dz=\frac{e^{-C}}{(\pi C)^{\frac{1}{2}}}.$$

Integrating with respect to C we find

$$T=-\frac{1}{\pi^{\frac{1}{2}}}\int^{C}e^{-C}\frac{dC}{C^{\frac{1}{2}}}=\frac{2}{\pi^{\frac{1}{2}}}\int_{C^{\frac{1}{2}}}e^{-u^2}du.$$

The upper limit of the last integral has to be chosen so that $T=1$ for $C=0$, which shows that the limit is $+\infty$. If therefore ϕ designates as usual the probability integral, we have by (4) and (7)

$$T=1-\phi((\pi S\alpha x)^{\frac{1}{2}}/d). \tag{8}$$

For small values of x this becomes equivalent to formula (2).

2. Large β

In this case we have from the second expression (5)

$$k=(S/d)\tanh 2\beta\cdot(1+\cos 2\tau/\cosh 2\beta).$$

Substituting in (6) we obtain

$$T=\frac{1}{2\pi}e^{-(Sx/d)\tanh 2\beta}\times\int_0^{2\pi}e^{-(Sx/d)\cdot\tanh 2\beta\cdot\cos 2\tau/\cosh 2\beta}d(2\tau)$$

$$=e^{-(Sx/d)\tanh 2\beta}J_0(i(Sx/d)\tanh 2\beta/\cosh 2\beta)$$

J_0 is the Bessel function of order zero and its argument is purely imaginary. Now $J_0(0)=1$ and the function increases at first extremely slowly with increasing imaginary argument, e.g. $J_0(1)=1.27$. The argument of the Bessel function is smaller than the argument of the exponential by a factor $1/\cosh 2\beta$. Furthermore the exponential decreases more rapidly with increasing argument than the Bessel function increases. The degree of approximation remains therefore almost unaffected by putting the Bessel function equal to unity throughout and writing

$$T=e^{-(Sx/d)\tanh(2\pi\alpha/d)}. \tag{9}$$

According to the derivation (9) is valid for large values of α/d. It appears however that it yields a fair degree of approximation for all other values of α/d. If for instance we make α/d small we have

$$T=e^{-2\pi S\alpha x/d}. \tag{10}$$

In order to compare this with formula (8) which is the correct expression for small α/d the functions e^{-2x} and $1-\phi(\sqrt{x})$ have been plotted together in Fig. 1. For thin layers where the square root formula (2) for the absorption is valid, (10) would of course be a poor approximation. It is seen however that for values of T which are not too close to unity or to zero the two curves do not differ largely from each other. Since this is true for small values of α/d, it will hold *a fortiori* for intermediate values of this quantity.

3. The intermediate case

In order to reduce (6) to a more convenient form in the general case, we introduce a new integration variable u by $k=Su/d$. From (5) we have then

$$T=\frac{1}{2\pi}\oint\frac{e^{-Sxu/d}\cdot du}{u(2u\coth 2\beta-u^2-1)^{\frac{1}{2}}},$$

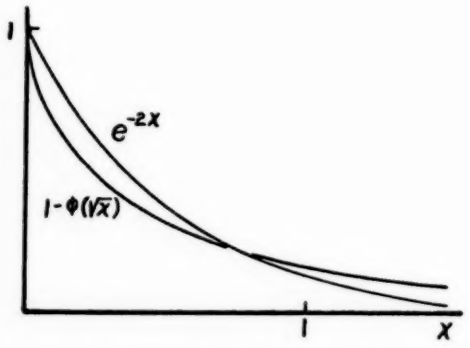

FIG. 1.

where the path of integration may conveniently be taken as a closed loop encircling the two singularities which arise from the zeros of the root ($u=\tanh\beta$ and $u=\coth\beta$, respectively). We introduce the abbreviation $A=Sx/d$. Differentiating with respect to A and introducing a variable v by $u=(v+\cosh 2\beta)/\sinh 2\beta$ we have

$$-\frac{dT}{dA}=\frac{1}{\pi}e^{-A\coth 2\beta}\int_{-1}^{+1}\frac{e^{-Av/\sinh 2\beta}}{(1-v^2)^{\frac{1}{2}}}dv$$

$$=e^{-A\coth 2\beta}J_0\left(\frac{iA}{\sinh 2\beta}\right)$$

by a well-known integral representation of the Bessel functions. Integrating the last equation with respect to A we obtain finally

$$T=\int_{Sx/d}^{\infty}e^{-A\coth 2\beta}J_0\left(\frac{iA}{\sinh 2\beta}\right)dA, \tag{11}$$

where the upper limit is again chosen so that $T=1$ for $x=\infty$. There seems to be no means of reducing (11) further in terms of elementary functions. The Bessel function can be replaced by its power series for small values of its argument and by its asymptotic expansion for large values of the argument; in both cases with two or three terms a good approximation is obtained.

Application

If the above formulae are to be applied to the absorption of band spectra, it must be remembered that the intensity of successive band lines decreases in most cases rather rapidly toward the edge of a band. This decrease is exponential and

is therefore much faster than the decrease of intensity in the wings of an individual line. The strong lines in the center of a band will therefore give rise to a continuous background at the edges of the band and with sufficient thickness of the absorbing layer the background may become comparable in intensity and may even become much stronger than the outer band lines themselves.[6]

We can now apply the above calculations to the problem of radiative transfer. The fundamental equation of transfer is

$$dI/dx = -kI + E, \tag{12}$$

where x is the optical thickness and E is the emissive power of the substance. The equation expresses the obvious fact that the change in intensity I of a beam when passing through an infinitesimal slab is equal to the emission minus the absorption of the slab. I, E, k will in general be functions of the thickness x, of the frequency ν and of the direction of the beam. It is obviously not permissible to carry out an average with respect to ν for each individual quantity in (12). If nevertheless we want to simplify the problem by calculating from the outset with an average value of k which is only slowly variable with frequency, we must determine the degree of approximation of such a procedure. A natural definition of an average absorption coefficient may be obtained in the following way. To each value of the absorption coefficient there corresponds a mean free path of the light which is obviously proportional to k^{-1}. We may define an equivalent mean absorption coefficient, say k', by the condition that the mean free path averaged over a spectral interval be equal to the mean free path resulting from the equivalent absorption coefficient k'. Thus

$$(k')^{-1} = [k^{-1}]_{Av} \tag{13}$$

and substituting the expression (5) for k

$$k' = (S/d) \tanh (2\pi\alpha/d).$$

This is precisely the absorption coefficient as derived above in the approximation formula (9).

The introduction of a mean free path has a good sense under physical conditions where the radiation will undergo a large number of absorption and emission processes before leaving the medium in which (12) is valid. The medium is then very *opaque*. If the opacity is high, the left hand side of (12) is small compared to each of the two terms on the right hand side. The solution of (12) can be found by a perturbation method;[7] the first terms are:

$$I = \frac{E}{k} - \frac{1}{k}\frac{d}{dx}\left(\frac{E}{k}\right) + \cdots. \tag{14}$$

Now, by Kirchhoff's law, E/k is nothing but the black-body radiation and it varies therefore only slowly with frequency. If (14) is averaged over a small frequency interval which however may contain several spectral lines, the equivalent mean absorption coefficient is just given by (13) provided E/k is kept constant in the averaging. The introduction of the equivalent absorption coefficient as defined above is therefore justified if the transmitting medium is sufficiently opaque.

[6] An example given by W. M. Elsasser, Phys. Rev. **53**, 768 (1938).

[7] E. A. Milne, *Handbuch der Astrophysik*, vol. 3, ch.2c.

The Theory of Excitation Functions on the Basis of the Many-Body Model

E. J. KONOPINSKI* AND H. A. BETHE
Cornell University, Ithaca, New York

(Received May 31, 1938)

The theory of transmutation functions for charged particles is examined in the light of recent developments in nuclear theory. It is found that ignoring all factors besides the penetrability of the incident particle is justifiable only for processes without effective competition. For these, the usual applications of the Gamow-Condon-Gurney theory must be modified to include the influence of incident particles with nonvanishing orbital momentum which causes a continued rise of the yield for energies greater than the Coulomb barrier. For processes subject to effective competition, the comparative density of residual states available to each alternative process is important in determining relative yields. The densities of the states are calculated on the basis of the liquid drop model for the nucleus and a table is obtained giving the relative probabilities of neutron and charged particle emissions. The overwhelming factor in favor of neutron emission by heavy nuclei seems to be confirmed by experiment. The shape of an excitation curve expected for the less probable of two processes is shown. Finally the effect of selection rules in the yield curves of reactions involving very light nuclei is considered. Special cases are discussed.

§1. INTRODUCTION

HERETOFORE, attempts to explain the variation of the yield from charged particle disintegrations as a function of the bombarding energy were largely limited to applications of the simple Gamow-Condon-Gurney (G-C-G) theory to the penetration of nuclear potential barriers by incoming particles. This was done with the hope that other factors, lumped together under the title "internal disintegration probability," would be comparatively unimportant in determining the variation. The development of the Bohr-Breit-Wigner theory of nuclear processes has made it clearer what some of the other factors are and encourages an attempt to evaluate their effects. The quantitative results of such an attempt must for the present remain very uncertain. However, they will show to what extent the neglect of influences other than that of the simple penetrability are justified.

When the penetration probability of the incoming particle is alone considered to vary with the energy in the evaluation of the excitation function for a given process, it is being assumed: first, that the probability of the nucleus' and particle's sticking together after the penetration does not depend importantly upon the energy, and secondly, that the formation of the compound nucleus itself guarantees the completion of the process. No improvement can be made on the first assumption until a more workable model of the nucleus presents itself. The second assumption is justified only if the completion of the process in question involves a type of emission which is much more probable than any other way in which the compound nucleus may disintegrate. Our evaluation of the excitation functions for such cases, presented in §4, differs from the usual procedure in one respect: The contributions of incident particles having orbital momenta other than zero are taken into account. When the process being considered meets with effective competition from other possible modes of disintegration of the same compound nucleus, the relative densities of the final states available to each process have an important effect on the excitation functions. This point is discussed in §5, for heavy nuclei. In §6, we treat the effect of selection rules, which have practical importance for very light nuclei.

The consideration of other influences besides the penetrability by particles making direct hits has a particularly important bearing on the deduction of nuclear radii from transmutation functions. It has been the practice to assume that the height of the Coulomb barrier of a nucleus is equal to the energy at which the yield reaches a maximum; such a behavior is expected on the basis of the "simple" ($l=0$) G-C-G theory. The practice is not justified, since it is now clear that the yield continues to rise rapidly beyond the barrier height energy because of the increasing contributions from particles having high orbital momenta and in some cases also because of the

* National Research Fellow.

greater density of available final states at higher excitations. (Fig. 3.)

§2. General Formulation

Most of the effects considered in this paper will be discussed in terms of a formulation which conveniently represents the Bohr picture and which may be derived either by the simple statistical method used in papers of Weisskopf[1] and Bethe[2] or by averaging the Breit-Wigner "dispersion" formula over the resonances in the neighborhood of the energy of the compound nucleus formed in the process. One obtains by the latter method (see I, Eq. (405)) for the cross section of a process in which a nucleus A is bombarded by particles P and from which there results the emission of a particle Q and the formation of a residual nucleus B:

$$(\sigma^{Ppi}{}_{Qq i'})_{\text{Av}}=\frac{2\pi^2\lambda\!\!\!^{-}{}_P{}^2}{(2i+1)(2s+1)} \times\sum_{Jlj l'j'}(2J+1)\left(\frac{\Gamma^J{}_{Pplj}\Gamma^J{}_{Qql'j'}}{\Gamma_J D_J}\right)_{\text{Av}}. \quad (1)$$

$2\pi\lambda\!\!\!^{-}{}_P$ is the de Broglie wave-length of P. $\Gamma^J{}_{Pplj}$ is a partial width of the compound nuclear level, corresponding to the emission of particles P having an energy denoted by p and orbital and total angular momenta l and j. $\Gamma^J{}_{Qql'j'}$ is a corresponding quantity for particles of kind Q. Γ_J is the *total* width of the level, i.e.,

$$\Gamma_J=\sum_{Q'q'}\Gamma^J{}_{Q'q'}=\sum_{Q'q'l''j''}\Gamma^J{}_{Q'q'l''j''}. \quad (2)$$

D_J is the average spacing of the levels of angular momentum J in the neighborhood of the compound level formed. i, s, J, i' and s' are the respective spins of A, P, C, B and Q in the states concerned.

When (1) is summed over all possible emission processes Qq, one obtains

$$\sigma^{Ppi}{}_C=\frac{2\pi^2\lambda\!\!\!^{-}{}_P{}^2}{(2i+1)(2s+1)}\sum_{Jlj}(2J+1)\frac{\Gamma^J{}_{Pplj}}{D_J}. \quad (3)$$

This must be the cross section for the formation of the compound nucleus since it must disintegrate in *some* way. At very high energies of the incident particle, classical concepts should hold, and $\sigma^{Ppi}{}_C$ must equal the geometrical cross section, πR^2, multiplied by the "sticking probability" ξ_{Pp} of P to A, i.e.,

$$\sigma^{Ppi}{}_C=\pi R^2\xi_{Pp} \quad \text{for} \quad \lambda\!\!\!^{-}{}_P\ll R. \quad (4)$$

It will be useful to extend the definition of the sticking probability to low energies. That will be done by assuming:

(1) For a given l, the probability of each j and J is given by the statistical weights, i.e.

$$\sigma^{Pplj}{}_J=(2J+1)/(2i+1)(2s+1)(2l+1)\cdot\sigma_{Pp\bar{l}}. \quad (5)$$

(2) The cross section for each l, σ_{Ppl}, is proportional to the statistical factor, $2l+1$, multiplied with the penetrability P_l of the barrier for particles of that orbital momentum,[3] i.e.,

$$\sigma^{Ppi}{}_C=c\sum_l(2l+1)P_l=cR^2/\lambda\!\!\!^{-}{}_P{}^2=\pi R^2\xi_{Pp} \quad (6)$$

(see (4) and §3, (13c)). Then, comparing (3), (5) and (6) we have

$$\sigma^{Pplj}{}_J=\frac{(2J+1)}{(2i+1)(2s+1)}\pi\lambda\!\!\!^{-}{}^2{}_P\xi_{Pp}P_l =\frac{(2J+1)}{(2i+1)(2s+1)}2\pi^2\lambda\!\!\!^{-}{}^2{}_P\frac{\Gamma^J{}_{Pplj}}{D_J},$$

from which

$$\xi_{Pp}=2\pi\Gamma^J{}_{Pplj}/D_JP_l. \quad (7)$$

This definition of the sticking probability from "correspondence" will be regarded as valid for all energies. It makes ξ nearly independent of energy since the penetrability factor is divided out from Γ and probably the "width without barrier" varies with the energy in about the same way as

[1] Weisskopf, Phys. Rev. **52**, 295 (1937).
[2] Bethe, Rev. Mod. Phys. **9**, 69 (1937). This reference will hereafter be denoted by "I".

[3] This is equivalent to assuming that the formation probability is proportional to the influx of particles, which is appropriate for a sticking probability near unity. If proportionality to the density of the particle wave function near the nucleus had been used instead of just the penetrability, a factor analogous to the inverse of the radial velocity in the classical picture, namely $[1-(l+\frac{1}{2})^2\lambda\!\!\!^{-}{}^2/R^2-zZe^2/ER]^{-\frac{1}{2}}$, would have entered. This would make the probability of sticking proportional to the "time of contact" and would be inconsistent with a unit sticking probability. The presence or absence of such a factor is of little consequence for the excitation functions.

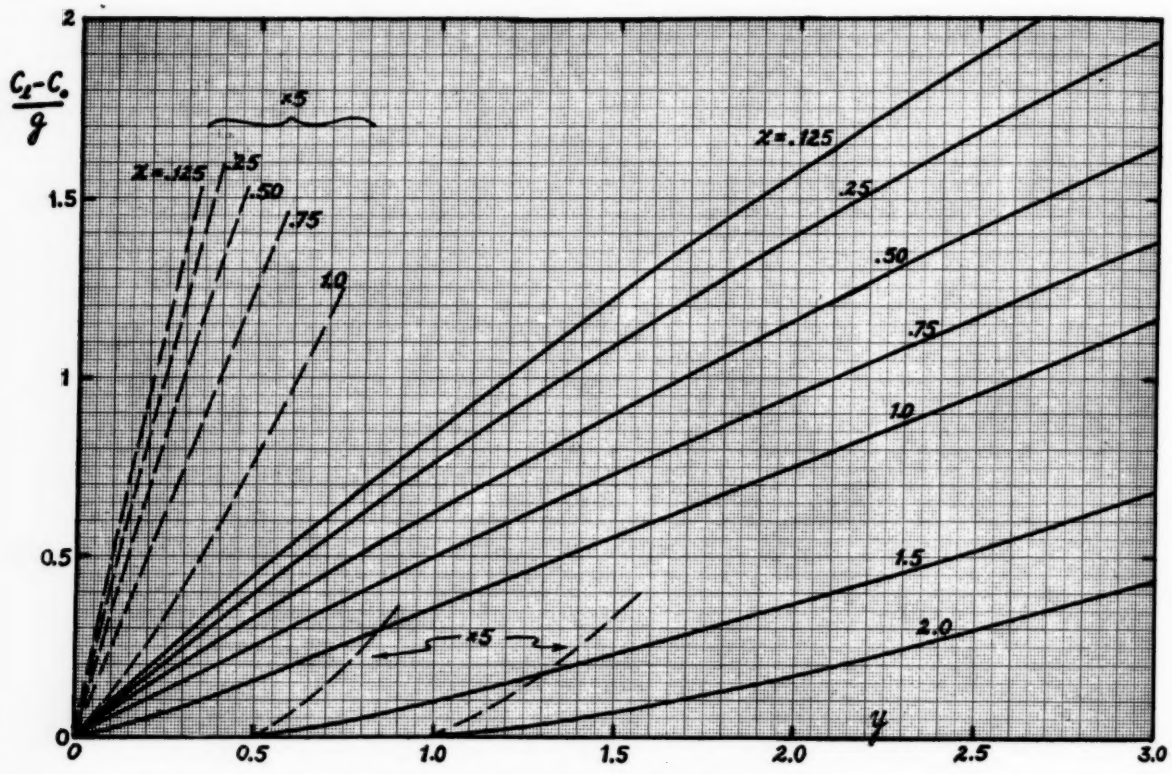

FIG. 1. $(C_l - C_0)/g$ as a function of y for seven values of x. The dashed curves are the same as the solid curves with ordinates multiplied by five.

the spacing D. (I, §54D). It enables the reduction of formula (1) to

$$(\sigma^{P_p i}{}_{Q_q i'})_{Av} = \frac{\pi\lambda^2 {}_P\xi_{P_p}\xi_{Q_q}}{(2i+1)(2s+1)} \cdot \sum_J \frac{(2J+1)}{\eta_J} \sum_{lj} P_l \sum_{l'j'} P'_{l'}, \quad (8)$$

where

$$\eta_J = 2\pi\Gamma_J/D_J. \quad (8a)$$

The summation over J is to be taken over all values of J available at the given excitation energy. The compound nucleus is usually highly excited (10 MV or more) so that except for very light nuclei the density of levels is great enough for each value of J up to a certain limit to be represented. It does no harm to include values of J up to infinity because, as we shall see, the factor P_l cuts down the contributions of high values of J so much that only values up to $J=3$ or 4 are important even for fairly heavy nuclei.

As it stands, (8) gives the cross section for a single "group" of particles which leave the residual nucleus in a definite excited state q with spin i'. To obtain the total yield of Q, (8) must be summed over all possible residual levels q, each properly weighted. For heavy enough nuclei this is done by multiplying with the number of residual states per energy interval,

$$(2i'+1)dW_B/D_{i'} \quad (9)$$

integrating, and summing over i'. $D_{i'}$ is the average spacing of levels with a given spin i' in the residual nucleus; it is probably almost independent of i'.

§3. The Penetrability Formulae

The penetration probability P_l as calculated by the W-K-B method is well known. It can be written

$$P_l = e^{-2C_l}, \quad (10)$$

in which C_l is a function given in I, Eq. (631). We give $(C_l - C_0)/g$ as a function of x and y in Fig. 1. For C_0, see I, Eq. (600) and Fig. 18. g is the "characteristic orbital momentum:"

$$g = (2MzZe^2R)^{\frac{1}{2}}/\hbar = 0.262(zZaAr_0/a+A)^{\frac{1}{2}}A^{1/6}, \quad (10a)$$

in which M is the reduced mass of the particle, a and A are the mass numbers of particle and

nucleus, respectively, and

$$r_0 = RA^{-\frac{1}{3}} \cdot 10^{+13}, \qquad (10b)$$

$$x = E_P/B = E/B', \qquad (10c)$$

in which E_P and E are relative and absolute kinetic energies of the particle, while

$$B = zZe^2/R = 1.43_5 zZ/r_0 A^{\frac{1}{3}} \text{ MV}, \qquad (10d)$$

$$B' = zZe^2(a+A)/RA = 1.43_5 zZ(a+A)/r_0 A^{4/3} \text{ MV}, \qquad (10e)$$

$$y = l(l+1)/g^2. \qquad (10f)$$

With $r_0 = 1.65$, which corresponds to a radius of 10^{-12} cm for the α-radioactive nuclei, the values of g and B' are given in Table I.

Certain approximations for $(C_l - C_0)/g$ will be useful.

$$(C_l - C_0)/g \approx y(1 - \tfrac{1}{2}x) \qquad \text{for } x < 1. \quad (11a)$$

$$C_l/g \approx 2(y - x + 1)^{\frac{1}{2}}/3(2x-1) \qquad \text{for } x > 1. \quad (11b)$$

For $y < (x-1)$, $C_l = 0$; for $x \gtrsim 1$, $C_0/g = 0$, $P_0 = 1$.

For many problems (cf. Eq. (6), (15), (16)) the quantity

$$l_c^2 = \sum_l (2l+1)(P_l/P_0) \qquad (12a)$$

is needed. It is shown as a function of x in Fig. 2, for two cases. For sufficiently heavy nuclei a great number of l's will contribute so that the sum may be replaced by the integral

$$l_c^2 = g^2 \int_0^\infty dy P(y)/P(0). \qquad (12b)$$

The integral may be extended to infinity except when the available J's are very restricted (§6). With the approximations (11),

$$l_c^2 = g/2 - x \qquad \text{for } x < 1, \quad (13a)$$

TABLE I. *Effective heights B' of Coulomb barriers in MV. Characteristic orbital momenta, $g(Z)$.*

	Z A NUCLEUS	2 4 He	4 9 Be	10 20 Ne	20 40 Ca	30 66 Zn	50 112 Sn	70 174 Yb	92 238 U
B'	Protons	1.4	1.9	3.4	5.2	6.6	9.1	11.0	12.9
	Deuterons	1.6	2.0	3.5	5.4	6.7	9.2	11.1	13.1
	α-particles	3.6	4.9	7.7	11.2	13.1	18.6	22.4	26.0
g	Protons	0.6	0.9	1.7	2.8	3.7	5.3	6.7	8.2
	Deuterons	0.7	1.3	2.3	3.9	5.2	7.4	9.5	11.5
	α-particles	1.2	2.2	4.5	7.5	10.3	14.7	18.8	22.9

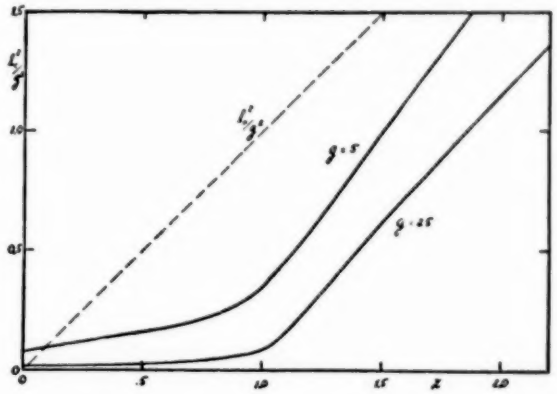

FIG. 2. The orbital momentum factor l_c^2/g^2 as a function of x for two values of g. $g \sim 5$ for deuterons bombarding Ne and $g \sim 25$ for alphas on U. All curves are asymptotic to $l_0^2/g^2 = x$ for very large x.

$$l_c^2 = g^2(x-1) + 0.744 g^{4/3}(2x-1)^{2/3} \qquad \text{for } x > 1. \quad (13b)$$

For $x \gg 1$,

$$l_c^2 = (R^2/\lambda^2)(1 - B/E) \approx R^2/\lambda^2 = l_0^2. \quad (13c)$$

This can also be derived from classical mechanics, $(l+\frac{1}{2})\lambda$ being identified with the collision parameter. The quantity l_c as given by (13) can easily be shown to represent the "critical orbital momentum" as defined by

$$2(C_l - C_0) = 1. \qquad (14)$$

Values of l greater than l_c yield only small contributions, better justifying the extension of the integration in (12) to infinity.

§4. Excitation Functions for Most Probable Reactions

The formula for the yield becomes most simple when the reaction in question is so much the most probable one that

$$\sum_q \Gamma^J{}_{Qq} \approx \Gamma_J.$$

In that case, (8), summed over all residual states q, becomes (cf. (13c))

$$\sigma^{Ppi}{}_Q = \pi R^2 \xi_{Pp} (l_c^2/l_0^2) P_0 \qquad (15)$$

after the summations over angular momenta are carried out with proper regard for their conservation. Eq. (15) is essentially the simple G-C-G formula except for the factor l_c^2 which

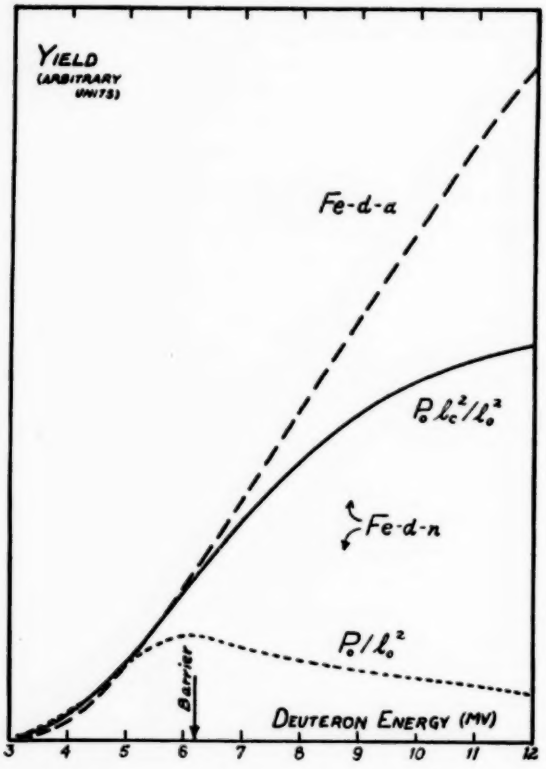

FIG. 3. Comparison of theoretical excitation functions for a most probable process (emission of neutrons) and a less probable one (alphas). Also shown is the excitation function calculated according to the usual G-C-G theory (factor l_c^2 omitted). Both reactions have been observed[9] but measurements of yield have not been yet carried to high enough energies. Ordinates of all curves were made equal at 5 MV.

represents the influence of higher orbital momenta. This factor is practically a constant for $E<B$ (see Fig. 2) and so the simple G-C-G formula gives a correct energy dependence for energies below the barrier. Also because of l_c^2, the yield will continue to rise quite rapidly even after the particles are able to pass over the barrier, contrary to frequent assumptions. An example of this behavior is shown in Fig. 3. When the energy becomes very great ($E\gg B$), (15) goes over into $\pi R^2 \xi_{P_p}$, simply. The usual G-C-G formula has for all energies the factor $1/E$, which (15) shows only for low energies. This point has led in the past to some confusion because of the apparent contradiction to the reasonable expectation that the cross section should go over into the geometrical cross section in the classical limit.

The validity of (15) for all reactions without effective competition accounts for some of the success the G-C-G theory has had in fitting transmutation data. Among the heavy elements ($A>40$), the reactions producing neutrons will usually be the most probable ones (§5). Among the somewhat lighter elements, the most probable reactions may be of almost any variety, depending on which lead to the most stable products. No excitation functions seem to be known at present for any reactions involving this class of elements ($5<Z<20$), which can safely be said to be much more probable than its alternatives. One reason is that, because such reactions usually lead to the most stable products, the observation of radioactivities is not often available as a method of measuring their excitation functions. Among the very light elements, the assumption made in deriving (15), that all J's are available, does not hold and selection rules become important (§6).

At present, there are among the heavy element reactions two sets of data[4] to which (15) is applicable and these seem to contradict each other. Mann[5] finds that a simple G-C-G penetrability function (P_0/E) fits the excitation curve he measured for the Cu^{65}-α-n reaction if he assumes $r_0=1.75$ (see (10b)). On the other hand, Thornton[6] is forced to assume $r_0=1.15$ to obtain approximate agreement of his data on the Ni^{60}-d-n reaction with the simple G-C-G theory. In view of the discrepancy between Mann's and Thornton's data, it may be significant that there seems to be a definite disagreement between Thornton's data and the G-C-G theory at the lowest energies, where the penetrability is almost independent of r_0. The factor l_c^2 plays no great part in the two cases discussed because the measurements were limited to energies below the barriers. Not only Mann's Cu^{65}-α-n curve but also his Cu^{63}-α-n data can be fitted within the theoretical and experimental uncertainties by $r_0=1.65$ (see §3).

Further measurements among the heavy elements would have some importance. In order to

[4] Recently there has been added a third, the measurement of the Se-p-n reaction by the Rochester group (to be published). Calculations for this case have been carried out by Mrs. Weisskopf. She finds that $r_0 \leqq 1.50$ fits the data best. We are indebted to Professor Weisskopf for communicating these results to us.

[5] Mann, Phys. Rev. **52**, 405 (1937).

[6] Thornton, Phys. Rev. **51**, 893 (1937).

test the theory, they should be done at the lowest possible energies, first, because there the variation of the penetrability is independent of the choice of r_0, and second, because at low energies the penetrability will be by far the most rapidly varying factor in the cross section and the variation of ξ_{Pp} can more safely be neglected in comparison.

§5. The Influence of Final States

The cross section for a reaction which meets with effective competition must involve the relative probabilities of the various types of emission possible for the same compound nucleus. To simplify the discussion, it will be assumed[7] that there is just one most probable process (e.g. for heavy nuclei, neutron emission). The formula (8) can then be shown to reduce to the cross section (15) for the most probable process, multiplied with

$$(2s'+1)\sum_q \xi_{Qq} l_c'^2 P_0' / (2s''+1)\sum_{q'} \xi_{Q'q'} l_c''^2 \quad (16)$$

$P_0''=1$ because the most probable process (the emission $Q'q'$) is certainly neutron emission;

$$l_c''^2 \approx R^2/\lambda_N^2 \quad (16a)$$

with λ_N the neutron wave-length. (16) is essentially the ratio of the "effective" densities of residual states available for the two processes, Q and Q', assuming that at least the ratio of the sticking probabilities is a constant nearly unity. The word "effective" is used here to denote the reduction of the states available by the penetrability factor, P_0'.

A computation of the density of states in residual nuclei must be based on some model such as the liquid drop model discussed in I, §53C. Although this may have no virtues over other possible models, it still seems to give correctly certain general features, namely the exponential increase of the level density with excitation energy and with mass number, and an approximately correct average spacing of the levels in heavy nuclei. For our purposes, there would be no essential differences arising from the use of other formulae for the density, such as the one involving the exponential of the square root of the excitation and empirical constants.[1]

Computations of the ratio (16), based on the liquid drop model formulae of I, §53C, have been carried out for various excitations of various compound nuclei and the results are shown in Table II. The second column gives the mass numbers A of the compound nuclei, the third their Coulomb barrier heights B in MV. The computations were made for excitations of 10, 15, 20, 25 and 50 MV for the compound nucleus. The first two rows give the deuteron bombardment energy necessary for each of the various excitations for mass numbers 50 and 200. A similar interpretation may be applied to the proton, alpha and neutron energies given in the next six rows, or, instead, each energy value may be regarded as the total energy available for the emission of the corresponding particle. The figures given are based on the semiempirical mass-defect curve which leads to Table XXXVIII of I. The remaining rows of Table II give the ratios of the probabilities of neutron and proton emission and of neutron and alpha-emission, as represented by (16).[8] The ratio of the ξ's was taken as unity.

Table II. *Energies available for various particle emissions starting from given excitations of the compound nucleus. Ratios of neutron emission probabilities to proton and alpha-emission probabilities.*

			Exc. Energy of Compound Nucleus (MV)				
	A	B (MV)	10	15	20	25	50
H^2 energy	50	5.3	—	—	3.5	8.5	33.5
	200	12	—	4	9	14	39
H^1 energy	50	5.3	1	6	11	16	41
	200	12	4	9	14	19	44
He^4 energy	50	11	2.5	7.5	12.5	17.5	42.5
	200	24	14	19	24	29	54
n^1 energy	50	—	0	5	10	15	40
	200	—	3	8	13	18	43
n/p	50		$3\cdot10^4$	12	10	8	7
	100		$5\cdot10^5$	96	70	44	24
	150		$3\cdot10^6$	1400	615	400	110
	200		$1.5\cdot10^7$	16000	6200	2600	410
	240		$2.3\cdot10^8$	32000	15000	12000	520
n/α	50		$2\cdot10^9$	700	84	65	30
	100		$3\cdot10^7$	4800	430	480	100
	150		$3\cdot10^8$	$7\cdot10^7$	$1.3\cdot10^4$	1800	250
	200		$2\cdot10^8$	$7\cdot10^5$	$9\cdot10^5$	18000	1800
	240		$2\cdot10^8$	$5\cdot10^6$	$1.2\cdot10^6$	$1.8\cdot10^5$	23000

[7] Also assumed is that the nuclei involved are heavy enough and the excitations high enough so that all values of the spin of the final nucleus are available both when the process in question takes place and when the most probable emission occurs. This assumption is of little importance for our results.

[8] The summing over states was done wherever possible by the methods suggested by (9) and by I, (346*b*). A few checks by numerical integration showed that these approximations are fair. When the available energies are lower

Table II must not be regarded as giving results with greater accuracy than by a factor of ten or so and then only when applied to elements at the bottom of the "Gamow valley," that is, those having the most stable mass number. In general, less energy is available for radioactive products than indicated in the table and so the probability of forming the radioactive nucleus is reduced accordingly. Contributing to the uncertainties are: the model employed, itself; possible deviations from the smooth mass defect curve which was assumed; the neglect of correlations such as are caused by selection rules.

The first point to be learned from Table II is that the emission of charged particles by nuclei having mass numbers greater than about 100 is practically forbidden. This comes about because neutrons, not having barriers to penetrate, may be emitted with lower kinetic energies than charged particles; then, not only is the region of easily available final states for the residual nucleus greatly widened, but more important, the region of high excitations of the residual nucleus, which is the most densely populated with levels, is easily available solely to the neutron process. On the whole, the experimental data[9] tend to confirm these considerations. Limiting the discussion to nuclei with $A>60$, we find:

(a) Three, not unquestionable, d-α reactions are suggested, with Cu, Zn and Sb, as against a half-dozen d-n reactions (Ni, Se, $Pd^{104, 105}$, Sn^{119}, $Sn^{(?)}$). The numerous d-p reactions found must be construed as an argument for the existence of the Oppenheimer-Phillips process of disintegration.[10]

(b) About five n-a (Zn, Ga, Ba, Th, U) and three n-p reactions (Cu^{65}, $Zn^{64, 66}$) have been postulated. The Ba-n-α, Th-n-α and U-n-α processes may plausibly be ascribed to short lived alpha-radioactivities following inelastic scattering of the neutron. The others all have $A<70$ so they may still be allowed.

(c) There are no p-α or α-p reactions known for $A>60$, although neutron emission processes have been observed for Ni (2 reactions), Zn(2), As (2), Se(3), Mo(2), Cd(4) and In when bombarded by protons, and for Ni, $Cu^{63, 65}$ and As when bombarded by alpha-particles.

Also shown by the table is the effect of competition on excitation functions. As the energy is increased, the probability of charged particle emission becomes more and more nearly comparable to neutron emission. At extremely high energies, all the processes tend to become equally probable. These effects will be reflected in the excitation functions of the less probable processes by a more rapid rise with energy than for the most probable processes. At the lowest excitations, this added rate of increase will be extremely great. Observations so far have been limited to higher excitations of the compound nucleus (15 MV or more), where the addition to the rate of increase is not quite so pronounced. An example is given in Fig. 3.

The methods of this section are too crude to be applied to elements of mass number smaller than about 50. Tentative calculations showed that the weights (e.g. statistical weights due to spin) given to the individual residual states are quite influential and not easily decided. Only qualitative considerations about the lighter elements seem to be feasible. The most interesting[11] of these deal with the striking decrease which may occur in the probability of a reaction when the bombarding energy is raised beyond a value which makes a competing reaction energetically possible. Haxel[12] reports such an interference of the N-α-p reaction with the yield from N-α-n, and Newson[13] found similar effects in the excitation functions for the reactions C-d-n, N-d-n and O-d-n. Newson points out that the surmounting of the thresholds of the C-d-α and N-d-α reactions are probably responsible for the decrease observed in his first two cases. There is no threshold for a new reaction which could interfere with the O-d-n reaction in the way observed. The low stability of the radioactive F^{17} against emission of protons probably is responsible for the lower probability of detecting it when it is formed with high energies.

§6. The Effect of Selection Rules

Finally, we shall consider the effect of the selection rules on excitation functions. As one might have expected, this effect has its greatest

than the Coulomb barriers, the most important contributions are made by a few levels for which the penetrability is most favorable. In these cases integration is too crude and so the sums over states were evaluated by adding together the penetrabilities for a few reasonably spaced levels. Often this gave about the same results as the crude integration.

[9] Cf. Livingston and Bethe, Rev. Mod. Phys. **9**, 245 (1937).
[10] Bethe, Phys. Rev. **53**, 39 (1938).
[11] Bohr and Kalckar, Kgl. Danske Selskab. **14**, 10 (1937).
[12] Haxel, Zeits. f. Physik **93**, 400 (1935).
[13] Newson, Phys. Rev. **51**, 620 (1937).

importance for reactions involving very light nuclei. For these, the formulation of the preceding paragraphs is not strictly valid since it was based on the participation in the process of a great many compound levels at every energy in the relevent range. In its place, the so-called "one-level" formula (I, (646))

$$\sigma=\pi\lambda_P^2\frac{2J+1}{(2i+1)(2s+1)}\frac{\Gamma^J{}_{Pp}\Gamma^J{}_{Qq}}{(E-E_r)^2+\frac{1}{4}\Gamma^2{}_J} \quad (17)$$

is sometimes useful, but it is applicable only in energy ranges for which just one level of the compound nucleus is effective. One may proceed with a detailed analysis of special cases which may decide to which (17) may be applied.

Another difficulty encountered when dealing with light elements is in the calculation of the penetrability itself. The W-K-B method should be expected to fail for the low and thin barriers possessed by the very light nuclei. One might instead make use of the exact wave functions for a Coulomb field calculated by Yost, Wheeler and Breit,[14] but now there arises the question of what boundary conditions to impose (see I, §54*A*). We have adopted the procedure of Kapur and Peierls,[15] according to which the width of a level depends on the particle energy as

$$\Gamma^J{}_{Pplj}\sim E^l/G_l^2, \quad (18)$$

where G_l is the irregular wave function for a Coulomb field as given in Yost, Wheeler and Breit's paper. For low energies and $l=0$, (18) reduces in its energy dependence to

$$\Gamma^J{}_{Pplj}\sim\exp(-2\pi zZe^2/\hbar v), \quad (18a)$$

with v the velocity of the particle. This is exactly what the W-K-B method gives for low energies (I, (589b)). The procedure we adopt here is quite consistent with our treatment of the penetrability for heavy nuclei (cf. footnote 3).

As a first illustration of how selection rules affect excitation functions, one may take the case of

$$\mathrm{Li}^7+\mathrm{H}^1\rightarrow 2\ \mathrm{He}^4. \quad (19)$$

The protons responsible for this process must have odd angular momenta since the parity of Li^7 is odd and the alphas obey Bose statistics.

[14] Yost, Wheeler and Breit, Terr. Mag., Dec. (1935). Also Phys. Rev. **49**, 174 (1936).

[15] Kapur and Peierls, Proc. Roy. Soc. **A166**, 277 (1938).

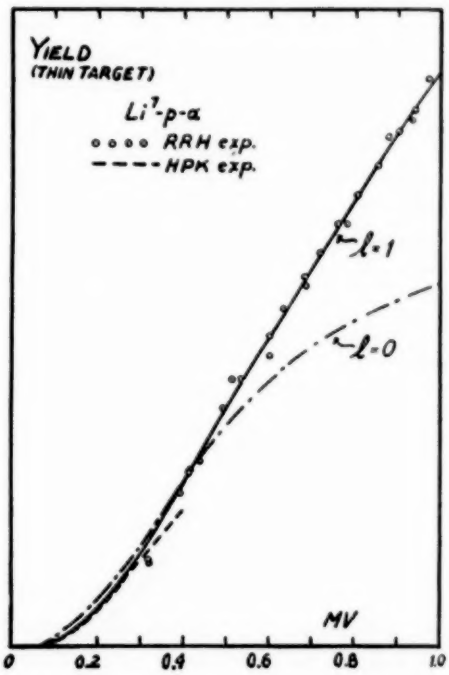

FIG. 4. The circles represent the data of Rumbaugh, Roberts and Hafstad,[16] the short dashed curve that of Herb, Parkinson and Kerst.[16] The solid curve is the theoretical excitation function for $l=1$ and $r_0=1.65$, the dot-dash curve for $l=0$ and $r_0=0$. Curves fitted at 0.4 MV.

The comparison of the theoretical with the experimental excitation functions[16] in Fig. 4 shows that indeed the $l=1$ protons account for the observed variation of the yield much better than $l=0$. A nuclear radius corresponding to $r_0=1.65$ was used for the $l=1$ curve while a zero radius was taken for the $l=0$ case in order to make its comparison as favorable as possible. The form (18) for Γ was employed in computing the $l=1$ function.[17]

Unfortunately, further illustrations of the importance of selection rules are obscured by other considerations. For example, consider the reactions

$$\mathrm{Li}^6+\mathrm{H}^2\rightarrow 2\ \mathrm{He}^4 \quad (20a)$$

and

$$\mathrm{Li}^6+\mathrm{H}^2\rightarrow\mathrm{Li}^7+\mathrm{H}^1. \quad (20b)$$

[16] The experimental data for low energies were taken from Herb, Parkinson and Kerst, Phys. Rev. **48**, 118 (1935). The measurements up to 1 MV are those of Rumbaugh, Roberts, and Hafstad (to be published). We are indebted to the authors and to the Drs. Fleming and Tuve of the Carnegie Institute at Washington for the communication of these results to us.

[17] It was not necessary to assume the existence of a resonance in these calculations in contrast to those of Ostrofsky, Breit and Johnson (Phys. Rev. **49**, 22 (1936)) who employed a one-body model.

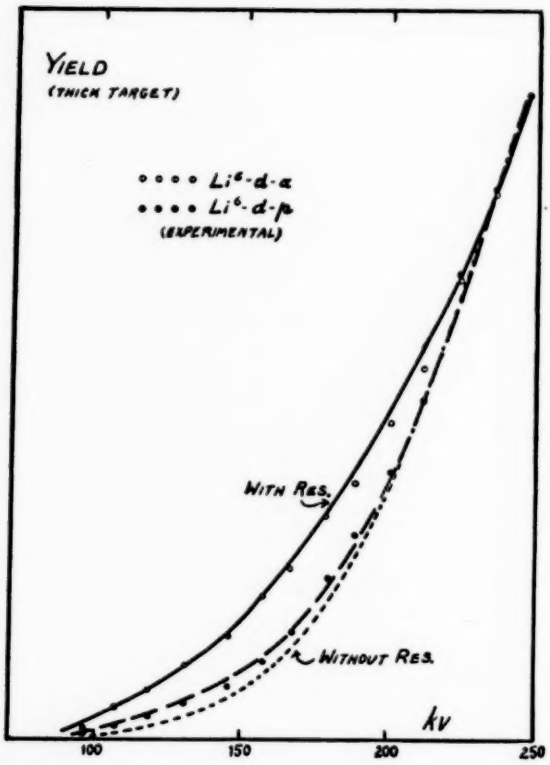

FIG. 5. Circles represent experimental points for the Li^6-d-α reaction, dots for Li^6-d-p, according to Williams, Shepherd and Haxby. The dotted curve is the theoretical excitation function for $l=0$ and no resonance. The solid curve includes a resonance at 40 kv, 50 kv wide. The dashed curve is the sum of the other two made equal at ~160 kv. All curves fitted at 240 kv.

Since the parity of every nucleus involved in (19a) as well as that of the relative motion of the alphas is even, the orbital momentum of the deuteron about Li^6 can only be even. Thus the selection rules require that the yield of protons increases more rapidly with bombarding energy than the alpha-yield, due to the contribution to (20b) of the $l=1$ deuterons which are barred for (20a). Actually, Williams, Shepherd and Haxby[18] do find a steeper curve for the excitation of (20). However, the relative steepness is much too great to be accounted for by the $l=1$ deuterons. With no resonance, the theoretical excitation function (cf. (17)) is given by (18) multiplied with λ^2. For the low energies used, (18a) was found to represent the energy dependence of (18) rather well, i.e., the results depend only slightly on the choice of the radius. Comparison in Fig. 5 shows that the theoretical curves, even with $l=0$, are too steep for both the alpha and proton yields. Even a radius as large as 10^{-12} cm fails to bring about sufficient improvement. A discrepancy in this direction perhaps may indicate that a resonance must be postulated. It was found that a resonance level for the Li^6-d-α reaction at about 40 kv deuteron energy and about 50 kv wide (depending on the position) could remove the discrepancy. It is satisfactory that this resonance is wide compared to the 10 kv or so found for the proton capture resonance widths.[9] Of the three spins, $J=0$, 1 and 2, possible for the compound nucleus with the slow deuterons ($l=0$), the Li^6-d-α resonance certainly has $J=0$ or 2 only. Since the Li^6-d-p reaction may also have $J=1$, only part of it will follow the same excitation function for $l=0$ as Li^6-d-α. We find that by equating the contributions of the cross section without resonance and that with the resonance at 160 kv agreement with the data is obtained. (Fig. 5.)

The excitation function[19] for

$$B^{11}+H^1 \rightarrow 3\,He^4 \qquad (20)$$

shows a behavior of the same kind. In this case the postulated resonance level has actually been observed; it lies at 180 kv proton energy and is 11 kv wide. The resonance is most clear for the long range alpha-particles whose emission leads to the ground state of Be^8. From the angular distribution of these alphas it seems plausible[20] that the resonance probably has $J=2$ and is therefore produced by protons of $l=1$. The observed yield curve for (20) is then probably a superposition of an $l=1$ curve showing resonance and a non-resonance function for $l=0$.

The experimental excitation functions for the Be-d-α, Be-d-H^3, Be-d-p and Be-p-α reactions[21] again seem to show too slow a rise compared to the theoretical curve without resonance, but in these cases the differences are too small to be very certain.

[18] Williams, Shepherd and Haxby, Phys. Rev. **52**, 390 (1937).

[19] Williams, Wells, Tate and Hill, Phys. Rev. **51**, 439 (1937).

[20] Oppenheimer and Serber, Phys. Rev. **53**, 636 (1938).

[21] Williams, Haxby and Shepherd, Phys. Rev. **52**, 1031 (1937).

Positive-Point-to-Plane Discharge in Air at Atmospheric Pressure

ARTHUR F. KIP
Department of Physics, University of California, Berkeley, California
(Received May 5, 1938)

Investigations have been carried out on current-voltage characteristics of positive-point-to-plane discharge. All currents start *abruptly* and increase at first linearly and then more steeply with voltage, until finally breakdown into a spark occurs. The corona process in air is shown to be a *discontinuous* one, involving the alternate propagation and space charge quenching of positive streamers out from the point. Photoelectric ionization in the gas is shown to account for the rapid self-propagation of streamers. Attachment of electrons to form negative ions and subsequent detachment of these electrons in the high field near the point provides means of starting new streamers for self-maintaining corona process. Fields at onset are calculated by the use of confocal paraboloids as electrodes, and it is shown that the fields necessary for such corona process are available. Introduction of a radioactive source into the gap indicates that the sharp cut-off of the corona current as the voltage is decreased is due to lack of electrons for initiating new streamers. Offset voltage marks the point at which the self-perpetuating ionization process begins. The initial current rise is found to increase as the gap distance is decreased and this is shown to be caused by the change in field distribution and consequent further extension of streamers into the gap. Below a certain minimum gap distance, depending on the point geometry, the initial streamers propagate completely across the gap and this introduction of the highly efficient ionization at the cathode causes spark breakdown. The initial current-voltage slopes are expressed as a resistance which is found to increase linearly with the gap and to account for approximately 1 percent of the total voltage drop in the gap. Extrapolation of resistance to zero resistance gives the minimum gap at which stable corona will flow. Above the initial current rise, the current increases as the square of the difference between the applied and offset voltage. Evidence indicates that this is caused by a superposition upon the otherwise linear rise in current with voltage, of an increase proportional to the current itself. Visual observation near breakdown indicates that this increase proportional to the current is associated with the utilization by later streamers of the residual paths of their predecessors. This becomes more pronounced as the current and voltage increase; the effect of earlier streamers in this way increases the current in later streamers. Spark breakdown occurs when the amalgamated streamers succeed in crossing to the plate.

INTRODUCTION

THE current-voltage characteristics of positive-point-to-plane discharge in air at atmospheric pressure have been investigated extensively in the past.[1–3] Unfortunately most of the work has consisted in finding empirical equations to satisfy the current-voltage curves for various gap geometries and to indicate the voltages at which the corona breaks down into a spark. This information, while of some importance from an engineering point of view, tells very little with respect to the fundamental processes taking place. In this laboratory, discussions with the late Professor Hillebrand led Professor Loeb[4] to observe, in positive point corona in air and in impure N_2, streamers coming out from the point in an ever-changing pattern, which indicated that there might be discontinuities in the current. It was known that while such discontinuities exist and can be observed on an oscilloscope when the point is at negative potential, no discontinuities can be observed by this means with a positive point. Thus it has always been assumed that positive corona at high pressure is a continuous phenomenon analogous to a glow discharge. Acting on the suggestion by Professor Loeb, G. W. Trichel in these laboratories has verified the existence of these discontinuities. Details of this work will be published soon. The present paper will describe experiments whose purpose was to investigate the fundamental processes occurring in positive point-to-plane discharge in air at atmospheric pressure principally by means of current-voltage measurements. The measurements have determined current-voltage characteristics of the corona as a function of gap geometry, and include the voltages at which the corona breaks down into a spark. Particular attention has been given to the conditions under which the corona begins and to the nature of the starting currents, since this

[1] Warburg, Ann. d. Physik **66**, 652 (1898); **67**, 69 (1899).
[2] Zeleny, Phys. Rev. **25**, 305 (1907); **26**, 129 (1908).
[3] *Handbuch der Physik*, Vol. 14, Chap. IV.
[4] Loeb and Leigh, Phys. Rev. **51**, 149 (1937).

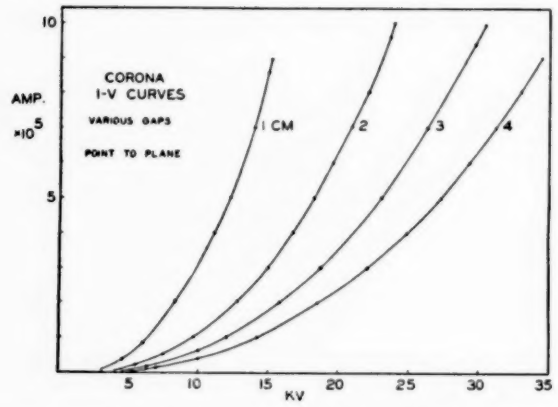

FIG. 1. Corona current-voltage curves for various gap distances. Curves end at voltage at which spark breakdown occurs. Hemispherical point 3*A*, diameter 0.5 mm.

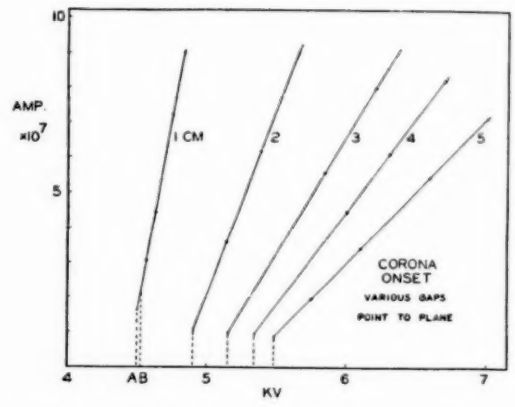

FIG. 2. Onset region of corona current-voltage curves, enlarged, showing initial linear current rise.

information gives many clues as to the kind of processes occurring.

APPARATUS

The essential features of the apparatus are the chamber wherein the discharge takes place, the voltage supply, and current and voltage measuring devices. Voltage is supplied by a 500 cycle generator to a 150 kv transformer, which leads to a full wave rectifier and filter circuit. The voltage is maintained and adjusted by a saturable reactor stabilizer in series with the transformer primary. Voltages from one to 50 kv, constant to better than 1 percent are thus available. The voltage is measured by a potentiometer put across a small fraction of a 50 megohm resistance tower in parallel with the discharge. Current is measured by the voltage drop across a resistance in series with the gap. This voltage drop is measured by means of an electrometer, and the resistance can be readily changed to make possible current readings from 10^{-10} to 10^{-3} ampere. The resistance is always small with respect to the gap resistance, so that it does not influence the discharge. In order to protect the electrometer from the large impulse which occurs when the corona goes into a spark, a neon lamp is put in parallel with the electrometer to take a major part of the spark current.

The discharge takes place inside a glass chamber made from a five gallon water bottle with the bottom cut off and replaced by a glass plate. This chamber is covered inside with a grounded monel screen to prevent the accumulation of electrostatic charges on its surface which would alter the field, and can be evacuated and filled with any desired gas. In most of the experiments, dried room air has been used.

The negative electrode is a brass plate 13 cm in diameter, and the positive electrode is a platinum wire with a hemispherical end. Platinum was chosen because it was found that its characteristics suffer a minimum change due to corona currents and sparking. The hemispherical end was used because of ease of maintaining constant point geometry. Various sizes of points have been used, with diameters from 0.5 to 4.7 mm. The gap distance can be varied while the chamber is isolated from room air by means of a threaded point holder which can be turned in a ground glass joint.

EXPERIMENTAL RESULTS

The general shape of the current-voltage curve is plotted in Fig. 1 for various gap distances and a 0.5 mm diameter point. The essential features are the initial sudden rise of current and the increase which is at first linear with voltage and then becomes steeper until finally breakdown into spark occurs, at which point the curves are ended. These curves were taken in dry air and are similar to those of other workers except that the initial sudden rise has not generally been noted.

Figure 2 shows an enlarged view of the onset region. The scale has been changed to show the linear increase after the initial sudden rise. If the voltage is increased gradually from zero to some

value B above A, as shown on the curve for a 1.0 cm gap, the current will suddenly start, and then follow the curve shown. The position of B varies with the time a given voltage has been applied. The time delay or lag before the current starts varies in a statistical manner, and is proportional on the average to the difference between the voltage applied and the critical or offset voltage A. The time of starting may vary from a fraction of a second to many seconds for a given applied voltage. If the voltage is decreased after the current has started, the current follows the curve shown until the *offset* voltage A is reached, at which point it goes off suddenly. In contrast to the statistical character of *onset*, the *offset* voltage is found to be extremely sharp, and to remain constant as long as the gap geometry is held constant.

The way in which the offset voltage and current vary with gap distance is shown in Fig. 3. The minimum current which will flow before the process stops completely is found to increase as the gap distance is decreased. When the gap has less than a certain critical length, called the *corona point distance*, the corona process no longer occurs and the gap breaks down completely into a spark.

In view of the theory of the processes occurring, to be discussed later, it was of interest to determine the cause for the sudden cutting off of the corona current at the critical voltage. This problem was attacked by means of inserting radioactive material into the gap and the results are shown in Fig. 4. If a very small quantity of radioactive material is placed in the gap, so as to provide an intermittent source of ions, the corona behaves exactly as without the auxiliary source of ions at voltages above the critical voltage A, except that the corona now goes on immediately when the critical voltage has been reached. Below the critical voltage the corona current is intermittent, with an average frequency which depends on the amount of radioactive material and the difference between the applied and critical voltage. The average current which flows in the voltage range between A and C is dependent on the radioactive strength, but for a particular strength, falls approximately on the broken line 1. A larger radioactive intensity gives no material change in the current when the voltage is above the critical value, but gives currents as shown in curve 2 below the critical voltage. The current in the region below the critical voltage (between A and C) has been found by Trichel to show the same discontinuities observed in regular stable corona at voltages above the critical point A. However, in this region the corona process occurs only by virtue of the auxiliary source of ions provided by the radioactive source. The exact shape of the current curve between A and C is dependent on the amount of radioactive material present. Below this region another process occurs, where the current is perfectly continuous, and decreases more rapidly. If a very intense ion source is provided, the discontinuous corona action no longer occurs until large voltages are applied, and in consequence the current-voltage curves are completely changed. Curve 3 was obtained by the use of an intense radioactive source.

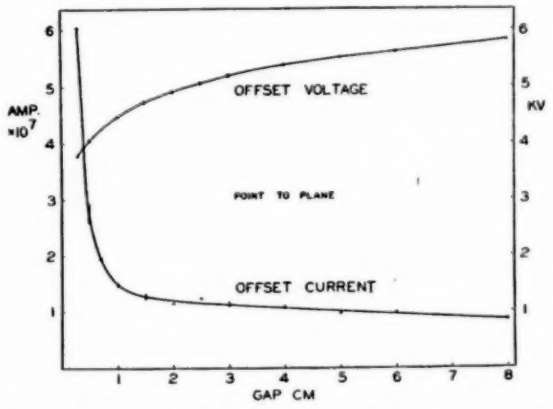

FIG. 3. Offset voltage and current *vs.* gap distance for hemispherical point 3A.

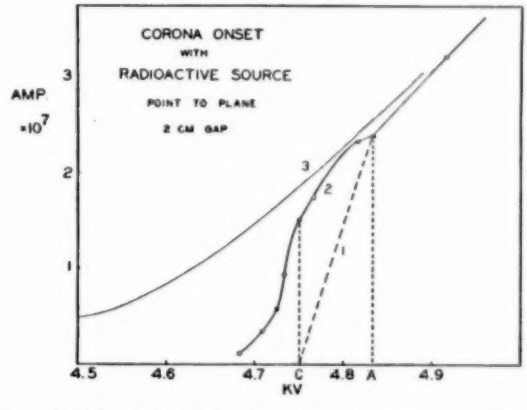

FIG. 4. Effect of radioactive source on corona onset, 2.0 cm gap, point 3A. Curve 1, weak source; curve 2, medium source; curve 3, strong source.

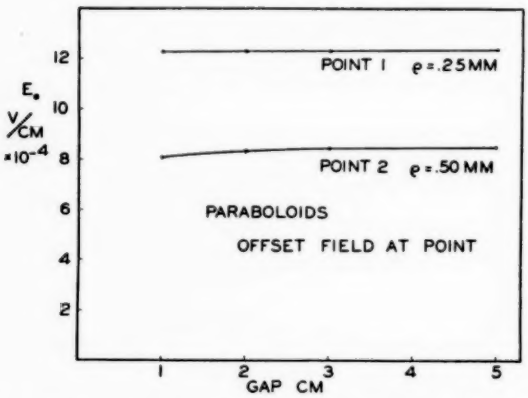

FIG. 5. Field at point surface at onset for confocal parabolic electrodes for various gap distances.

The voltages at current-onset shown in Fig. 3 give no information as to the fields existing, since calculation of the field for the geometry used is not possible. Knowledge of the field strengths existing is of prime importance for the understanding of the processes occurring. To make such calculations possible, the gap geometry was altered by making a set of confocal paraboloids of revolution, one being used for the point, and the others replacing the plate. One pair was used for each gap distance tested. Observation of onset voltages and subsequent calculation of the electrostatic field at the surface of the point just prior to onset gave the curves shown in Fig. 5. Two different points were used, as indicated. The maximum field at onset was thus found to be the same for all gap distances for a given point. The slight curvature in the curve for the larger point is probably due to the fact that necessary departure from true parabolic shape becomes of some importance in the larger point.

The voltages at which the corona breaks down into a spark as a function of gap distance are plotted for a 0.5 mm diameter point in Fig. 6. The maximum current before breakdown occurs is plotted in Fig. 7.

THEORY

The existence of a discontinuous process in positive point corona at once indicated that the character of the discharge mechanism is basically that indicated by Loeb and Cravath[5] for the propagation of the positive leader stroke in lightning discharge. Such a mechanism occurs upon the appearance in the high field region of the gap of either a free electron at E/p of about 30, where E is the field in volts/cm and p is the pressure in mm of Hg, or a negative ion where the value of E/p is greater than 90. Loeb[6] has shown that negative ions lose their electrons in such fields, hence at lower fields if free electrons are present, and in any case in fields extending into the gap space with a value of E/p greater than 90, a single electron will ionize by collision, produce an electron *avalanche* and leave behind a positive ion space charge of high ion density which effectively extends the point out into the gap. This positive column will be relatively stationary because of the very small mobility of the ions as compared to the electron mobility. Such a single electron avalanche does not constitute the discontinuous current observed, inasmuch as the magnitude of the electron multiplication is entirely inadequate. This is evidenced by the fact that the single electron avalanches with medium radioactive source (below C in Fig. 4) do not register any discontinuities. Another indication that a single avalanche does not account for the

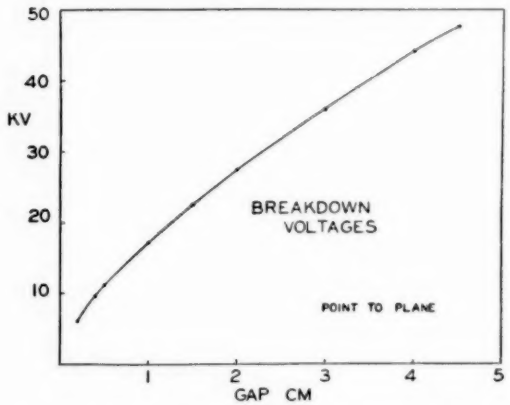

FIG. 6. Breakdown voltage *vs.* gap distance, hemispherical point.

discontinuities is the fact that under certain conditions visible streamers extend out into the gap into regions where the electrostatic fields are entirely inadequate for avalanche formation.[4] Thus a mechanism must be looked for which will allow for the self-extension of the avalanches out into the gap. Accompanying the avalanche there has been intense excitation and the region for

[5] Loeb and Cravath, Physics **6**, 125 (1935).

[6] L. B. Loeb, Phys. Rev. **48**, 684 (1935).

some distance around the positive point is photoelectrically ionized. Evidence of this has recently been obtained by W. S. Gorrill in these laboratories, with the use of a Wilson cloud chamber. The intense field around the extended positive point gives rise to further electron avalanche formation. Thus a positive corona streamer propagates outward from the positive point into the gap space.[5] This propagation continues until the dissipative action of diffusion, space charge and the random entry of electron avalanches into the extended point so distorts the field and reduces the gradients that further propagation is no longer possible. It is clear that the higher the field is in the active region around the point the greater the length of the streamer before the dissipative forces, which require time, choke it off. Under suitable conditions the existence of these individual streamers can be seen; their presence is characterized in air and impure nitrogen by the characteristic brilliant blue color of the spark spectrum of nitrogen, indicating the existence of intense fields along the tip of the propagating channel. The exact duration of propagation of such a streamer has not yet been determined. Evidence based on Trichel's work and knowledge of the propagation time of lightning discharge streamers indicate duration less than 10^{-7} and more likely 10^{-8} second. Once the streamer has ceased propagating, there must follow a period of relaxation in which the positive space charge which has accumulated is swept away from the region around the point by the clearing field until the high field region is again made active.

The period of time during which the clearing field dissipates the positive space charge to an extent sufficient to permit of a new avalanche must depend largely on gap geometry and the potential applied to the positive point; that is, on the steepness of the gradient throughout a considerable portion of the gap. Once the clearing field has acted, the positive point is again in a position to produce a discharge by propagating a new streamer. It can do this *only when a negative ion or a free electron* is available in the limited high field region about the point. The normal ionic and electronic content in the atmosphere is so weak that the chance of a new avalanche *without an auxiliary source of electrons*,

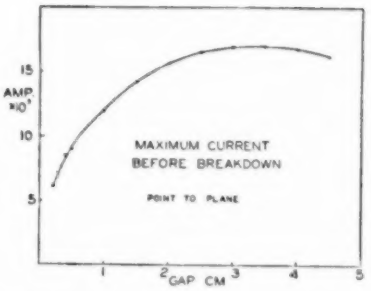

FIG. 7. Maximum current before spark breakdown vs. gap distance.

in a reasonable time is very small. If electrons were available, the streamers would propagate at the rate of electron appearance in the sensitive region up to a frequency more or less dictated by the time of relaxation necessary to restore the high fields. Owing to the rapid sweeping of electrons, the only possibility in the absence of radioactivity for a repetition of streamer formation lies in a supply of electrons through detachment of electrons from the surviving negative ions produced in the weak field region by ultraviolet light action. The existence of these negative ions is proven by direct evidence from the cloud chamber studies of Gorrill. This mechanism was proposed by Trichel as the mechanism of starting of the new streamer. As has been explained, this necessitates a value of E/p greater than 90 at some distance away from the positive point which is in conformity with observations. On this basis it is *only gases in which the free electrons are trapped to form negative ions which are capable of giving a positive corona showing the characteristics of that in air*. Thus with pure nitrogen in which electrons do not attach, Trichel has shown that the discontinuous process does not occur. The discontinuities which characterize the positive point corona in air are caused by the alternate propagation and choking off of the lightning-like positive streamers.

It is therefore necessary in order to have a stable self-maintaining corona discharge that there be a region in the vicinity of the point where E/p is greater than 90, a supply of negative ions, and in addition there must be a weak field region such as to prevent the positive streamers from propagating completely across the gap to produce spark breakdown. With this picture in mind one may now discuss the results observed.

Discussion of Results

Onset phenomena

The phenomena observed in the onset region of the current-voltage curves may now be explained. The voltage B (Fig. 2) at which onset occurs is determined by the arrival of an ion in the sensitive volume around the point, which starts the stable corona process. As explained, this value of voltage for *onset* depends on the time the given voltage has been applied and on the difference between A and B. The greater the applied voltage, the greater is the sensitive high field region around the point wherein a negative ion can lose its electron and start the corona process and therefore the shorter on the average is the time lag before such action occurs. The *offset* voltage A is an important characteristic of the corona. It marks the lowest potential at which the presence of an ion in the sensitive region from the preceding streamer is assured, and therefore the *lowest potential at which the corona process is self-maintaining*. Below this potential, single streamers, or many, may occur before statistical fluctuations in ion arrival cause the final streamer to be unproductive of an effective ion and therefore cause cessation of the process. The lower the potential the smaller on the average is the number of streamers which will succeed in following each other before extinction, and probably eventually only single streamers will be propagated. When an auxiliary source of ions from radioactive material is supplied in this region, between A and C in Fig. 4, the positive point acts as a Geiger point counter for ions entering the sensitive region of the gap, each ion or group of ions causing the initiation of one or a series of streamers. This action can be clearly seen in the current measuring instrument, as the current appears in bursts which become less frequent below A as the potential is lowered and as the strength of the auxiliary ion source is decreased. This production of separate bursts of current stops abruptly below C, which is presumably the voltage below which streamer propagation ceases. With a very weak radioactive source, C marks the point below which no current above 10^{-10} ampere is observed. As the voltage approaches A, the average strength of the current bursts becomes greater because of the increased number of streamers which occur before the process is cut off.

With stronger radioactive sources there is an asymptotic rise in current below C with no discontinuities, as shown in Fig. 4. This current obviously represents a mere multiplication of the radioactively produced ions in the strong field about the point, which is great enough to cause multiplication of ions but not enough to allow streamer propagation. With the more intense ionization the current between C and A represents a superposition of the current due to almost continuous streamer formation made possible by the auxiliary nearly continuous source of ions upon a background of the multiplication current. Above A the current is nearly unaffected by the externally supplied ions and follows the initial linear rise which occurs in the absence of radioactive material. This is no doubt due to the fact that above A, the auxiliary ion source is small with respect to the photoelectrically produced ions and therefore the modification of the weak field region which limits the current is small.

When even stronger radioactive intensity is used, as mentioned in the section on experimental results, streamer propagation no longer occurs until large voltages far above the onset value are applied. In consequence the current-voltage curve is completely changed as shown. The curve no longer shows any discontinuities and the slope of the linear part is changed. This change in the kind of process occurring is unquestionably caused by the change in the character of the field as a result of the large amount of ionization present, and the current is due to simple multiplication of ions. In this case, even above A, the auxiliary source of ions is very much greater than the ionization caused by the photoelectric process in the gap, and hence the space charge is profoundly modified. In effect, the space charge due to the intense radioactive source causes the intense field to be spread out through the weak field region of the gap to such an extent that the intense field necessary for the propagation of streamers no longer exists until voltages are much greater than otherwise would be sufficient. If the ionization is great enough, it may be impossible to establish the discontinuous corona process before breakdown occurs.

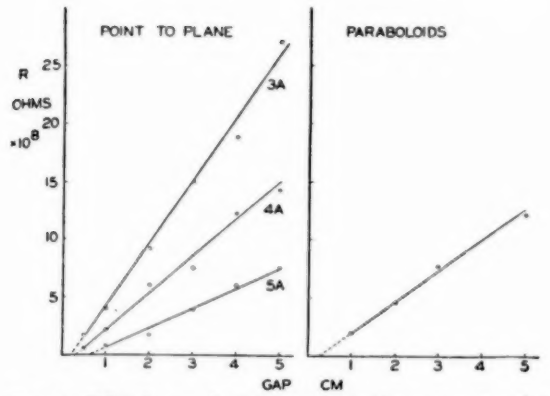

FIG. 8. Effective resistance interposed by clearing field region of gap *vs.* gap distance for point to plane and parabolic gaps. Point 3*A*, diameter 0.5 mm; point 4*A*, diameter 1.5 mm; point 5*A*, diameter 4.7 mm.

Field intensities at onset

As has been stated, confocal paraboloids were used to make possible calculation of the field in the region of the point at onset. Calculations from the data obtained show that the field at the surface of the point is 80 and 120 kv/cm for the small and large points respectively. These may be in error by as much as 10 percent but in any case it is seen that they lie well above the 69 kv necessary for $E/p=90$. Thus fields sufficient for dissociating the electrons from negative ions as well as for multiplication of electrons exist in a considerable region out from the point at onset, as is necessary. Calculation shows that for the unmodified electrostatic field, the region of $E/p>90$ extends out to 0.05 mm along the axis of the point for point 1, and out to 0.1 mm for point 2, at onset voltages. The space charge will of course modify this when current starts to flow, but also the field at the tip of the self-propagating streamer will be greater than as calculated for the electrostatic field. At onset voltages, the electrostatic field in which multiplication of electrons can occur ($E/p>20$), extends out approximately 1 mm from the point.

Under reasonable assumptions as to the time of relaxation and the field existing during this time, calculations show that negative ions formed from 0.5 to 1 cm out from the point will be available to re-kindle the corona process after the time of relaxation.

Effect of gap distance

The manner in which the offset current varies with gap distance (Fig. 3) clearly indicates the effect of the weak field region. For large gaps, d/ρ, the ratio of gap distance to radius of curvature of the point, is large and consequently the clearing field is weak. Therefore at voltages just sufficient to give the necessary high fields for the generation of corona currents, the sweeping out of the positive space charge is relatively slow and the current is correspondingly low, presumably because of a long time of relaxation. As the gap is made smaller, d/ρ becomes smaller and the field consequently tends to be spread out more uniformly across the gap. This gives greater sweeping fields which correspond to voltages just sufficient to produce an active high field region. The minimum current for stable self-maintaining corona is consequently larger for small gaps. As the gap is further decreased, the high field region extends over a still larger proportion of the gap. Finally when the *corona point distance* is reached, the low field region no longer exists, and the stabs propagate themselves completely across the gap. Immediate breakdown into a spark then occurs without the appearance of stable corona.

The spark represents a changed condition in which the streamer reaches the cathode. This introduces a new efficient electron source into the process and the corona current no longer depends on the relatively inefficient photoelectric effect in the gas. Thus it is seen that the low field region is essential for maintenance of stable corona.

The voltage at which breakdown into a spark occurs for various gap distances, as shown in Fig. 6, is determined by the fact that at this point the low field region is no longer sufficient to prevent the streamers from propagating completely across the gap. The maximum in Fig. 7 is due to the fact that the collecting plate does not receive all of the current at high voltages when the gap distance is greater than 3 cm. Thus if the *total* current were taken, the maximum current before breakdown would steadily rise as the gap distance is increased. This instrumental error also affects the 4 cm gap curve in Fig. 1, which gives currents smaller than the total current.

Effective resistance

The fact that the initial rise of current after onset with applied voltage is linear, as shown in

Fig. 2, makes possible further demonstration of the necessity of the low field region in the maintenance of stable corona. The reciprocal of the slope of this initial rise in current may be considered as an effective resistance interposed by the weak field region of the gap. Fig. 8 shows the variation of this effective resistance with gap distance, for various sizes of points. As is shown, the resistance increases linearly with gap distance, and as to be expected, is less for points with larger diameters since for larger points d/ρ is smaller and consequently the fields are more uniform. This means that the sweeping action is more effective and less resistance is interposed by the weak field part of the gap. It is of further interest to note that if these effective resistance curves are extrapolated to zero resistance, they cross the axis at gap distances corresponding within the experimental error to the *corona point*, that is, the distance below which spark breakdown occurs without the formation of stable corona. This corresponds to the fact that when the gap distance is such that the weak field part of the gap no longer interposes a resistance, the streamers propagate completely across the gap, and cause breakdown. It is to be noted that while the resistance so calculated is only of the order of magnitude of 10^8 ohms, the total effective resistance in the gap must be of the order of 10^{10} ohms to account for the magnitude of the current which flows. Thus only about 1 percent of the total IR drop is due to the weak field part of the gap. However, it is to be expected that most of the energy provided by the potential source is used in the intense field region in producing ionization and the shape of this intense field region will be only slightly modified by changes in gap distances, whereas the sweeping fields will be greatly changed.

The effective resistance of the weak field region has also been plotted for the confocal paraboloid geometry. In this case, both the points used yield the same values for effective resistance at different gap distances. This is as to be expected, since with the paraboloids, the lines of force in the weak field regions are independent of the size of the point, as long as all surfaces remain confocal, and therefore the sweeping field current-limiting action is the same for both points used.

Shape of current-voltage curves

Above the initial linear rise, it is found that the current is roughly proportional to the square of the difference between the applied and offset voltage. This is to be expected from a visual observation of the streamers at voltages approaching breakdown values. It is seen that the visible streamers have a tendency to follow along somewhat the same paths of others which have gone before. Apparently, at high voltages the new streamer may start propagating before the column of positive ions from the last one in the weak field region has been completely swept away, and the resulting uneven ion distribution around the old positive column out in the gap will give rise to regions where the field is considerably higher than is the case where the last positive column is more completely removed before the starting of the new streamer. This increase in the field in regions contiguous to an old streamer will allow the new streamer to propagate further than would otherwise be the case. Thus two factors influence the increase of current with voltage, first the linear increase in sweeping fields and second the effect of old streamers. The latter effect would be expected to be at least roughly proportional to the size and frequency of the preceding streamers, and thus also to the current which is dependent on the difference between applied and offset voltage. It is thus seen that the nonlinear region of the current-voltage relationship may be ascribed to effects of the preceding discharge proportional to the current, which act to augment the current by modifying the otherwise linear space charge limitations.

In conclusion, the author wishes to express his appreciation to Professor Loeb for his guidance throughout the prosecution of this work and particularly for his aid in the interpretation of the results. He is also indebted to his colleagues, G. W. Trichel and W. S. Gorrill, the results of whose coordinate researches on different aspects of the same problem have been of the greatest help. Finally he wishes to express his appreciation to the Research Corporation of New York whose Research Fellowship Grant at the University of California for the last two years has made this work possible.

LETTERS TO THE EDITOR

Prompt publication of brief reports of important discoveries in physics may be secured by addressing them to this department. Closing dates for this department are, for the first issue of the month, the eighteenth of the preceding month, for the second issue, the third of the month. Because of the late closing dates for the section no proof can be shown to authors. The Board of Editors does not hold itself responsible for the opinions expressed by the correspondents.

Communications should not in general exceed 600 words in length.

The Viscosity of Liquid Helium II

As is well known, the properties of liquid helium undergo a rapid change near 2.19°K, the so-called "lambda point." Below this temperature the liquid is ordinarily referred to as helium II. Recently Kapitza[1] has reached the conclusion that the viscosity of liquid helium II must be less than 10^{-9} poise and Allen and Misener[2] similarly have concluded that their experiments place the possible upper limit as 4×10^{-9} poise.

However, in connection with another experiment it has been pointed out by Kurti, Rollin and Simon[3] that rather phenomenal surface films of liquid helium II spread over surfaces brought into contact with it. Their experiments show that the films can climb for a considerable distance above the surface of the liquid. This deduction is supported by observations of Kamerlingh Onnes[4] and more recently by experiments of Daunt and Mendelssohn[5] which show that a body of liquid helium II rapidly comes to a common level in two vessels in contact with it. In our own experiments we have, on numerous occasions, obtained results that are in agreement with the above explanation. Thus it seems rather obvious that the conclusions as to the limiting value of viscosity, referred to above, are not valid because of the fact that under the conditions of the experiment most of the liquid helium would be transferred over the outer surface of the apparatus instead of through the small capillaries as supposed. Nevertheless it is known that the viscosity of liquid helium decreases rapidly with decreasing temperature near the "lambda point" since Wilhelm, Misener and Clark[6] and Burton[7] have shown, by measurements with an oscillating cylinder, that it changes from 2.7×10^{-4} poise at 24°K to 3.3×10^{-5} poise at 2.2°K.

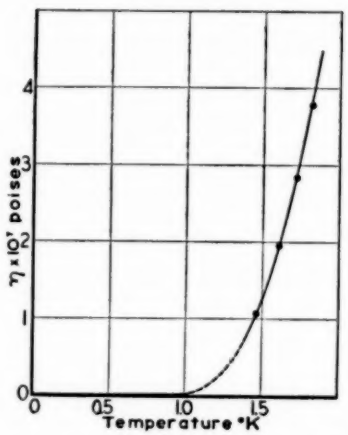

FIG. 1. The viscosity of liquid helium II measured by flow through a 10^{-4} cm channel.

We have measured the flow of liquid helium II through a small capillary into an enclosed space so that there was no possibility of transfer outside the capillary by a surface film. The capillary was calibrated in terms of the viscosity of helium gas at 4.225°K. The viscosity of the gas at this temperature was taken as 1.267×10^{-5} poise from the work of van Itterbeek and Keesom.[8] The more important results are given in Table I and are shown graphically in Fig. 1.

TABLE I. *The viscosity of liquid helium from the flow through a 10^{-4} cm channel.*

T°K	1.468	1.610	1.725	1.823
$\eta\times10^7$ poises	1.1	2.0	2.8	3.8

The values given in Table I are based on a preliminary calculation. Final corrections may increase the values at 1.823 and 1.725°K by small amounts.

The capillary channel which approximated the parallel plate type was obtained by casting a cylinder of solder in a glass tube and taking advantage of differential temperature contraction. The Reynolds number at the lowest temperature was $R=2v\rho h/\eta=179$, where v represents the average velocity, ρ the density and h equals one-half the plate separation. Davies and White[9] have shown that R for the upper limit of laminar flow between parallel plates is 890. The plate separation was about 1×10^{-4} cm which is about the same as that used by Kapitza and considerably smaller than the capillaries used by Allen and Misener.

From Fig. 1 it appears that the viscosity of liquid helium II drops to a very low value near 1°K and will presumably vanish at the absolute zero of temperature.

A detailed account of the experiments will be published in the near future, probably in the *Journal of the American Chemical Society.*

W. F. GIAUQUE
J. W. STOUT
R. E. BARIEAU

Department of Chemistry,
University of California,
Berkeley, California,
June 23, 1938.

[1] Kapitza, Nature **141**, 74 (1938).
[2] Allen and Misener, Nature **141**, 75 (1935).
[3] Kurti, Rollin and Simon, Physica **3**, 266 (1936); Rollin, Actes 7th Cong. int. du Froid **1**, 189 (1936).
[4] Kamerlingh Onnes, Comm. Phys. Lab. Leiden, No. 159 (1922); Trans. Faraday Soc. **18**, part 2, No. 53 (1922).
[5] Daunt and Mendelssohn, Nature **141**, 911 (1938).
[6] Wilhelm, Misener and Clark, Proc. Roy. Soc. London **A151**, 342 (1935).
[7] Burton, Nature **135**, 265 (1935).
[8] van Itterbeek and Keesom, Physica **5**, 257 (1938).
[9] Davies and White, Proc. Roy. Soc. London **A119**, 921 (1928).

The Identification of Auroral Radiations

Vegard and his collaborators have acquired a large number of data on the spectrum of the aurora which are collected in a recent publication.[1] Some 109 wave-lengths are given, most of which can be identified with lines and bands of oxygen and nitrogen. A few of the lines in the aurora are identified with the so-called ϵ system, which are described as follows,[2] "$\epsilon(n', n'')$ are bands of the ϵ system discovered by Vegard in the luminescence from solid nitrogen and interpreted by him as being due to the transitions between the electronic levels $A^3\Sigma$ and $X'\Sigma$ of the nitrogen molecule."

The writer[3] later discovered corresponding bands in the spectrum of an uncondensed electrical discharge which was capable of producing a strong nitrogen afterglow. These bands were recognized by the writer and Herzberg, who gave the analysis, as the $A^3\Sigma - X'\Sigma$ transition in nitrogen. The role these bands have played in the clarification of light of the night sky has been adequately treated by Déjardin.[4]

It is the purpose of this note to point out again a difference between the spectra which we designate $A^3\Sigma - X'\Sigma$ (solid) and $A^3\Sigma - X'\Sigma$ (gas). There is a difference in the wave-lengths (see Tables I and II, reference 3) and the gaseous bands are single headed bands whereas the ϵ bands (solid nitrogen) are double. The frequency difference between the stronger of the bands from the solid and the gaseous bands may have some significance in the structure of solid nitrogen.

For several years now, Vegard and his collaborators have been publishing identifications of certain auroral radiations and calling them ϵ bands.[5] A reference to the wave-lengths of the ϵ bands with which they identify the auroral radiations shows that the wave-length differences between the two vary from 8.6A to as high as 20.35A, the variations being fairly irregular. Comparison of the auroral radiations with members of the $A^3\Sigma \rightarrow X'\Sigma$ system in gaseous nitrogen shows an agreement which is probably within the errors of measurement. These comparisons are made in Table I.

It is difficult to understand why Vegard and his collaborators have failed to compare the auroral radiations with the bands which are emitted by gaseous nitrogen. The fallacy of comparing with the ϵ bands of solid nitrogen is shown not only by the failure to obtain agreement between the wave-lengths, but also by the incorrect identification of eight of the bands. A detailed discussion of several of these cases may be of interest. The band at 3603 was identified as either $\epsilon(0\text{–}10)$ or $\epsilon(3\text{–}12)$. $\epsilon(0\text{–}10)$ is correct, if we use the wave-length observed in the gas, 3601.4. $\epsilon(3\text{–}12)$, however, is obviously incorrect even though the wave-length of the weaker head is 3600.5, since one would hardly expect such accurate agreement in an isolated case, and with the weaker head. Again, 3728.6 is identified as $\epsilon(5\text{–}14)$. Aside from the fact that the evidence, based on actual study of these bands in the gas, is overwhelmingly against the excitation of $v' = 5$, the wave-length of the $\epsilon(5\text{–}14)$ band in Vegard's table is 3770, a difference of 42A. Other comparisons are made in Table I.

TABLE I.[6] *Identification of auroral radiations.*

AURORA	$A^3\Sigma \rightarrow X'\Sigma$(solid)	$A^3\Sigma \rightarrow X'\Sigma$(gas)	$\Delta\lambda_V$	$\Delta\lambda_K$
3202.7	3211.3 3217.2	3197.5	8.6	5.2
3429.0	3440.3 3446.8	3424.6	15.7	4.4
3603.0	3619.7 3627.0 $\epsilon(0,10)$ $\epsilon(3,12)$	3601.4	16.7	1.6
3685.3	3701.0 3709.7	3682.0	15.7	3.3
3728.6	$\epsilon(5,14)$	—	—	—
3769	3784.9 3789.8	3769	15.9	0
3872.0	$\epsilon(3\text{–}13)$	—	—	—
3981	3995.64 4001.56	3979	12.64	2
4076	4089.99 4096.44	4073	13.99	3
4092.0	$\epsilon(5,15)$	—	—	—
4176.2	4188.05 4195.26	4171	11.85	5
4218	4238.69 4247.3	4220	20.69	2
4319.5	4339.02 4345.34	4321	19.52	1.5
4375.6	$\epsilon(5,16)$	—	—	—
4424	4444.35 4451.56	4425	20.35	1
4507	$\epsilon(4,17)$	—	—	—
4535	4554.63 4562.55	4536	19.63	1
4858	$\epsilon(2,15)$	—	—	—
5238	$\epsilon(5,18)$	—	—	—

In conclusion, we wish to point out that as a result of this failure on the part of Vegard and his collaborators to consider the wave-lengths in gaseous nitrogen in interpreting their auroral data, not only have many of the bands been incorrectly identified, but the feeling has been left that they are identifying auroral radiations with the luminescence of solid nitrogen. Readers who are not very familiar with the development of the auroral problem might even think that Vegard and his school still believe in the existence of solid nitrogen in the upper atmosphere.

We wish finally to suggest a nomenclature for the two band systems which correspond to the $A^3\Sigma \rightarrow X'\Sigma$ transition in the nitrogen molecule. Since both systems correspond to some important radiant phenomena, and because of the large and real differences in wave-lengths, it is suggested that the system discovered by Vegard be called the "$A^3\Sigma \rightarrow X'\Sigma$ (solid)" and that discovered by the writer be called the "$A^3\Sigma \rightarrow X'\Sigma$ (gas)."

JOSEPH KAPLAN

Department of Physics,
University of California,
Los Angeles, California,
December 31, 1937.

[1] Vegard and Tonsberg, Geofysiski Publikasjoner, Vol. XI, No. 16.
[2] Reference 1, page 3.
[3] Kaplan, Phys. Rev. **45**, 675 (1934).
[4] Déjardin, Rev. Mod. Phys. **8**, 1 (1936).
[5] Reference 1 for complete bibliography.
[6] Vegard, Zeits. f. Physik **75**, 30 (1932).

Note on Internal Conversion of Arbitrary Multipole Order

In the activity coming down with gallium chemically separated from a zinc target bombarded with deuterons, Alvarez[1] found two homogeneous groups of electrons near 100 kev energy. The sharpness and spacing of these groups, the presence of zinc x-rays, and the relative intensities indicated that the electrons were the secondaries of an internally-converted γ-ray of about 100 kev energy. Few γ-rays of this energy were observed, though radiative transitions cannot be completely forbidden in an odd nucleus like Zn^{67}. The study of the internal conversion in natural radioactive elements has revealed[2] no cases of a conversion as high as that indicated here in zinc. The approximate formulae given by Rasetti[3] and Bethe[4] give values of a few percent for this case, and the Z^3 dependence of the conversion coefficient suggests that conversion becomes unimportant for the lighter elements. The formulae cited, however, were for the conversion of radiation from an electric dipole. One expects conversion to vary with multipole order, 2^l, roughly as the parameter $(\lambda^2/\lambda^2e)^l$, where λe is the de Broglie wave-length of the emitted electron, λ the γ-ray wave-length. Thus for low energy γ-rays, the conversion could increase greatly with multipole order.

Making a nonrelativistic calculation, neglecting spin, and neglecting the ratio $n=Ze^2/\hbar v$ of the velocity of the electron in its bound state to its velocity v after emission, one obtains a simple formula. We take the internal conversion coefficient a_K as

$$\frac{\text{number of electrons emerging from the atom}}{\text{number of } \gamma\text{-rays emerging from the atom}}.$$

For conversion by one electron in the K shell, we have for an electric 2^l pole:

$$a_K=\frac{l}{l+1}\cdot\alpha^4\cdot Z^5\left(\frac{2mc^2}{E}\right)^{l+5/2}. \qquad (1)$$

Z = effective nuclear charge; $\alpha=e^2/\hbar c$; E = energy of γ-ray; m = electron rest mass. If the effective nuclear charge were the same for both shells, the lowered electron density for the L shell would introduce a factor $\frac{1}{8}$. Screening will still further reduce the L conversion. In this limit, where we neglect the orbital motion of the bound electron, magnetic multipole radiation is not converted. This corresponds physically to the absence of radial forces on a stationary charge in a magnetic multipole field.

For Zn, $n\sim0.3$, and neglect of the binding is hardly justified. We have therefore made calculations using the nonrelativistic wave functions for the Coulomb field; for the electric dipole we find:

$$a_K=\alpha^4Z^5\left(\frac{2mc^2}{E}\right)^{7/2}\frac{\pi n}{1-e^{-2\pi n}}\left|\left[1+\frac{8}{1+n^2}\left(f+\frac{k}{2p}g\right)\right]\right|^2 \qquad (2)$$

where $f=[x(1-x)(1-u)+(in/2)(1-2x)+n^2/2]$;
$g=[(1-2x)(1-u)-in(1+u)]$;
$u=(-x/(1-x))^{in}$; $\quad|arg\,(-u)|<\pi$;
$x=\rho/2ip$; $\quad n=a/p$.

Here: $\rho=a+i(p-k)$; $\quad a=Ze^2m/\hbar^2$; $\quad p=mv/\hbar$; $\quad k=E/\hbar c$.

The other multipole orders lead to analogous but longer formulae. Numerical results for this case of a 100 kev γ-ray and atomic number 30 are:

	a_k	a_k from (1)
electric dipole	0.03	0.1
electric quadripole	0.7	1.4
electric octupole	5.	16.

The same trend with multipole order appears here. It is clear that the large conversion observed by Alvarez can be understood if the radiation is not dipole radiation.[5]

These nonrelativistic formulae fail if the γ-ray energy becomes of the order mc^2. Since $\lambda/\lambda e\to|$ for high γ-ray energies, one would expect the change with multipole order to become much less marked as the γ-ray energy increased, and relativistic calculations confirm this. Casimir has published[6] a formula for the electric dipole valid in the limit of very high γ-ray energies. Since the multipole order is unimportant here, Casimir's formula will give the order of magnitude of the conversion for all multipole orders, if only the γ-ray energy is $\gg mc^2$.[7]

All results are here stated for one electron. There are ordinarily two electrons in the K shell, but in cases like Alvarez', where K electron capture occurs, it is possible that the nuclear transition which causes electron emission precedes the atomic transition which refills the depleted K shell. Further work on internal conversion in the artificially radioactive nuclei may help to settle this question, and to determine the angular momenta of the states involved.

We are happy to acknowledge the continual kind guidance of Professor J. R. Oppenheimer and Dr. R. Serber.

S. M. Dancoff
P. Morrison

Department of Physics,
University of California,
Berkeley, California,
June 17, 1938.

[1] Alvarez, Phys. Rev. **53**, 606 (1938).
[2] Hulme, Mott, F. Oppenheimer and Taylor, Proc. Roy. Soc. **155A**, 315 (1936).
[3] Rasetti, *Elements of Nuclear Physics* (Prentice-Hall 1936), p. 139 et seq.
[4] Bethe, Rev. Mod. Phys. **9**, 228 (1937). The formulae given by Bethe and Rasetti do not agree as published. In the limit of $n\to0$ they agree with each other, but differ from our formula (1) by a factor 2. The consistency of the approximations employed in their derivation is not clear.
[5] We have to thank Dr. Alvarez for informing us that there are at least as many secondaries as 100 kev quanta emerging.
[6] Casimir, Physik. Zeits. **32**, 665 (1931).
[7] A more detailed discussion of the relativistic formulae and the derivation of those given above will be published later.

Radioactive As Isotopes

Germanium samples activated last year at Berkeley with 5.5 Mev deuteron beam from the cyclotron were brought back by one of the authors to Tokyo. The study of the activity shows the existence of two long periods. According to the data so far obtained, the periods are estimated to be about 17 days and 50 days, respectively. The decay curves are still being followed in order to determine the periods more accurately. Chemical separations show that both activities are due to arsenic isotopes.

The shorter period was also obtained by bombarding arsenic with fast neutrons from Li+D in the Tokyo cyclotron. This neutron loss process was first reported by

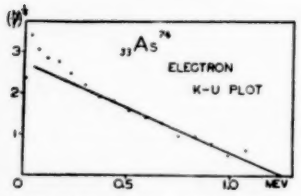

FIG. 1(a). K-U plot for electrons.

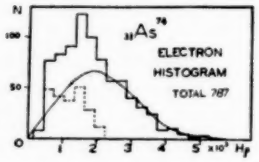

FIG. 1(b). Energy histogram for electrons. The part drawn by a broken line is considered to be due to annihilation rays.

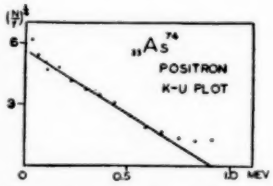

FIG. 1(c). K-U plot for positrons.

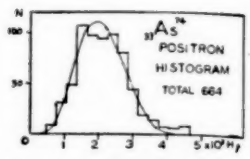

FIG. 1(d). Energy histogram for positrons.

Pool, Cork and Thornton,[1] and Curtis and Cork[2] who reported that it has the half-life of 13.5 days and emits both positive and negative electrons. The upper limit of the positron is said to be 0.65 Mev but for negative electrons, relative numbers emitted and chemical separations have not been reported yet.

The study of the β-ray histogram of the germanium samples with a hydrogen-filled Wilson chamber gave results as shown in Fig. 1. The upper limit for positive and negative electrons reduced from the K–U plots are 0.9 Mev and 1.25 Mev, respectively. Although the value for positrons is a little higher than that obtained by the Michigan group, we are certain that the process should be written as follows:

$$Ge^{73}+D^2\rightarrow As^{74}+n'$$
$$As^{75}+n'\rightarrow As^{74}+2n'.$$

To check the fact that As^{74} emits positive and negative electrons three series of photographs were taken on the same sample on three different dates about two weeks apart. The ratios of the number of positive and negative electrons are nearly constant as shown in Table I. The branching ratio is thus estimated to be 0.9. As for the longer period it is most probable that it is due to the following process:

$$Ge^{76}+D^2\rightarrow As^{77}+n'.$$

This isotope emits very soft β-rays which can be absorbed completely by 4/1000″ Al sheet. A study with a low pressure chamber is now in progress.

TABLE I. *Relative number of positive and negative electrons.*

Date	pos.	neg.	ratio
March 23	255	233	0.92
April 6	146	113	0.78
April 24	263	212	0.81
Total	664	558	0.84

It is a pleasure to express our thanks to Professor E. O. Lawrence for the privilege of using his cyclotron. Thanks are also due to Dr. Y. Nishina and Professor K. Kimura for their valuable help and encouragement. We wish to acknowledge the assistance given to us by Mr. K. Sinma, Mr. F. Yamasaki and Mr. N. Mori. The experiment has been aided by grants from the Research Corporation, the Chemical Foundation, the Josiah Macy, Jr. Foundation, the Japan Society for the Promotion of Scientific Research, Oji Paper Manufacturing Company, Mitsui Ho-onkwai Foundation, Tokyo Electric Light Company and Japan Wireless Telegraph Company.

R. SAGANE
S. KOJIMA
M. IKAWA

Department of Physics (R. S. and S. K.),
Department of Chemistry (M. I.),
Tokyo Imperial University,
Tokyo, Japan,
May 28, 1938.

[1] Pool, Cork and Thornton, Phys. Rev. **52**, 239 (1937).
[2] Curtis and Cork, Phys. Rev. **53**, 681 (1938).